Study on Dynamic Performance of Grid Connected Doubly-Fed Induction Generator

Dissertation submitted in partial fulfillment of the requirements for the award of degree of

Master of Engineering

in

Power Systems & Electric Drives

By:

Ashwani Kumar

(Roll. No. 801141008)

Under the supervision of:

Dr. Sanjay K. Jain
Associate Professor, EIED

ELECTRICAL AND INSTRUMENTATION ENGINEERING DEPARTMENT

THAPAR UNIVERSITY

PATIALA – 147004

JULY, 2013

CERTIFICATE

I hereby certify that the work which is being presented in the dissertation entitled, **"Study on Dynamic Performance of Grid Connected Doubly-Fed Induction Generator"**, in partial fulfillment of the requirements for the award of degree of Master of Engineering in Power Systems and Electric Drives submitted in Electrical and Instrumentation Engineering Department of Thapar University, Patiala is an authentic record of my own work carried out under the supervision of Dr. Sanjay K. Jain, Associate Professor, EIED.

The matter presented in this dissertation has not been submitted for the award of any other degree of this or any other university.

Ashwani

(Ashwani Kumar)
Roll. No. – 801141008

This is to certify that the above statement made by the candidate is correct and true to best of my knowledge.

Sanjay
13/07/2013

(Dr. Sanjay K. Jain)
Associate Professor
EIED, Thapar University

Countersigned by :

S. Ghosh

(Dr. S. Ghosh)
Professor & Head, EIED
Thapar University

(Dr. S. K. Mohapatra)
Sr. Professor & Dean (Academic Affairs)
Thapar University

ACKNOWLEDGEMENT

Foremost, I feel great pleasure in acknowledging a deep sense of gratitude and regards to my supervisor, Dr. Sanjay K. Jain, Associate Professor, EIED, Thapar University, whose guidance, motivation, critical observation and whole hearted support helped me in the successful completion of the dissertation work.

I would like to thanks Dr. S. Ghosh, Professor and Head, Department of Electrical & Instrumentation Engineering, Thapar University, for providing the necessary facilities to carry out the dissertation work.

I also take this opportunity to express my sincere appreciation to Ms. Manbir Kaur, Associate Professor & PG Coordinator (Power Systems & Electric Drives), EIED, Thapar University, for her motivation and immense support.

I am highly thankful to the entire faculty and staff members of department for their cooperation throughout this work.

I am grateful to all whosoever have enlightened me throughout my life

Ashwani Kumar

ABSTRACT

Due to the environmental concern, the effort is being made to generate electricity from renewable energy sources. Among various renewable sources, one efficient alternative is wind energy. Large wind farms are being connected to grid. As the wind speed does not remain constant, Doubly-fed Induction Generator (DFIG) is being used to extract maximum power from the wind. In DFIG, the stator is directly connected to the grid while the rotor is connected through back-to back converter.

The work is carried out with the objective to study the operational aspects of grid connected DFIG and simulate the dynamic performance of grid connected DFIG. The various aspects of aerodynamic conversion using wind turbine, dynamic model, converter model has been studied. The dynamic model and control scheme of grid connected DFIG has been realized under simulink environment. The stator flux oriented (SFO) and stator voltage oriented (SVO) control schemes are implemented on the rotor and grid side converter respectively. The DFIG is operated in speed control mode. The modeling and dynamic performance of the wind driven DFIG system is studied for change in wind speed, change in reference speed, change in DC link reference voltage, DC link capacitance and line inductance.

TABLE OF CONTENTS

PAGE NO.

CERTIFICATE i

ACKNOWLEDGEMENT ii

ABSTRACT iii

TABLE OF CONTENTS iv

LIST OF FIGURES vii

LIST OF TABLES x

NOMENCLATURE xi

CHAPTER-1 INTRODUCTION 1-13

1.1 OVERVIEW 1

1.2 LITERATURE REVIEW 2

1.3 OBJECTIVE OF THE WORK 13

1.4 ORGANISATION OF THE DISEERTATION 13

CHAPTER-2 AERODYNAMIC CONVERSION THROUGH WIND TURBINE .14-23

2.1 INTRODUCTION 14

2.2 CLASSIFICATION OF WIND TURBINES 14

2.2.1 Horizontal Axis Wind Turbine 15

2.2.2 Vertical Axis Wind Turbine 16

2.2.3 Fixed Speed Wind Turbine 16

2.2.4 Variable Speed Wind Turbine 17

2.2.4.1 WECS with stator side converter 18

2.2.4.2 WECS with both stator and rotor side converter 18

2.3 WIND TURBINE MODEL AND CHARACTERISTICS 19

2.3.1 Wind Turbine Modeling 19

2.3.2 Power Characteristics 21

2.3.3 Pitch and Stall Control 22

CHAPTER-3 MODELING AND OPERATION OF DOUBLY-FED INDUCTION GENERATOR **24-34**

3.1 INTRODUCTION 24

3.2 OPERATION OF DFIG 25

3.2.1 Super-Synchronous Mode 26

3.2.2 Sub-Synchronous Mode 26

3.3 DYNAMIC MODEL OF INDUCTION MACHINE 28

3.3.1 Reference Frame Theory 28

CHAPTER-4 POWER CONVERTER CONTROL AND DESIGN **35-47**

4.1 INTRODUCTION 35

4.1.1 Rotor Side Converter 36

4.1.2 Grid Side Converter 37

4.1.3 Converter Losses 38

4.2 CONVERTER CONTROL SYSTEM 38

4.2.1 Rotor Side Control Scheme 39

4.2.2 Decoupling Control Scheme 41

4.2.3 Grid Side Control Scheme 42

4.3 CONTROLLER DESIGN 44

4.3.1 Grid Side Current Control Loop 44

4.3.2 DC Link Voltage Control Loop 45

4.3.3 Rotor Side Current Control Loop 45

4.3.4 Speed Control Loop 46

CHAPTER-5 SIMULATION AND RESULTS **48-77**

5.1 SYSTEM MODEL 48

5.1.1 Induction Generator Model 49

5.1.2 Converter Control Model 50

5.1.2.1 Discrete Phase-Locked Loop 50

5.1.2.2 Grid Side Converter Control Block 51

5.1.2.3 Rotor Side converter control block 52

5.1.3 Wind Turbine Model 53

5.2 RESULTS AND DISCUSSION 54

5.2.1 Effect of change in wind speed on DFIG performance 54

5.2.2 Effect of change in parameter on DFIG performance 66

5.2.3 Effect of change in rotor reference speed on the performance of DFIG 70

CHAPTER-6 CONCLUSION AND FUTURE SCOPE 75

6.1 CONCLUSION 75

6.2 FUTURE SCOPE OF WORK 75

APPENDIX-A 76-78

APPENDIX-B 79

LIST OF PUBLICATIONS 80

REFERENCES 81-89

LIST OF FIGURES

Fig. No.	Name of Figure	Page No.
Fig.2.1	Horizontal axis wind turbine	15
Fig.2.2	Vertical axis wind turbine	16
Fig.2.3	Fixed speed wind turbine generator configuration with soft starter	17
Fig.2.4	Variable speed wind turbine generator configuration with full capacity power converter	18
Fig.2.5	Variable speed wind turbine generator configuration with reduced capacity power converter	19
Fig.2.6	Illustration of forces around the moving blade	21
Fig.2.7	The Operating modes of wind turbine	22
Fig.3.1	Grid connection of DFIG	25
Fig.3.2	Power flow in DFIG WECS under super-synchronous mode of operation	26
Fig.3.3	Power flow in DFIG WECS under sub-synchronous mode of operation	27
Fig.3.4	Co-linearity of q^s-axis with the a- phase axis	29
Fig.3.5	Projection of stationary reference to synchronous reference frame	30
Fig.3.6	Projection of rotor reference to synchronous reference frame	31
Fig.3.7a	q-axis model of induction machine	32
Fig.3.7b	d-axis model of induction machine	32
Fig.4.1	Back-to-Back PWM structure	35
Fig.4.2	Rotor side converter control scheme	36

Fig.4.3	Grid side converter control scheme	37
Fig.4.4	Current-control loop of stator side converter	44
Fig.4.5	DC link voltage control loop	45
Fig.4.6	Current-control loop of rotor side converter	46
Fig.4.7	Speed control loop of DFIG	47
Fig.5.1	System model of DFIG grid integration	48
Fig.5.2	Model of induction generator	49
Fig.5.3	Sub-system of control system	50
Fig.5.4	Grid side control model	51
Fig.5.5	Rotor side control model	53
Fig.5.6	Wind turbine model	54
Fig.5.7	Coefficient of performance Cp model	54
Fig.5.8	Effect of wind speed on turbine torque	55
Fig.5.9	Effect of wind speed on electromagnetic torque	56
Fig.5.10	Effect of wind speed on active power generated by DFIG	57
Fig.5.11	Effect of wind speed on reactive power	58
Fig.5.12	Illustration of (i) Rotor speed (ii) Stator voltage (iii) DC-link voltage	59
Fig.5.13	Effect of wind speed on 3-phase stator current	60
Fig.5.14	Effect of wind speed on 3-phase rotor current	61
Fig.5.15	Effect of wind speed on rotor current in (d-q) terms	62
Fig.5.16	Effect of wind speed on stator current in (d-q) terms	63

Fig.5.17	Effect of wind speed on rotor side reference voltage	64
Fig.5.18	Effect of wind speed on stator side reference voltage	65
Fig.5.19	Effect of change in parameters on electromagnetic torque	66
Fig.5.20	Effect of change in parameters on active power	67
Fig.5.21	Effect of change in parameters on 3-phase stator current	67
Fig.5.22	Effect of change in parameters on 3-phase rotor current	68
Fig.5.23	Effect of change in parameters on (d-q) rotor current	68
Fig.5.24	Effect of change in parameters on rotor ref. voltage in (d-q) terms	69
Fig.5.25	Effect of change in parameters on stator ref. voltage in (d-q) terms	69
Fig.5.26	Turbine torque for different rotor ref. speed	70
Fig.5.27	Rotor speed for different rotor ref. speed	71
Fig.5.28	3-phase stator current for different rotor ref. speed	72
Fig.5.29	3-phase rotor current for different rotor ref. speed	72
Fig.5.30	d-q rotor ref. voltage for different rotor ref. speed	73
Fig.5.31	d-q rotor current for different rotor ref. speed	73
Fig.5.32	Active and reactive power for different rotor ref. speed	74

List of Tables

Table No.	Name of Table	Page No.
Table 5.1	Steady state torque for different wind speeds	56
Table 5.2	Peak value of Active power for different speeds	58
Table 5.3	Peak value of reactive power for different speeds	59
Table 5.4	Summary of stator current for different rotor speeds.	61
Table 5.5	Summary of rotor current for different rotor speeds.	62
Table 5.6	summary of rotor current in d-q terms	63
Table 5.7	summary of stator current in d-q terms	64

NOMENCLATURE

p	:	The time derivative (d/dt)
V_{qs} ,V_{ds}	:	Stator side quadrature and direct axis voltage, respectively
i_{qs} ,i_{ds}	:	Stator side quadrature and direct axis current, respectively
φ_{qs} ,φ_{ds}	:	Stator side quadrature and direct axis flux, respectively
V_{qr} ,V_{dr}	:	Rotor side quadrature and direct axis voltage, respectively
i_{qr} , i_{dr}	:	Rotor side quadrature and direct axis current , respectively
φ_{qr} ,φ_{dr}	:	Rotor side quadrature and direct axis flux, respectively
r_s ,r_r	:	Stator and Rotor resistances of machine per phase, respectively
L_{ls}, L_{lr}	:	Leakage inductances of stator and rotor windings, respectively
ω_e ,ω_r	:	Supply and Rotor angular frequency (electrical speed), respectively
θ_s ,θ_r	:	Stator and Rotor flux angle, respectively
T_e ,T_m	:	Electromagnetic and Mechanical torques, respectively
P_s ,Q_s	:	Stator-side active and reactive powers, respectively
P_r ,Q_r	:	Rotor-side active and reactive powers, respectively
J, D	:	Moment of inertia and Damping coefficient, respectively
P	:	Number of poles
M_1,M_2	:	Stator and Rotor modulation depths, respectively
V_{tri}	:	Triangular voltage signal
R,L	:	Resistance and Inductance of input filter, respectively
V_1, I_1	:	Input filter line voltage and current, respectively
E	:	DC-link voltage
C	:	DC-Link capacitance
P_{DC}	:	DC-link active power
σ	:	Leakage factor
k_p ,k	:	Proportional and Integral gain, respectively
α	:	Bandwidth of the closed-loop system
α_{cs}	:	Bandwidth of supply-side current controller
α_E	:	Bandwidth of DC-link voltage controller
α_{cr}	:	Bandwidth of rotor-side current controller
α_ω	:	Bandwidth of speed controller
‘Comp’	:	Compensation term
superscript‘e’	:	synchronously rotating reference frame

CHAPTER - 1

INTRODUCTION

1.1 OVERVIEW

The wind energy is a by-product of solar energy. Approximately 2% of the solar energy that is reaching the earth is converted into wind energy. The surface of the earth heats and cools unevenly. Thereby, creating atmospheric zones that makes the air to flow from the region of higher atmospheric pressure to the lower atmospheric pressure.

The wind has played an important role in the history of human civilization. Around 5000 years back the wind energy was used to sail boats from shore to shore. In Egypt the first wind mill have been built around 2000 B.C. in ancient Babylon. By the 10^{th} century, wind mills of about 30ft high with large wind catching surfaces were used for grinding grain in the areas in eastern Iran and Afghanistan. In 12^{th} century wind mills were used for milling grains in western world.

After few hundred years, the wind mills were modified to pump water in 1889 in Europe. The multi vane wind mill farm was invented in the United States of America during the latter half of the 19th century. Until the diesel engine came along, many transcontinental routes in the USA depended on large multi vane wind mills to pump water for steam locomotives.

In the 1930s and 1940s, thousands of electricity producing wind turbines were built in U.S. They had two-three thin blades which rotate at high speed to drive the electric generators to provide electricity to farms beyond the reach of power lines and were typically used to charge storage batteries, operate radio receivers and power a light bulb. In early 1950s, the central power grid has been extended to nearly every American household, thus eliminated the market for these machines. Wind turbine development has again got momentum after the oil crises in seventies. Thereafter the wind energy technology developed rapidly and large wind turbines were set in the operation.

The major factors which triggered the harnessing of renewable resources including

wind energy are:

- Finite nature of fossil fuel
- Increasing prices of conventional fuel resources
- Emission of harmful gases during the combustion of fossil fuel

Initially, the cost of production of electricity from wind energy was 8-10 times more than that produced by the conventional sources. The factors such as technological advancement in the field of engineering and the growing awareness for clean and green energy contributed in the development and utilization of wind energy. It is the fastly growing source for electric power generation and it is expected to remain so in future. Various countries namely United States of America, Germany, China and India are leading to harness this non-polluting and renewable source of energy.

Harnessing wind energy for electric power generation is an area of research interest. Among various techniques, the use of the doubly fed induction generator appeared to be good solution for such application. The induction generator is favored for wind power plants because of its simplicity, robustness and small size per generator kW, lower maintenance and ease of control.

For, wind power generation both fixed speed and variable speed turbines can be used. These turbines are classified in to four major types by the Western Electricity Coordinating Council (WECC). These are **Type I:** Pitch regulated squirrel cage induction generator directly connected to the grid. **Type II:** Variable slip squirrel cage induction generator directly connected to the grid. **Type III:** Wound rotor induction generator with an AC/DC/AC power converter connected between the rotor terminals and the grid and is pitch regulated. **Type IV:** Synchronous or asynchronous machine connected to the grid using full rated AC/DC/AC power converters and is pitch regulated.

1.2 LITERATURE REVIEW

Many investigations in the field of wind power generation have taken place over the past few decades. These investigation deals with behavior, modeling, speed control of doubly fed induction generator. A literature on the modeling and control of DFIG is briefly summarized here with.

The doubly-fed induction generator (DFIG) is an induction generator with both stator and rotor windings. The DFIG is nowadays widely used in variable-speed wind energy applications with a static converter connected between the stator and rotor. Currently, this topology occupies close to 50% of the wind energy market. There is numerous literatures [1]-[88] on the operation of WECSs based on DFIGs for the integration to the grid.

Green house gas reduction and global warming has been one of the crucial and inevitable global challenges. These issues have drawn increasing attention to renewable energies including wind energy [1]. WECS has annual installation growth rate of 31.7% in 2009 with its growth rate is continuously increasing for the last few years [2]. The increasing price-competitiveness of wind energy against other conventional fossil fuel energy sources such as coal and natural gas is another positive [3].

WECS consists of three major aspects; aerodynamic, mechanical and electrical. The electrical aspect of WECS can further be divided into three main components, which are wind turbine generators (WTGs), power electronic converters (PECs) and the utility grid. With the consideration to its operation speed and the size of the associated converters, WTGs can be classified into three categories namely: Fixed Speed Wind Turbine (FSWT), Variable Speed Wind Turbine (VSWT) with partial scale frequency converter (PSFC), Variable Speed Wind Turbine (VSWT) with full scale frequency converter (FSFC). FSWT including Squirrel-Cage Induction Generator (SCIG), led the market until 2003. The Doubly-Fed Induction Generator (DFIG), which is the main concept of VSWT with PSFC, overtook FSWT and has been leading WTG concept. It nearly has 85% of the market share [3]. The functional structure of a wind energy conversion system is presented in [4]. A comparison between the constant and variable speed wind turbine model and dynamic behavior with pitch control capability is explained.

The wind turbines may be of horizontal axis or vertical axis types. These turbines can be fixed speed and variable speed wind turbines. The fixed-speed wind turbines rotate at almost a constant speed and the maximum conversion efficiency can be achieved only at a given wind speed. The turbine is protected by aerodynamic control of the blades from possible damage caused by high wind gusts. This type of turbine also requires a sturdy mechanical design to absorb high mechanical stresses [5]. The variable-speed wind turbines can achieve maximum energy conversion efficiency over a wide range of wind

speeds. The turbine can continuously adjust its rotational speed according to the wind speed. In doing so, the tip speed ratio, which is the ratio of the blade tip speed to the wind speed, can be kept at an optimal value to achieve the maximum power conversion efficiency at different wind speeds [6]. To make the turbine speed adjustable, the wind turbine generator is normally connected to the utility grid through a power converter system [7]. The converter system enables the control of the speed of the generator that is mechanically coupled to the rotor (blades) of the wind turbine. The influence of wind turbines on the behavior of electrical power systems is presented [8]. A dynamic model of a doubly fed (wound rotor) induction generator with a voltage source converter feeding the rotor is presented. The dynamic performance of fixed speed wind turbine and Doubly-fed induction wind turbine is compared by deriving a reduced-order dynamic machine model using control scheme, speed control characteristics and converter protection of DFIG [9].

The Doubly-fed induction generator's are mostly utilizes slip ring induction generator. In the slip ring induction generator topology, the stator circuit is directly connected to the grid while the rotor circuit is connected to grid via slip rings and three-phase converter. The DFIG is currently the system of choice for multi-MW wind turbines. The DFIG system operates in both sub- and super-synchronous modes with a rotor speed range around the synchronous speed. The stator flux oriented VSCF Doubly-fed power system model is presented and the sub-synchronous and super-synchronous mode of operation of Doubly-fed induction generator is studied [10]. The slip is negative in the super-synchronous mode and becomes positive in the sub-synchronous mode [11]. For variable-speed systems where the speed range requirements are around ±30% of synchronous speed, the DFIG offers adequate performance. The DFIG generates high power when operating in the super-synchronous mode, the power rating for the converter is determined by the rated or maximum slip in the super-synchronous mode. The authors [12] suggested that large wind farms will employ doubly fed induction generator (DFIG) variable speed wind turbines. The dynamic model of DFIG wind turbine using a single-cage and double-cage representation of the rotor with associated control and protection circuits was given

An AC-DC-AC converter is included in the rotor circuit. The converters need only be rated to handle a fraction of the total power – the rotor power – typically about 30% nominal generator power. Therefore, the losses and the cost associated with the converter

are lower compared to a system where the converter has to handle the entire power. As the rotor speed of the DFIG is adjustable, the maximum power point tracking (MPPT) schemes can be implemented to harvest the maximum available power from the wind turbine.

Recently, brushless DFIG are also investigated. The most significant features of the brushless DFIG are that a) it is brushless in operation, b) it utilizes a fractionally rated converter, and c) it shows greater compatibility with grid codes than the conventional DFIG. The brushless DFIG is attractive as brushless operation reduces the maintenance requirements and increases reliability. These advantages are even more significant for offshore applications.

The contemporary BDFIG is single frame induction machine, without any brushes. It has two 3-phase stator windings of different pole numbers. Typically the two stator supplies are of different frequencies, one a fixed frequency supply connected to the grid, and the other a variable frequency supply derived from a power electronic frequency converter. The BDFIG may be thought of as the combination two induction machines, of different stator pole, these machines will have different synchronous speeds, for the same supply frequency. With their rotors connected together both physically and electrically. Physically this machine is very similar to the self-cascaded machine proposed by Hunt [13]. The main distinction is that the BDFIG is explicitly a doubly-fed machine. It can be operated in asynchronous or synchronous mode of operation.

During the asynchronous mode of operation, the shaft speed is dependent on the loading of the generator, as well as the supply frequency. When either of the stator winding is excited while leaving the other supply unconnected, the mode of operation is referred to as simple induction mode. The characteristics of the BDFIG in this mode are the same as those of a standard induction generator, except that the performance will be poor. However, if the non-supplied stator winding is short-circuited, then the behavior of the generator is like that of a cascaded induction generator and is referred to as cascade induction mode.

The design of the machine is to be optimized for synchronous mode of operation. The synchronous mode of operation of the BDFIG relies on cross-coupling between the stator and rotor fields [14]. When the second stator winding is fed from DC, the operating

speed is regarded as natural speed and this operating condition has been noted by Broadway and Burbridge [15]. Furthermore, it can be shown that the power factor of the machine can be controlled in this synchronous mode, and, subject to inverter capacity, the grid-connected winding may run at leading power factor.

The variable speed configuration of DFIG is the same as that of the WRIG system except that (1) the variable resistance in the rotor circuit is replaced by a grid-connected power converter system, and (2) there is no need for the soft starter or reactive power compensation. The power factor of the system can be adjusted by the power converters. The converters only have to process the slip power in the rotor circuits resulting in reduced converter cost in comparison to the wind energy systems using full-capacity converters [16]-[18]. The use of the converters also allows bidirectional power flow in the rotor circuit and increases the speed range of the generator. This system features improved overall power conversion efficiency and enhanced dynamic performance as compared to the fixed-speed WECS and the variable resistance configuration. These features have made the DFIG wind energy system widely accepted in today's market. A two-level IGBT voltage source converter (VSC) system in a back-to-back configuration is normally used. Since both stator and rotor can feed energy to the grid, the generator is known as a doubly fed generator. The dynamics of DFIG connected to the grid is explained [19]. The stator was connected directly to grid and by two back-to-back PWM voltage source converter connected by a common D.C. link between the rotor and the grid. The study was carried out in rotor reference frame using dynamic vector approach. The paper [20] presented a model using the current controllers for the rotor-side and grid-side converter.

The rotor-side converter (RSC) controls the torque or active/reactive power of the generator while the grid-side converter (GSC) controls the DC-link voltage and its AC-side reactive power. Since the system has the capability to control the reactive power, external reactive power compensation is not needed.

There are mainly three configurations of power converters through which the operation of DFIG is realized. These are (i) Static Kramer drive and SCR Converter (ii) Back-to-back PWM converter and (iii) Matrix converter configurations.

The Static Kramer Drive consists of a diode rectifier on the rotor side and a line commutated inverter connected to the supply-side [21]. With this converter, a sliding mode

control is developed which provides a suitable compromise between conversion efficiency and torque oscillation smoothing. The controller regulates the thyristor inverter firing angle to attain the ideal compromise. The sliding mode control law forces the generator torque to be a linear function of the generator speed around the operating point of maximum power transfer. This converter is only able to provide power from both stator and rotor circuits, under super-synchronous operation. To solve this problem, the diode rectifier is replaced with thyristor rectifier (SCR) [22,23]. The inclusion of a second SCR allows the generator reactive power demand to be satisfied by the rotor-side converter system [22]. In comparison to the Kramer Drive, this system produces more power output due to the lack of reactive power available with a diode rectifier. The detailed control of the two rectifiers in sub- and super-synchronous modes is presented [23]. This approach, however, results in firing and commutation problems with the rotor-side converter and harmonic distortion to the grid.

The use of technologically advanced back-to-back converters is giving more flexibility for control [24]-[29]. The vector control is applied to the supply-side converter, with a reference frame orientated with the d-axis along the stator voltage vector [24,25]. The supply-side converter is controlled to keep the DC-link voltage constant through regulation of the d-axis current and reactive power control through alteration of the q-axis current. The paper [30] compared the vector control and direct power control of DFIG under grid connection and steady state.

For the rotor side, the decoupled control of the electrical torque and the rotor excitation current is presented [24]. Conversely, the rotor current decomposed into d-q components, where the d-axis current is used to control the electromagnetic torque and the q-axis current controls the power factor [25]. Both types of rotor-side converter control employ PI controllers, with PWM switching techniques, and space vector modulation (SVM) . A full ordered DFIG model based on stator voltage oriented with the stator flux transients and then implementing internal model control (IMC) in designing the DFIG rotor current controller was described [31].

To accompany the capacitor in the DC-link, a battery is used as a storage device, thereby, the supply-side converter controls the transfer of real power between the grid and the battery [26]. The supply-side controller is made up of PI controllers. Energy is stored during high winds and is exported to the grid during calm conditions to compensate for the

drop in stator power. The algorithm searches for the peak power by varying the rotor speed, and the peak power points are recognized as zero slopes on the power speed curves. The control works continuously, as a significant shift in power causes the controller to shift the speed the d-q axis control is used to control the real and reactive power of the machine. It is stated that the dynamics of the speed controller should not be extremely fast, else large transients in generator torque may occur [27].

The control scheme [28] is based on voltage space vectors (VSV). The application of certain voltage vectors may accelerate the rotor flux, and increase the active power generated by the stator. However the application of other voltage vectors may decreases the reactive power drawn by the stator and thus results into improved power factor. To facilitate this direct power control, the controller tables and details are provided.

The control scheme, uses information on shaft speed and turbine output power to estimate the wind speed and is applied to brushless DFIG [29]. The turbine output power is described as a function of TSR. The system is commanded to the desired shaft speed and the output power is measured, to guarantee the control.

The design of DFIG using back-to-back PWM converter is given in [32-37]. The paper [38] presented the switch-by-switch representation of the PWM converters with a carrier-based Sinusoidal PWM modulation for both rotor- and stator-side converters and evaluated the IMC control technique. The paper [39] presents a review on the typical dq concept used widely in DFIG converter control and examined the power control characteristics of DFIG PWM converter under different dq control conditions The decoupled d-q vector control scheme is implemented in [32-35] for the independent control of active, reactive power and to provide wide speed operation using back-to-back PWM converter connected between the rotor side and the utility grid. The converter performance of grid connected wind energy conversion system is analyzed in [36]. To overcome this harmonics generated by PWM used and the design the LCL filters for the back-to-back PWM converter in DFIG is presented in[37].

The matrix converter is capable of converting the variable AC from the generator into constant AC to the grid in one stage. This converter does not require bulky energy storage or DC-link and control is performed with one converter only. The utilization of a matrix converter with a DFIG has been explored [40-41]. The stator-flux oriented control was employed on the rotor matrix converter. The d-axis current was aligned with the

stator-flux linkage vector. The regulation of the d-axis current allows the control of the stator-side reactive power flow, where as the q-axis current helps regulate the stator-side active power [40].

The rotor voltage is controlled to control the power factor of the DFIG [41]. The matrix converter consists of nine bidirectional switches arranged in a manner such that any input phase may be connected to any output phase at any time. Each individual switch is capable of rectification and inversion. The matrix converter is controlled using double space vector PWM, employing the use of input current and output voltage SVM.

The grid connected wind-power generation scheme using DFIG in conjunction with a direct AC-AC matrix converter is proposed in [42-43] performance of grid–connected WECS based on DFIG fed by matrix converter is proposed in [44]. A simple and easy modulation scheme called DDPWM is proposed in [45] to confirm reliable application of matrix converter for the DFIG. The paper [46] summarizes a control strategy for a DFIG using an indirect matrix converter. The terminal voltage and frequency control along with the power factor at the interface with the grid was discussed [47].

Mainly three control system are used with grid connected DFIG. These are-

- Maximum Power Point Tracking (MPPT) Control
- Rotor side converter control
- Grid side converter control

The control of a variable-speed wind turbine below the rated wind speed is achieved by controlling the generator. The main goal is to maximize the wind power capture at different wind speeds, which can be achieved by adjusting the turbine speed in such a way that the optimal tip speed ratio λ_{opt} is maintained.

The relations between the mechanical power, speed, and torque of a wind turbine can be used to determine the optimal speed or torque reference to control the generator and achieve the MPP operation. The operation of the wind turbine can be divided into three modes: parking mode, generator-control mode, and pitch-control mode:

• Parking mode: When the wind speed is below cut-in speed, the turbine system generates less power than its internal consumption and, therefore, the turbine is kept in

parking mode. The blades are completely pitched out of the wind, and the mechanical brake is on.

• Generator-control mode: When the wind speed is between the cut-in and rated speed, the blades are pitched into the wind with its optimal angle of attack. The turbine operates with variable rotational speeds in order to track the MPP at different wind speeds. This is achieved by the proper control of the generator.

• Pitch-control mode: For higher than rated wind speeds but below the cut-out limit, the captured power is kept constant by the pitch mechanism to protect the turbine from damage while the system generates and delivers the rated power to the grid. The blades are pitched out of the wind gradually with the wind speed, and the generator speed is controlled accordingly.

The paper [48] compared the DFIG performance in terms of power reference tracking, response to sudden speed variation, sensitivity to perturbation and robustness against machine parameters variation regulation by simulating the system with PI and RST controllers. The authors [49] suggested that variable speed wind turbine based DFIG is frequently used in grid connected mode and this variable operation can be achieved by four-quadrant AC-DC-AC converter. The maximum power control with the DFIG and applied stator voltage oriented Vector control were applied to decouple the control of active and reactive power generated by DFIG. The authors [50] studied the system dynamic characteristics using stator flux oriented excitation, vector control strategy under speed control mode and current control mode in the process of MPPT. The parameters of PI controllers in current and speed control modes were selected using internal model control (IMC) and pole assignment method.

The rotor-side converter (RSC) provides the excitation for the induction machine rotor. With this PWM converter it is possible to control the torque hence the speed of the DFIG and also the power factor at the stator terminals. The rotor-side converter provides a varying excitation frequency depending on the wind speed conditions. The function of the receiving end converter is to feed in the active power transmitted by the sending end converter while maintaining the DC voltage at the desired level. Additionally, the reactive power channel can be used to support the grid voltage during faults and also in steady-state. The authors [51] proposed a decoupled control of DFIM used in generating mode,

by providing decoupled regulation of the primary side active and reactive power and makes it suitable for both electric energy generation and drive application.

The grid-side converter controls the flow of real and reactive power to the grid, through the grid interfacing inductance. The objective of the grid-side converter is to keep the DC-link voltage constant regardless of the magnitude and direction of the rotor power. The sending end converter is responsible for transmitting the active power produced by the wind farm, while maintaining the AC voltage in the wind farm grid. Furthermore, it can be used for frequency control which in turn controls the changes in the generator slip of the connected DFIG wind turbines. Thus, active power transfer through the low-rated converter in the rotor circuit of the DFIG can be limited without a reduction of total Power. As the power control is performed by the wind turbines, a simple voltage magnitude controller can be used for the sending end converter, thus fulfilling the aforementioned requirements. The frequency can be directly regulated without the need for a closed loop structure. The paper [52] analyzed the dynamic performance of DFIG using PI controller in the WECS.

In the grid integration of DFIG, the stator windings are directly connected to the grid and the wound rotor is connected to the grid via two back-to-back voltage source inverters. The paper [53] presents a model of variable speed wind turbine with doubly-fed induction generator and back-to-back voltage source converter along with speed, pitch and voltage controls to study the DFIG integration in a large scale power system. The grid side converter is connected via inductors to filter the current harmonics. Hence rotor currents can be controlled with a wished frequency and power quality of grid currents can be guaranteed. The operation influences system stability and reliability, power quality and power transmission.

The power system stability could be categorized into voltage stability, frequency stability and rotor angle stability [54]. VSWTSs have the ability to control reactive power and decouple active and reactive power control through electronic converters. Thus, the voltage stability of power systems is improved. Besides that wind energy could be restored as rotating kinetic energy in blade and hub, and then released by DFIG if necessary. So the frequency stability of grids could be enhanced temporarily. Different types of reduced order stability models for DFIGs are discussed and compared in study [55].

The voltage support and fault-ride through capability of DFIG are discussed in

studies [56]-[61]. In study [56], a reactive power control scheme is proposed for voltage regulation at a remote location with taking into account its operating state and limits. The study [57] derives a steady state PQ-diagram for a DFIG and concluded the reactive power production limitation is the rotor current limit. As the DFIG is quite sensitive to grid fault a voltage control scheme is designed to coordinate the rotor-side and grid-side converter [58].

Studies [62]-[67] discuss the effect on frequency stability by grid connected wind farm with VSWTSs. A control scheme that allows DFIGs to participate effectively in system frequency regulation is proposed in study [50]. A controller is designed in study [66], which helps to reduce the frequency drop following the transient period after the loss of network generation. The study [67] highlighted the advantages such as the improved power quality, high energy efficiency and controllability of fundamental frequency model of DFIG and simulated the power converter as a controlled voltage source.

There is no exact and accepted rotor angle concept for variable speed generators especially DFIG. The papers [68] propose a control scheme "Rotor Flux Magnitude and Angle" (FMAC) which defines the angle between the rotor flux vector and the d-axis of the reference frame as rotor angle. In study [69], above definition is used to design a power system stabilizer (PSS)

Studies [70,71] are concern with the modeling, algorithm and the evaluation method of reliability. The Power fluctuation caused by a large penetration of wind generation will influence on power quality such as voltage flicker, frequency deviation significantly. Meanwhile the harmonics current sourced from control system also increases the THD (Total Harmonic Distortion) index of power systems. Several studies [72]-[81] focus on these topics.

Studies [73]-[75] evaluate the flicker effect by wind farm. The frequency deviation caused by power fluctuation for a long term is just inevitable. Studies [76]-[78] discuss on this problem. Variable speed turbines are equipped with power PWM inverters, and uses insulated gate bipolar transistor (IGBT) technology. This gives rise to harmonic currents. Studies [79]-[80] discuss the effect of the harmonic current injected. In study [79], important general characteristics of the harmonic behavior of WTs are outlined. Study [80] analyzes the repercussions from the connection of wind farms with variable speed generators on the operation of weak electric distribution systems.

With wind being an uncontrollable resource, power delivery from a large-scale wind-farm into a power system poses challenges [82]-[88]. The papers [82]-[84] consider a solution for integration of large offshore doubly fed induction generator-based wind farms with a common collection bus controlled by a STATCOM into the main onshore grid using line-commutated high-voltage dc connection. The papers [85, 86] describe the use of voltage source converter (VSC)-based HVDC transmission system technology for connecting large DFIG-based wind farms over long distance. The paper[87] reports the impact of static synchronous compensator (STATCOM) to facilitate the integration of a large wind farm (WF) into a weak power system. Study [88] concerns with the issue of the fault ride-through capability of a wind farm of induction generators. The wind farm is connected to an AC grid through a VSC based HVDC link.

1.3 OBJECTIVE OF THE WORK

The WECS mostly utilize variable-speed variable-pitch wind turbine with DFIG. The DFIG-based WECS has efficient power conversion capability at variable wind speed, however, the system has limited reactive power capability.

The dissertation work has been carried out with the objective to study the operational aspects of WECS mainly through DFIG based system and to analyze the dynamic performance of wind driven grid connected doubly fed induction generator for varying parameters through simulation by implementing speed control mode.

1.4 ORGANISATION OF THE DISSERTATION

The work carried out in this dissertation has been summarized in six chapters. The **Chapter 1** summarizes the overview of thesis, brief literature review, objectives of work and organization of the thesis. The **Chapter 2** describes the power from the wind, description of wind turbine technology, modeling and control of wind turbine. The **Chapter 3** summarizes the operation and modeling of doubly fed induction generator. The **Chapter 4** explains the converter control and design. The **Chapter 5** presents the simulation and results obtained from developed simulink models. The **chapter 6** presents the summary of major conclusions and the scope of future work.

CHAPTER - 2

AERODYNAMIC CONVERSION THROUGH WIND TURBINE

2.1 INTRODUCTION

A wind energy conversion system (WECS) transforms wind kinetic energy to mechanical energy by using rotor blades. This energy is then transformed into electric energy by a generator. The system is made up of several components, participating directly in the energy conversion process. There are also other components that assist the system to achieve this task in a controlled, reliable, and efficient way. In order to better understand the process of wind energy conversion, descriptions of the wind turbine technology is given in this chapter.

Since the energy source for a WECS is wind kinetic energy, wind speed plays a key role in several aspects of the conversion process, especially in relation to the maximum power output. Therefore, this chapter introduces basic concepts of and relations between wind speed and power captured by the blades. This provides the necessary insight to explain how the power output of a wind turbine can be regulated by adjusting the blade pitch angle or stall control.

The wind turbine is one of the most important elements in wind energy conversion systems. Over the years, different types of wind turbines have been developed. This section also provides an overview of wind turbine technologies, including horizontal/ vertical-axis turbines and fixed/variable-speed turbines.

2.2 CLASSIFICATION OF WIND TURBINES

Wind turbines are classified into two ways one on the basis of their constructional feature and other on the basis of their speed [5, 91].

On the basis of constructional feature wind turbines are classified into two types:

- Horizontal Axis Wind Turbine
- Vertical Axis Wind Turbine

On the basis of speed wind turbines are also classified into two types:

- Fixed Speed Wind Turbine
- Variable Speed Wind Turbine

2.2.1 Horizontal Axis Wind Turbine

Horizontal-axis wind turbines, as shown in Fig.2.1, have the main rotor shaft and electrical generator at the top of a tower. The gearbox turns the slow rotation of the blades into a quicker rotation that is more suitable to drive an electrical generator.

Since a tower produces turbulence behind it, the turbine is usually pointed upwind of the tower. Turbine blades are made stiff to prevent the blades from being pushed into the tower by high winds. Additionally, the blades are placed at a considerable distance in front of the tower and are sometimes tilted up slightly.

Downwind machines have been built, despite the problem of turbulence, because they don't need an additional mechanism for keeping them in line with the wind. Additionally, during high winds, the 3-blades can be allowed to bend which reduces their swept area and thus their wind resistance. Since cyclic (that is repetitive) turbulence may lead to fatigue failures, most horizontal-axis wind turbines are upwind machines.

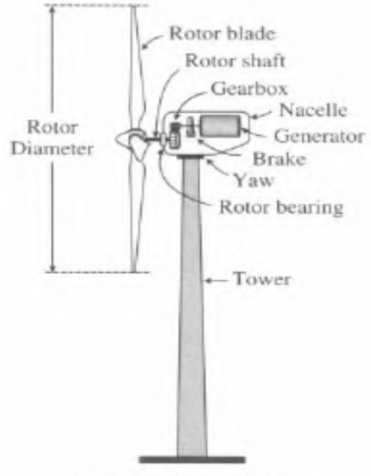

Fig.2.1 Horizontal Axis Wind Turbine

Horizontal-shaft turbines may have one blade or multiple blades. The sails are also used in place of blades in double opposite blade arrangement.

2.2.2 Vertical Axis Wind Turbine

Vertical-axis wind turbines, as shown in Fig.2.2, have the main rotor shaft arranged vertically. With this arrangement, the turbine need to be pointed into the wind to be effective. This is an advantage on sites where the wind direction is highly variable. Vertical-axis wind turbines can utilize winds from varying directions.

With a vertical axis, the generator and gearbox can be placed near the ground, so the tower doesn't need to support it, and it is more accessible for maintenance. Drawbacks are that some designs produce pulsating torque. Drag may be created when the blade rotates into the wind.

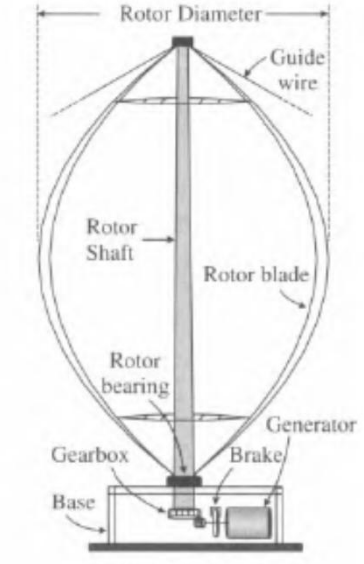

Fig. 2.2 Vertical axis wind Turbine

2.2.3 Fixed Speed Wind Turbine

The fixed speed wind turbine schematic is shown in Fig.2.3. For fixed speed wind turbines, the generator (induction generator) is directly connected to the grid. A soft starter is normally used in order to reduce the inrush current during start-up.

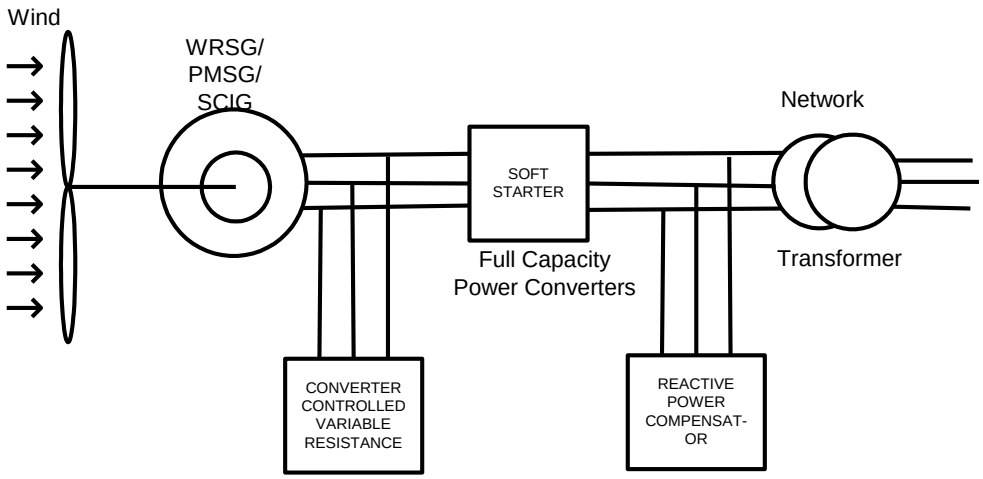

Fig. 2.3 Fixed Speed Wind Turbine Generator Configuration with Soft Starter

Also a reactive power compensator is needed to reduce the reactive power demand from the wind generator. Since the speed is almost fixed to the grid frequency, and certainly not controllable, it is not possible to store the turbulence of the wind in the form rotational energy. Therefore, for a fixed-speed system the turbulence of the wind will result in power variations, and thus affect the power quality of the grid. The advantage of a fixed speed turbine is that it is, relatively simple and therefore the investment cost tends to be slightly lower. These turbines have to be more mechanically robust than other designs, because of the higher structural loads involved. With a fixed speed WECS, it may be necessary to use aerodynamic control of the blades to optimize the whole system performance, thus introducing additional control system complexities, and costs.

2.2.4 Variable Speed Wind Turbine

For a variable-speed wind turbine, the generator is controlled by power electronic equipment, which makes it possible to control the rotor speed. The power fluctuations caused by wind variations can be more or less absorbed by changing the rotor speed and thus power variation originating from the wind conversion and the drive train can be reduced. Hence, the power quality impact caused by the wind turbine can be improved as compared to a fixed-speed turbine. Another advantage is that variable-speed turbine also allows the grid voltage to be controlled, as the reactive generation can be varied. The rotational speed of a wind turbine is fairly low and must therefore be adjusted to the electrical frequency. The major drawbacks of variable speed systems are that the, built-in power electronics are sensitive to voltage dips caused by faults or switching.

Variable Speed WECS can further be divided into two configurations depending on the power rating of the system with respect to the power of the system. These are

- WECS with stator side converter
- WECS with both stator and rotor side converter

2.2.4.1 WECS with stator side converter

The performance of the wind energy system can be greatly enhanced with the use of a full-capacity power converter. The schematic, shown in Fig. 2.4, shows such a system in which the generator is connected to the grid via a full-capacity converter system. Squirrel cage induction generators, wound rotor synchronous generators, and permanent magnet synchronous generators (PMSG) have all found applications in this type of configuration with a power rating up to several megawatts. The power rating of the converter is normally the same as that of the generator. With the use of the power converter, the generator is fully decoupled from the grid, and can operate in full speed range. This also enables the system to perform reactive power compensation and smooth the grid connection. The main drawback is a more complex system with increased costs.

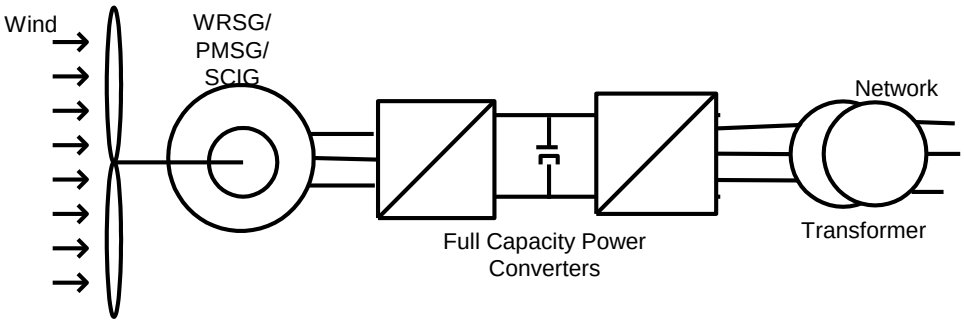

Fig. 2.4 Variable Speed Wind Turbine generator Configuration with Full-capacity power converter

2.2.4.2 WECS with both rotor and stator side converter

This system consist of a wind turbine with DFIG, as shown in Fig.2.5. This means that the stator is directly connected to the grid while the rotor winding is connected via slip rings toa a converter. This system have recently become very popular as generators for variable speed turbines. This is mainly due to the fact that the power electronic converter only has to handle a fraction of the total power. Therefore, the losses in the power

electronic converter can be reduced, compared to a system where the converter has to handle the total power and also the cost of converter is very low.

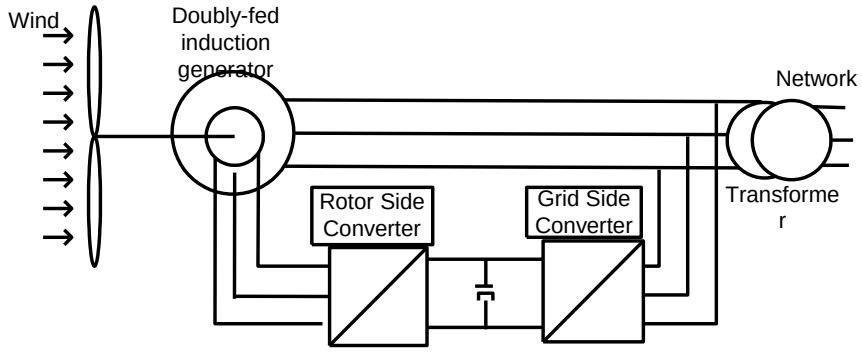

Fig. 2.5 Variable-speed wind turbine Generator With Reduced-Capacity Converter

2.3 WIND TURBINE MODEL AND CHARACTERISTICS

The mathematical modeling of wind turbine is explained along with the power characteristics, stall and pitch control of wind turbine.

2.3.1 Wind Turbine Modeling

The static characteristics of a wind turbine rotor can be described by the relationships between the total power in the wind and the mechanical power of the wind turbine. This relationship describes starting with the incoming wind in the rotor swept area. The kinetic energy of a cylinder of air of radius 'R' travelling at wind speed 'V_{wind}' corresponds to a total wind power 'P_{wind}' within the rotor swept area of the wind turbine. The 'P_{wind}' can be expressed as,

$$P_{wind} = 0.5\rho_{air}\pi R^2 \left(V_{wind}\right)^3 \tag{2.1}$$

Where, 'ρ_{air} is the air density (1.225 kg/m3), 'R' is the rotor radius and 'V_{wind}' is the wind speed. It is not possible to extract all the kinetic energy from the wind since this would mean that the air would stand still directly behind the wind turbine. This would not allow the air to flow away from the wind turbine, and clearly this cannot represent a physical steady-state condition. The wind speed is only reduced by the wind turbine, which thus extracts a fraction of the power in the wind. This fraction is expressed as the power efficiency coefficient, 'C_p', of the wind turbine. Therefore the mechanical power output of

the wind turbine 'P_{mech}' considering the definition of 'C_p' can be stated as given by

$$P_{mech} = C_p P_{wind} \tag{2.2}$$

Therefore, eq. 2.1 can be written as,

$$P_{mech} = 0.5 C_p \rho_{air} \pi R^2 \left(V_{wind}\right)^3 \tag{2.3}$$

It can be shown that the theoretical static upper limit of 'C_p' is approximately 0.59. This suggests that 59% of the maximum kinetic energy can be extracted from the wind. This 59% is known as Betz limit. A modern three bladed wind turbine has an optimal 'C_p' value in the range of 0.52-0.55 when measured at the hub of the turbine.

$$P_{mech} = f\left(\omega_{turb,}, V_{wind}, \beta\right) \tag{2.4}$$

From a physical point of view the power, 'P_{mech}' that is extracted from the wind will depend on rotational speed, wind speed and blade angle, 'β'. Therefore, 'P_{mech}' and 'C_p' are functions of these parameters.

The forces of the wind on a blade section and thereby the possible energy extraction will depend on the angle of incidence 'φ' between the plane of the moving rotor blades and the relative wind speed 'V_{rel}' as seen from the moving blades. Simple geometrical considerations are shown in Fig. 2.6. The wind turbulence created by the blade tips has been ignored and the angle of incidence 'φ' is determined by the incoming wind speed 'V_{wind}' and the speed of the blade. The blade tip is moving at speed 'V_{wind}', equal to (ω_{turb}*R). The highest values of 'C_p' are typically obtained for values in the range 8 to 9 (i.e. when the tip of the blade moves 8 to 9 times faster than the incoming wind). This means that the angle between the relative air speed from the blade tip and the rotor plane is rather a sharp angle.

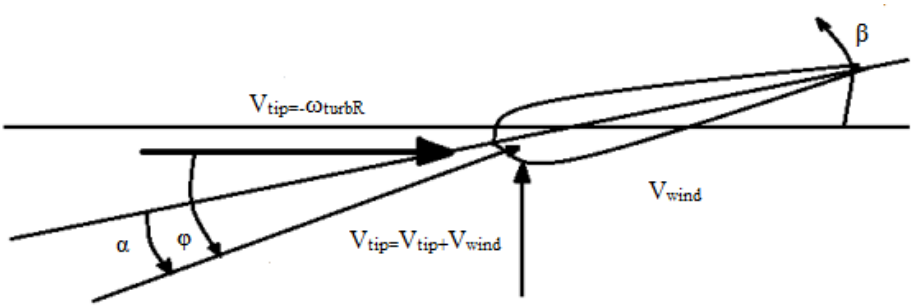

Fig. 2.6 Illustration of forces around the moving blade

Where, V_{tip} = tip speed; ω_{turb} = turbine rotational speed; R = rotor radius; V_{rel} = relative wind speed; V_{wind} = wind speed; α = angle of attack; φ = angle of incidence between the plane of the rotor and V_{rel}; β= blade angle.

On modern wind turbines, it is possible to adjust the pitch angle 'β' of the entire blade through a servo mechanism. If the blade is turned, the angle of attack 'α' between the blade and the relative wind 'V_{rel}' will be changed accordingly. Again, it is clear from a physical perspective that the forces of the relative wind on the blade, and thereby the energy extraction, will depend on the angle of attack 'α' between the moving rotor blades and the relative wind speed 'V_{rel}' as seen from the moving blades. Hence 'C_p' can be expressed as a function of 'λ' and 'β':

$$C_p = f(\lambda, \beta) \tag{2.5}$$

$$C_p(\lambda,\beta) = c_1\left(\frac{c_1}{\lambda_i} - c_1\beta - c_1\right)e^{\frac{-c_1}{\lambda_i}} + c_6\lambda \tag{2.6}$$

with

$$\frac{1}{\lambda_i} = \frac{1}{\lambda + 0.08\beta} - \frac{0.035}{\beta^3 + 1} \tag{2.7}$$

2.3.2 Power Characteristics of Wind Turbine

A typical power curve [91], as shown in Fig. 2.7, is characterized by three wind speeds: cut-in wind speed, rated wind speed, and cut-out wind speed. The 'P_m' is the mechanical power generated by the turbine and 'V_w' is the wind speed. The cut-in wind speed, as the name suggests, is the wind speed at which the turbine starts to operate and deliver power. The blade should be able to capture enough power to compensate for the

turbine power losses. The rated wind speed is the speed at which the system produces nominal power, which is also the rated output power of the generator. The cut-out wind speed is the highest wind speed at which the turbine is allowed to operate before it is shut down. For wind speeds above the cut-out speed, the turbine must be stopped, preventing damage from excessive wind.

As can be seen from Fig. 2.7, the wind turbine starts to capture power at the cut-in wind speed. The power captured by the blades, as expressed by eq. 2.3, is a cubic function of wind speed, until the wind speed reaches its rated value. To deliver captured power to the grid at different wind speeds, the wind generator should be properly controlled with variable speed operation when the wind speed increases beyond the rated speed.

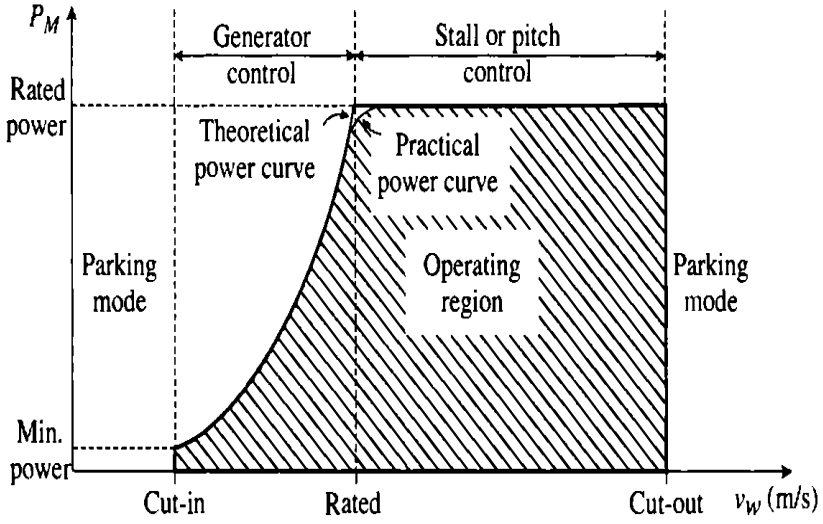

Fig. 2.7 The Operating Mode of Wind Turbine

2.3.3 Pitch and Stall Control of Wind Turbine

An effective control system should be designed to control the output power of wind turbine to maximize their output. In case of stronger winds it becomes necessary to waste part of the excess energy of the wind in order to avoid damaging the wind turbine. The wind turbines are designed to yield maximum output at wind speeds of 12-15 m/s because the probability of this speed of wind is very high. It is not economical to design turbines that maximize their output at stronger winds because such strong winds are rare. The pitch control and stall control are used in wind turbines.

The propellers pitch needs to be controlled whenever, the average of wind speed changes over a propeller. Commercial wind turbines are designed to produce optimum power with 11 m/s of wind speed. However, the wind speed always fluctuates up and down around this optimum. To generate the optimum power, the turbine blades have to adjust accordingly. This adjustment comes from turning the blades around their longitudinal axis (to pitch). When the wind speed decreases, the blade pitch is adjusted such that it exposes more surface area to the wind. Conversely, when wind speed picks up, the blade pitch is adjusted such that it exposes less surface area to the wind. If a blade is not designed for stall, increased wind speeds will force the rotor to turn faster without a pitch control mechanism. The pitch mechanism allows the wind to flow around the blade as smoothly as possible. To do this, air particles cannot hit the blade head on, rather they must flow almost tangent to the blade just as in an airplane's wing operating in the air.

The stall control of wind turbine works by increasing the angle at which the relative wind strikes the blades (angle of attack), and it reduces the induced drag (drag associated with lift). Stalling increases automatically when the winds speed up. The rotor blade has been aerodynamically designed to ensure that the moment wind speed becomes too high. Stalling creates turbulence on the side of the rotor blade not facing the wind. This stall prevents the lifting force of the rotor blade from acting on the rotor. A rotor blade for a stall controlled wind turbine is twisted slightly along its longitudinal axis. This is partly done in order to ensure that the rotor blade stalls gradually rather than abruptly when the wind speed reaches its critical value. The basic advantage of stall control is that one avoids moving parts in the rotor itself, and a complex control system.

CHAPTER - 3

MODELING AND OPERATION OF DOUBLY-FED INDUCTION GENERATOR

3.1 INTRODUCTION

The evolution of wind energy conversion technology gives rise to the development of different types of wind turbine configurations that make use of a variety of electric generators. The wound-rotor induction generator, also known as the doubly fed induction generator (DFIG), is one of the most commonly used and widely accepted generators in the wind energy industry. The DFIG is essentially a wound rotor induction generator in which the rotor circuit can be controlled by external devices to achieve variable speed operation. The stator of the generator is connected to the grid through a transformer, whereas the rotor connection to the grid is done through power converters and the harmonic filters.

The power rating for the DFIG is normally in the range of a few hundred kilowatts to several megawatts. The stator of the generator delivers power from the wind turbine to the grid and, therefore, the power flow is unidirectional. However, the power flow in the rotor circuit is bidirectional, depending on the operating conditions. The power can be delivered from the rotor to the grid and vice versa through rotor-side converter (RSCs) and grid-side converters (GSCs). Since the maximum rotor power is approximately 30% of the rated stator power, the power rating of the converters is substantially reduced in comparison to the WECS with full-capacity converters.

With variable speed operation, a DFIG wind energy system can harvest more energy from the wind than a fixed-speed WECS of the same capacity when the wind speed is below its rated value. The system can provide leading or lagging reactive power to the grid without additional devices. These features have made the DFIG wind energy system one of the preferred choices in the wind energy market.

3.2 OPERATION OF DFIG

The stator of DFIG is made of thin silicon steel laminations. The laminations are insulated to minimize iron losses caused by induced eddy currents. The laminations are basically flat rings with openings disposed along the inner perimeter of the ring. When the laminations are stacked together with the openings aligned, a canal is formed, in which a three-phase copper winding is placed.

The rotor of the DFIG has a three-phase winding similar to the stator winding. The rotor winding is embedded in the rotor laminations but in the exterior perimeter. This winding is usually fed through slip-rings mounted on the rotor shaft. In DFIG wind energy systems, the rotor winding is normally connected to a power converter system that makes the rotor speed adjustable, where the multiple coils in the stator and multiple bars in the rotor are grouped and represented by a single coil for each phase.

The Fig. 3.1 shows the basic scheme adopted in the WECS. The stator is directly connected to the AC mains, whilst the wound rotor is fed from the back-to-back IGBT voltage-source inverters with a common DC bus via slip rings to allow DFIG to operate at a variety of speeds in response to changing wind speed. Indeed, the basic concept is to interpose a frequency converter between the variable frequency induction generator and fixed frequency grid. The DC capacitor linking stator- and rotor-side converters allows the storage of power from induction generator for further generation. To achieve full control of grid current, the DC-link voltage must be boosted to a level higher than the amplitude of grid line-to-line voltage.

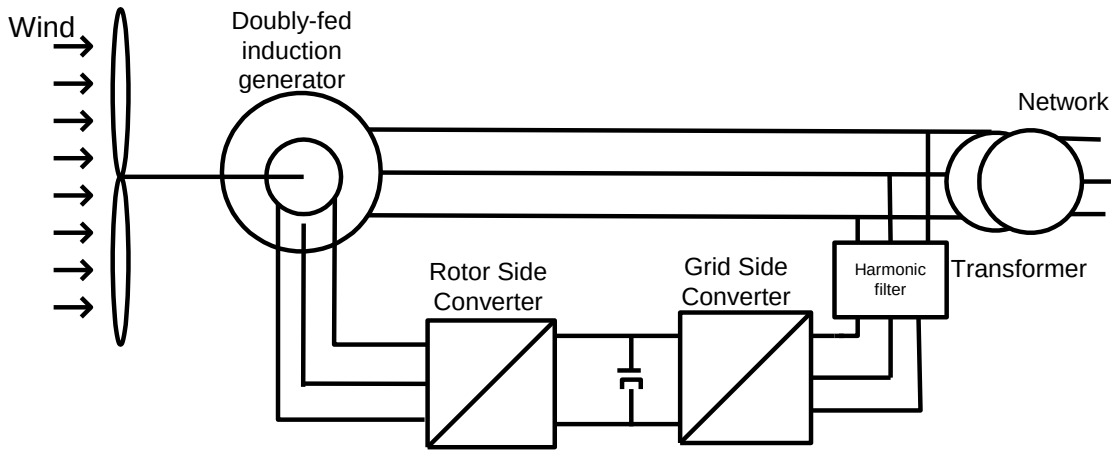

Fig.3.1. Grid Connection of DFIG

Depending on the rotor speed, there are two modes of operation of DFIG WECS; namely:

- Super-synchronous mode: The slip is negative in the super-synchronous
- Sub-synchronous mode: The slip is positive in sub-synchronous mode.

3.2.1 Super-Synchronous Mode

In the super-synchronous operation mode, as shown in Fig. 3.2 the mechanical power $|P_m|$ from the shaft is delivered to the grid through both stator and rotor circuits. The rotor power $|P_r|$ is transferred to the grid by power converters in the rotor circuit, whereas the stator power $|P_s|$ is delivered to the grid directly. Neglecting the losses in the generator and converters, the power delivered to the grid $|P_g|$ is the mechanical power $|P_m|$ of the generator, as illustrated in Fig. 3.2.

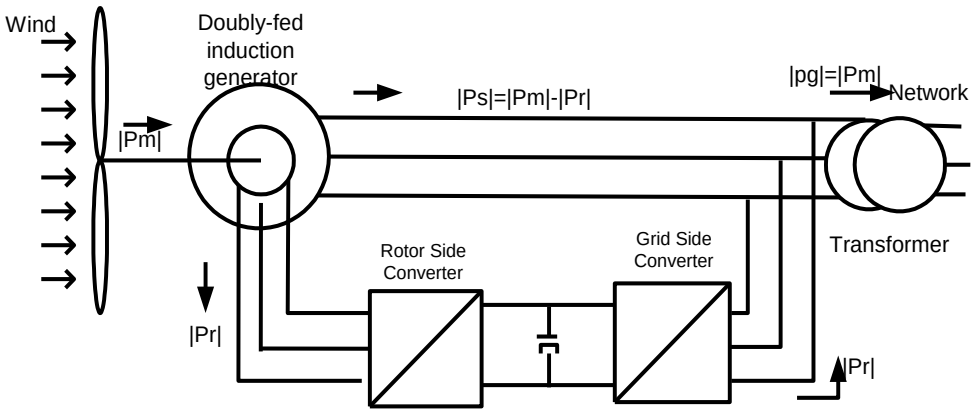

Fig. 3.2 Power flow in DFIG WECS under super-synchronous mode of operation

3.2.2 Sub Synchronous Mode

In sub-synchronous mode of operation, as shown in Fig. 3.3 the rotor receives the power from the grid. Both mechanical power $|P_m|$ and rotor power $|P_r|$ are delivered to the grid through the stator. Although the stator power $|P_S|$ is the sum of $|P_m|$ and $|P_r|$, it will not exceed its power rating since in the sub-synchronous mode the mechanical power $|P_m|$ from the generator shaft is lower than that in the super-synchronous mode. As in the previous case, neglecting the losses, the total power delivered to the grid $|P_g|$ is the input mechanical power $|P_m|$.

Since the DFIG generates high power when operating in the super-synchronous mode, the power rating for the converter is determined by the rated or maximum slip in the super-synchronous mode.

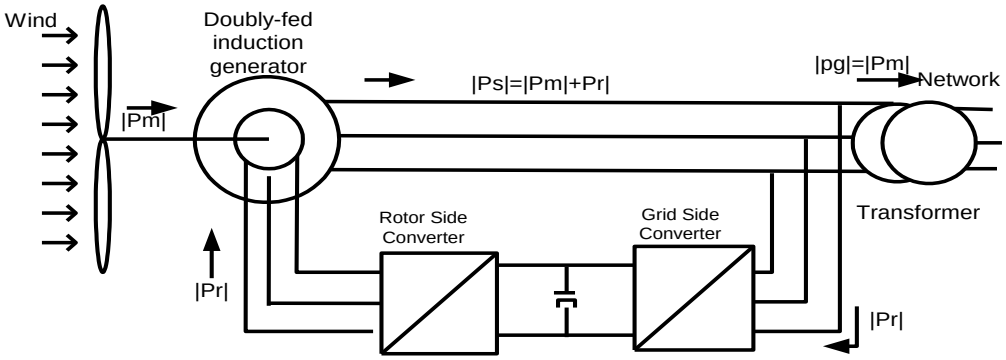

Fig. 3.3 Power flow in DFIG WECS under sub-synchronous mode of operation

The mechanical power and the stator electric power output are computed as

$$P_m = T_{em} * \omega_m \tag{3.1}$$

$$P_s = T_{em} * \omega_s \tag{3.2}$$

For a loss less generator the mechanical equation is:

$$J \frac{d\omega_r}{dx} = T_m - T_{em} \tag{3.3}$$

In steady-state at fixed speed for a loss less generator

$T_m = T_{em}$ and $P_m = P_s + P_r$

And it follows that:

$$P_r = P_m - P_s = T_m \omega_r - T_{em} \omega_s = -sP_s$$

Where,

$S = \frac{\omega_r - \omega_s}{\omega_s}$ is defined as the slip of the generator.

Generally the absolute value of slip is much lower than '1' and consequently, 'P_r'

is only a fraction of 'P_s'. Since 'T_m' is positive for power generation and since 'ω_s' is positive and constant for a constant frequency grid voltage, the sign of 'P_r' is a function of the slip sign. 'P_r' is positive for negative slip (speed greater than synchronous speed) and it is negative for positive slip (speed lower than synchronous speed). For super synchronous speed operation, 'P_r' is transmitted to DC bus capacitor and tends to rise the DC voltage. For sub-synchronous speed operation, 'P_r' is taken out of DC bus capacitor and tends to decrease the DC voltage. 'C_{grid}' is used to generate or absorb the power 'P_{gc}' in order to keep the DC voltage constant. In steady-state for a lossless AC/DC/AC converter 'P_{gc}' is equal to 'P_r' and the speed of the wind turbine is determined by the power 'P_r' absorbed or generated by 'C_{rotor}'. The phase-sequence of the AC voltage generated by 'C_{rotor}' is positive for sub-synchronous speed and negative for super synchronous speed. The frequency of this voltage is equal to the product of the grid frequency and the absolute value of the slip. 'C_{rotor}' and 'C_{grid}' have the capability for generating or absorbing reactive power and could be used to control the reactive power or the voltage at the grid terminals.

3.3 DYNAMIC MODEL OF INDUCTION MACHINE

There are two commonly used dynamic models for the induction generator. One is based on space vector theory and the other is the d-q axis model derived from the space vector model. The space vector model features compact mathematical expressions and a single equivalent circuit but requires complex (real and imaginary part) variables, whereas the dq-frame model is composed of two equivalent circuits, one for each axis. These models are closely related to each other and are equally valid for the analysis of transient and steady-state performance of the induction generator. But here only the reference frame theory and dq-frame model of induction machine is discussed.

3.3.1 Reference Frame Theory

The reference frame theory can be used to simplify the analysis of electric machines and also to facilitate the simulation and digital implementation of control schemes in wind energy conversion systems. A number of reference frames have been proposed over the years. There are three main transformations of interest in designing control strategies for DFIGs: stationary reference frame, synchronous reference frame, and rotor reference frame.

3.3.1.1 Stationary Reference Frame

The stationary reference frame can be thought of as projecting three-phase voltages (or currents) varying in time along the a, b, and c phase axes onto two-phase voltages varying in time along a pair of orthogonal axes d^s and q^s fixed on the stator.

We assume for convenience, without loss of generality, that the q^s axis is collinear with the a-phase axis, as shown in Fig.3.4.

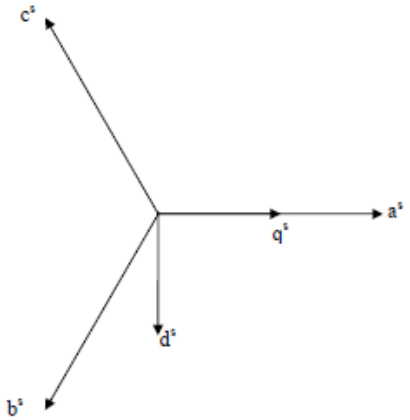

Fig.3.4 shows the collinearity of q^s axis with the a-phase axis

The transformation to the stationary reference frame is given by

$$\begin{bmatrix} v_q^s \\ v_d^s \\ v_0^s \end{bmatrix} = B \begin{bmatrix} 1 & 0 & 0 \\ 0 & \frac{-\sqrt{3}}{2} & 1 \\ \frac{1}{2} & \frac{1}{2} & \frac{1}{2} \end{bmatrix} \begin{bmatrix} v_a \\ v_b \\ v_c \end{bmatrix} \tag{3.4}$$

The transformation to the stationary reference frame is given by

The inverse transformation is given by

$$\begin{bmatrix} v_a \\ v_b \\ v_c \end{bmatrix} = \begin{bmatrix} 1 & 0 & 0 \\ \frac{-1}{2} & \frac{-\sqrt{3}}{2} & 1 \\ \frac{-1}{2} & \frac{\sqrt{3}}{2} & 1 \end{bmatrix} \begin{bmatrix} v_q^s \\ v_d^s \\ v_0^s \end{bmatrix} \tag{3.5}$$

This reference frame is useful for integrating the DFIG quantities with the power system network.

3.3.1.2 Synchronous Reference Frame

The synchronous reference frame corresponds to a rotating reference frame moving at synchronous speed, denoted by ω_e. The projection of q^s-d^s onto q^e-d^e is shown in the Fig. 3.5.

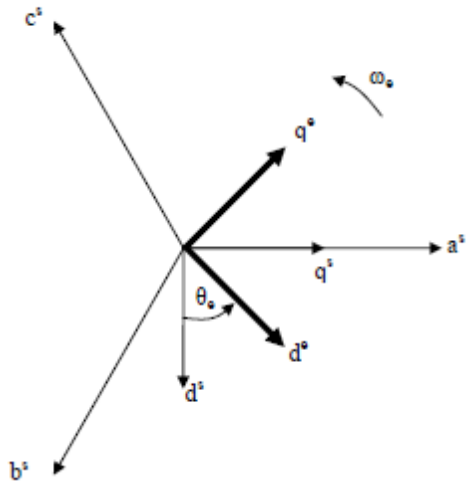

Fig.3.5 Projection of stationary reference to synchronous reference frame

Projection of a vector expressed in the stationary reference frame q^s-d^s into the synchronous reference frame q^e-d^e is obtained via

$$\begin{bmatrix} v_q^e \\ v_d^e \end{bmatrix} = \begin{bmatrix} \cos\theta_e & -\sin\theta_e \\ \sin\theta_e & \cos\theta_e \end{bmatrix} \begin{bmatrix} v_q^s \\ v_d^s \end{bmatrix} \tag{3.6}$$

The inverse transformation from the synchronous reference frame q^e-d^e to the stationary reference frame q^s-d^s is given by

$$\begin{bmatrix} v_q^s \\ v_d^s \end{bmatrix} = \begin{bmatrix} \cos\theta_e & \sin\theta_e \\ -\sin\theta_e & \cos\theta_e \end{bmatrix} \begin{bmatrix} v_q^e \\ v_d^e \end{bmatrix} \tag{3.7}$$

The inverse transformation from the synchronous reference frame q^e-d^e to the stationary reference frame q^s-d^s is given by (3.7)

3.3.1.3 Rotor Reference Frame

An important concept underlying the rotor reference frame is that in the induction machine, the rotor is also a three-phase system. Therefore, it too will have an a-phase axis. The rotor reference frame will maintain it's d-axis collinear with the axis of the rotor a phase. The speed of rotation of this reference frame is ωr. The projection of q^s-d^s onto q^r-d^r is shown in Fig. 3.6.

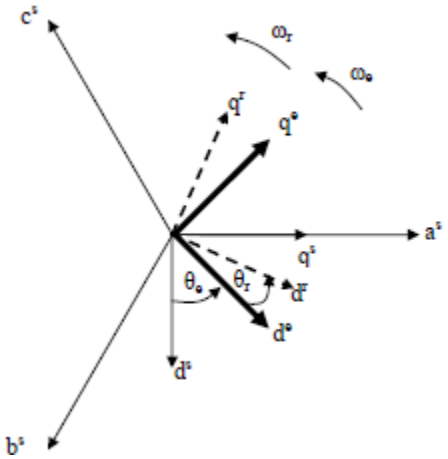

Fig.3.6 Projection of rotor reference to synchronous reference frame

Projection of a vector expressed in the stationary reference frame q^s-d^s into the rotor reference frame q^r-d^r is obtained via

$$\begin{bmatrix} v_q^r \\ v_d^r \end{bmatrix} = \begin{bmatrix} \cos(\theta_e + \theta_r) & -\sin(\theta_e + \theta_r) \\ \sin(\theta_e + \theta_r) & \cos(\theta_e + \theta_r) \end{bmatrix} \begin{bmatrix} v_q^e \\ v_d^e \end{bmatrix} \tag{3.8}$$

The inverse transformation from the synchronous reference frame q^e-d^e to the stationary reference frame q^s-d^s is given by

$$\begin{bmatrix} v_q^s \\ v_d^s \end{bmatrix} = \begin{bmatrix} \cos(\theta_e + \theta_r) & \sin(\theta_e + \theta_r) \\ -\sin(\theta_e + \theta_r) & \cos(\theta_e + \theta_r) \end{bmatrix} \begin{bmatrix} v_q^e \\ v_d^e \end{bmatrix} \tag{3 9}$$

We may also project from the synchronous rotor frame to the rotor reference frame according to:

$$\begin{bmatrix} v_q^r \\ v_d^r \end{bmatrix} = \begin{bmatrix} \cos\theta_r & -\sin\theta_r \\ \sin\theta_r & \cos\theta_r \end{bmatrix} \begin{bmatrix} v_q^e \\ v_d^e \end{bmatrix} \tag{3.10}$$

And the inverse transformation is

$$\begin{bmatrix} v_q^e \\ v_d^e \end{bmatrix} = \begin{bmatrix} \cos\theta_r & -\sin\theta_r \\ \sin\theta_r & \cos\theta_r \end{bmatrix} \begin{bmatrix} v_q^r \\ v_d^r \end{bmatrix} \tag{3.11}$$

3.3.2 D-Q model of induction machine

The asynchronous machine block operates in either generator or motor mode. The mode of operation is dictated by the sign of the mechanical torque:

- When T_m is positive, the machine acts as a motor.
- When T_m is negative, the machine acts as a generator.

The electrical part of the machine is represented by a fourth-order state-space model and the mechanical part by a second-order system. All electrical variables and parameters are referred to the stator. This is indicated by the prime signs in the machine equations given below. All stator and rotor quantities are in the arbitrary two-axis reference frame (dq-frame). The q-axis equivalent of induction machine is shown in Fig. 3.7(a) While, the d-axis equivalent of induction machine is given in Fig. 3.7(b).

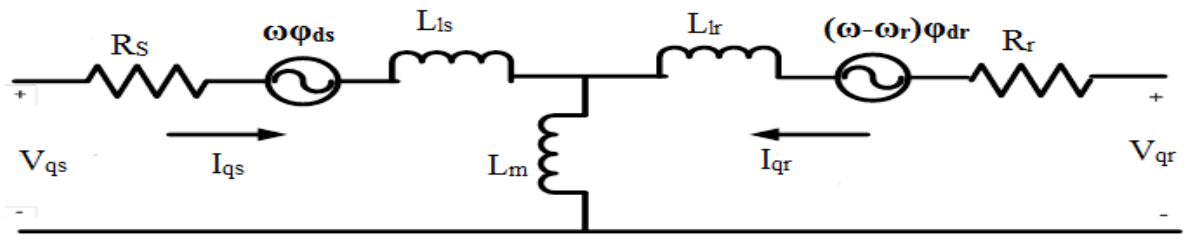

Fig.3.7a q-axis model of induction machine

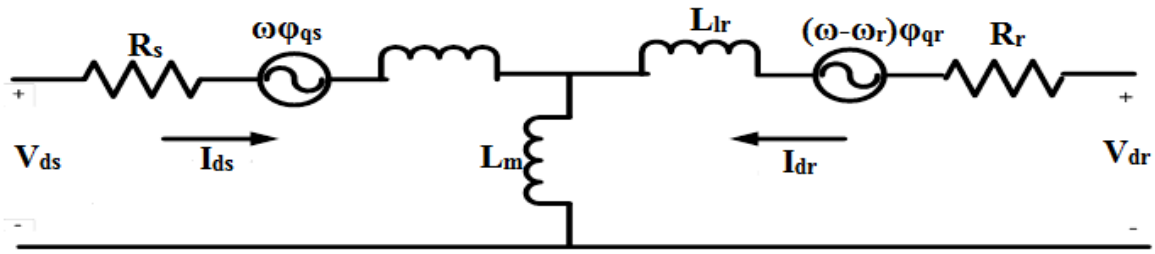

Fig.3.7b d-axis model of induction machine

The voltage equations, flux linkage relation and power-torque relations associated with d-q variables are expressed as-

1. **Voltage equations:**
   - Stator Voltage Equations:

$$V_{qs} = R_s i_{qs} + p\ \varphi_{qs} + \omega\varphi_{ds} \tag{3.12}$$

$$V_{ds} = R_s i_{ds} + p\ \varphi_{ds} - \omega_s\varphi_{qs} \tag{3.13}$$

   - Rotor Voltage Equations:

$$V_{qr} = R_r i_{qr} + p\ \varphi_{qr} + (\omega - \omega_r)\ \varphi_{dr} \tag{3.14}$$

$$V_{dr} = R_r i_{dr} + p\ \varphi_{dr} + (\omega - \omega_r)\varphi_{qr} \tag{3.15}$$

2. **Flux Linkage Equations:**
   - Stator Flux Equations:

$$\varphi_{qs} = (L_{ls} + L_m)\ i_{qs} + L_m i_{qr} \tag{3.16}$$

$$\varphi_{ds} = (L_{ls} + L_m)\ i_{ds} + L_m i_{dr} \tag{3.17}$$

   - Rotor Flux Equations:

$$\varphi_{qr} = (L_{lr} + L_m)\ i_{qr} + L_m i_{qs} \tag{3.18}$$

$$\varphi_{dr} = (L_{ls} + L_m)\ i_{dr} + L_m i_{ds} \tag{3.19}$$

3. **Power and Torque Equations:**

All the equations above are induction motor equations. When the induction motor operates as a generator, current direction will be opposite. Assuming negligible power losses in stator and rotor resistances, the active and reactive power outputs from stator and rotor side are given as:

$$P_s = -3/2\left(V_{ds} i_{ds} + V_{qs} i_s\right) \tag{3.20}$$

$$Q_s = -3/2\left(V_{qs} i_{ds} - V_{ds} i_{qs}\right) \tag{3.21}$$

$$P_r = -3/2\left(V_{dr} i_{dr} + V_{qr} i_r\right) \tag{3.22}$$

$$Q_s = -3/2\left(V_{qr} i_{dr} - V_{dr} i_{qr}\right) \tag{3.23}$$

The total active and reactive power generated by DFIG is:

$$P_{Total} = P_s + P_r \tag{3.24}$$

$$Q_{Total} = Q_s + Q_r \tag{3.25}$$

If 'P_{Total}' and 'Q_{Total}' are positive, DFIG is supplying power to the power grid, else it is drawing power from the grid. Total 'P' Total 'Q'. In the induction machine, the electromagnetic torque is developed by the interaction of air-gap flux and the rotor magneto-motive force (MMF). At synchronous speed, the rotor cannot see the moving magnetic field; as a result, there is no question of induced EMF as well as the rotor current, so the torque becomes zero. But at any speed other than synchronous speed, the machine will experience torque. That is true in case of motor, where as in case of wind turbine generator; electromechanical torque is provided by means of prime mover which is wind turbine in DFIG-based WECS.

The rotor speed dynamics of the DFIG is given as:

$$\frac{d}{dt}\omega_r = \frac{P}{2J}(T_m - T_e - F\omega_r) \tag{3.26}$$

where P is the number of poles of the machine, is friction coefficient, J is inertia of the rotor, Tm is the mechanical torque generated by wind turbine, and Te is the electromagnetic torque generated by the machine which can be written in terms of flux linkages and currents as follows:

$$T_e = -3/2\left(\varphi_{qs} i_{ds} - \varphi_{ds} i_{qs}\right) \tag{3.27}$$

Where, negative (positive) values of Te means DFIG works as a generator (motor).

CHAPTER - 4

POWER CONVERTER CONTROL AND DESIGN

4.1 INTRODUCTION

Power Converters are widely used in wind energy conversion systems (WECS). The schematic of back-to-back PWM converter is shown in Fig. 4.1. In fixed-speed WECS, the converters help to reduce inrush current and torque oscillations during the system start-up, whereas in variable-speed WECS they control the speed/torque of the generator and also the active/reactive power to the grid. According to the system power ratings and type of wind turbines, a variety of power converter configurations are available for the optimal control of wind energy systems. Their models are categorized into two groups: Mathematical functional models and Mathematical physical models.

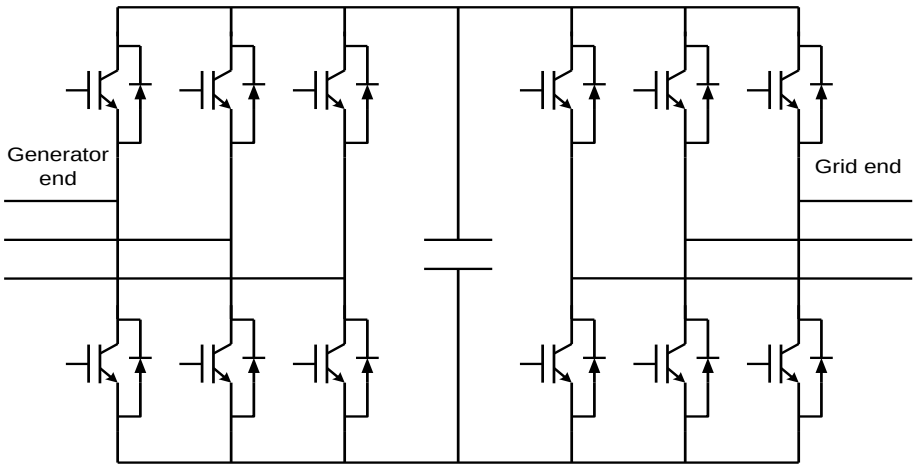

Fig.4.1 Back-to-Back PWM structure

Functional model express the relationship between the input and output signal of the system in form of mathematical function(s) and therefore constituting elements of the system are not modeled separately. Simplicity and fast time-domain simulation are the main advantages of this mathematical function(s) modeling, however it may lose accuracy. In this it is assumed that the converters are ideal and the DC-link voltage between them is constant. Consequently, depending on the converter control, a controllable voltage or current source can be implemented to represent the operation of the rotor-side of the converter in the model.

Physical model, on the other hand, models constituting elements of the system separately and also considers inter-relationship among different elements within the system, where type and structure of the model is normally dictated by the particular requirements of the analysis, e.g. steady-state, fault studies, etc. Indeed, Due to the importance of more realistic production of the behavior of DFIG, it is intended to adopt physical model rather than functional model in order to accurately assess performance of DFIG. In this the physical model is implemented.

4.1.1 Rotor Side Converter

The rotor-side converter (RSC), as illustrated in Fig. 4.2, applies the voltage to the rotor windings of the doubly-fed induction generator. The purpose of the rotor-side converter is to control the rotor currents such that the rotor flux position is optimally oriented with respect to the stator flux to develop desired torque the shaft of the machine. The rotor-side converter uses a torque controller to regulate the wind turbine output power and the voltage (or reactive power) measured at the machine stator terminals. The power is controlled in order to follow a pre-defined turbine power-speed characteristic to track the maximum power point. The actual electrical output power from the generator terminals, added to the total power losses (mechanical and electrical) is compared with the reference power obtained from the wind turbine characteristic.

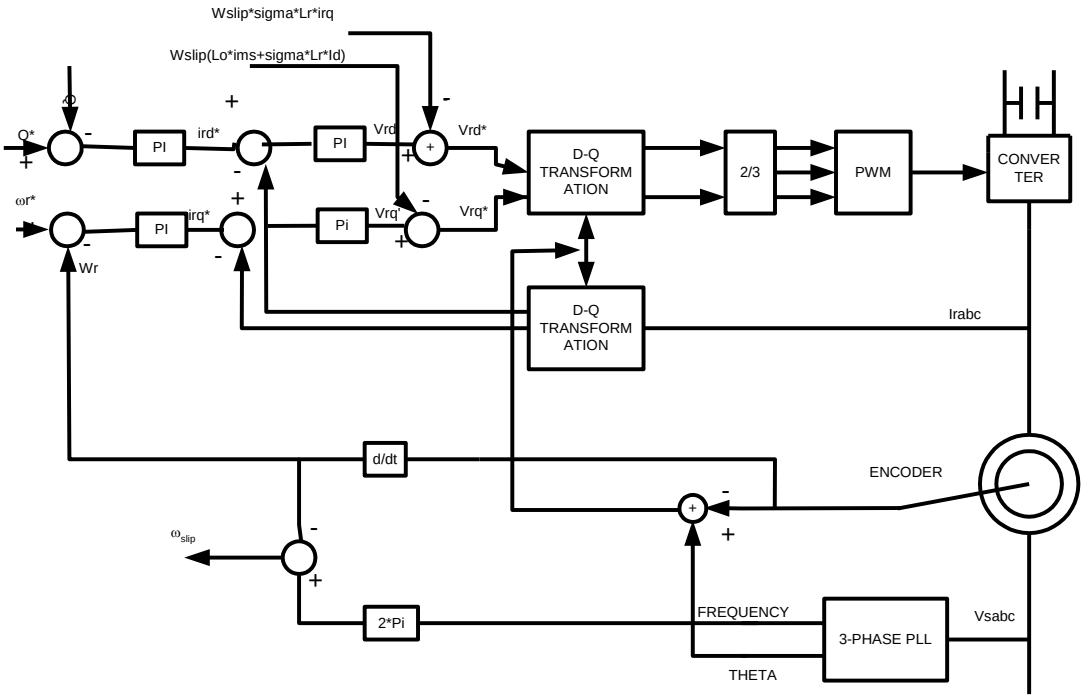

Fig.4.2 Rotor Side Converter Control Scheme

Usually, a Proportional-Integral (PI) regulator is used at the outer control loop to reduce the power error (or rotor speed error) to zero. The output of this regulator is the reference rotor current 'i_{qr_ref}' that must be injected in the rotor winding by rotor-side converter. This *q*-axis component controls the electromagnetic torque 'T_e'. The actual 'i_{qr}' component of rotor current is compared with 'i_{qr_ref}' and the error is reduced to zero by a current PI regulator at the inner control loop. The output of this current controller is the voltage 'v_{qr}' generated by the rotor-side converter. With another similarly regulated 'i_{dr}' and 'v_{dr}' component the required 3-phase voltages applied to the rotor winding are obtained.

4.1.2 Grid Side Converter

The grid-side converter, as illustrated in Fig.4.3, aims to regulate the voltage of the dc bus capacitor. Moreover, it is allowed to generate or absorb reactive power for voltage support requirements. The function is realized with two control loops as well: an outer regulation loop consisting of a dc voltage regulator. The output of the dc voltage regulator is the reference current 'i_{dc_ref}' for the current regulator. The inner current regulation loop consists of a current regulator controlling the magnitude and phase of the voltage generated by converter from the 'i_{dc_ref}' produced by the dc voltage regulator and specified *q*-axis 'i_{qc_ref}' reference.

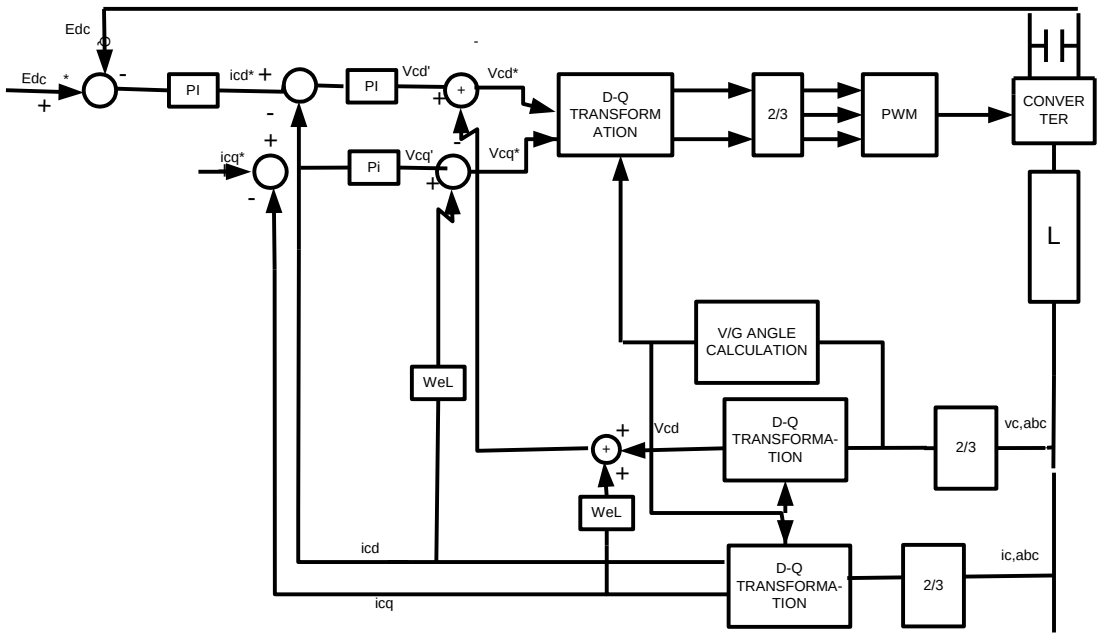

Fig.4.3 Grid side converter control scheme

4.1.3 Converter Losses

The losses of the converters can be divided into switching losses and conducting losses. The switching losses of the transistors are the turn-on and turn-off losses. For the diode the switching losses mainly consist of turn-off losses, i.e., reverse-recovery energy. The turn-on and turn-off losses for the transistor and the reverse-recovery energy loss for a diode can be found from data sheets. The conducting losses arise from the current through the transistors and diodes. The transistor and the diode can be modeled as constant voltage drops, and a resistance in series. The switching losses of the transistor can be considered to be proportional to the current, for a given dc-link voltage. For a given dc-link voltage and switching frequency, the switching losses of the IGBT and diode can be modeled as a constant voltage drop that is independent of the current rating of the valves. DC link model

The dc-link model describes the dc-link capacitor voltage variations as a function of the input power to the dc-link. The energy stored in the dc capacitor is:

$$W_{dc} = \int P_{dc} dt = \frac{1}{2} C V_{dc}^2 \tag{4.1}$$

Where C is the capacitance, V_{dc} is the voltage, W_{dc} is the stored energy, and P_{dc} is the input

power to the dc link. The voltage and energy derivatives are

$$\frac{dV_{dc}}{dt} = \frac{P_{dc}}{CV_{dc}}, \frac{dW_{dc}}{dt} = P_{dc} \tag{4.2}$$

The 'P_{dc}' is calculated as $P_{dc} = P_{in} - P_c$. Where *Pin* is the input power from rotor-side converter and P_c is the grid-side converter output power. The dc-link voltage varies as 'P_{dc}' and is a constant when $P_{dc} = 0$.

4.2 CONVERTER CONTROL SYSTEM

A voltage-source, current controlled PWM converter is used in the DFIG system. The main task of the current controlled PWM converter is to force the current to follow their reference signals. By comparing desired and actual values of the phase currents, the current controller generates the switching states for converter which decreases the current

errors. There are various ways to obtain the switching signals for the inverter switches in order to control the inverter output current. The simplest is hysteresis control, where the actual current is compared to the desired current in each phase leg of the converter output. Sinusoidal Pulse Width Modulation (SPWM) method is adopted, which is based on a triangular carrier signal. By comparison of the common carrier signal with three reference sinusoidal signals the switching instants of the IGBTs are obtained. In order to maintain the switching frequency within the switch-mode converter constant, it is a best to calculate the required rotor voltages that the converter must supply to the machine, making the rotor currents equal to their reference values. The control of generator and converter can be explained as by using, the vector-control technique for the independent control of torque and rotor excitation current in the DFIG and decouple control of the active and reactive power supplied to the grid.

4.2.1 Rotor side control scheme

The rotor-side converter (RSC) provides the excitation for the induction machine rotor. With this PWM converter, it is possible to control the torque and the speed of the DFIG and also the power factor at the stator terminals. The rotor-side converter provides a varying excitation frequency depending on the wind speed conditions. The induction machine is controlled in a synchronously rotating *dq*-axis frame, with the *d*-axis oriented along the stator-flux vector position in one common implementation. This is called stator-flux orientation (SFO) vector control. In this way, a decoupled control between the electrical torque and the rotor excitation current is obtained. Consequently, the active power and reactive power are controlled independently from each other. The control scheme of the rotor-side converter is organized in a generic way with two series of two PI-controllers. Fig 4.2 shows a schematic block diagram for the rotor-side converter control. The reference *q*-axis rotor current i_{qr}^{*} can be obtained either from an outer speed control loop or from a reference torque imposed on the machine. These two options may be termed a speed-control mode or torque-control mode for the generator, instead of regulating the active power directly. For speed-control mode, one outer PI controller is to control the speed error signal in terms of maximum power point tracking. Furthermore, another PI controller is added to produce the reference signal of the *d*-axis rotor current component to control the reactive power required from the generator. Assuming that all reactive power to the machine is supplied by the stator, the reference value i_{dr}^{*} may set to

zero. The switching dynamics of the IGBT-switches of the rotor converter are neglected and it is assumed that the rotor converter is able to follow demand values at any time.

The control system requires the measurement of the stator and rotor currents, stator voltage and the mechanical rotor position. There is no need to know the rotor-induced EMF, as is the case for the implementation with naturally commutated converters. Since the stator is connected to the grid, and the influence of the stator resistance is small, the stator magnetizing current 'i_{ms}' can be considered constant.

Rotor excitation current control is realized by controlling rotor voltage. The 'i_{dr}' and 'i_{qr}' error signals are processed by associated PI controllers to give 'v_{dr}' and 'v_{qr}', respectively.

Aligning the d-axis of reference frame to be along the stator flux linkage (stator flux oriented control) will result in:

$$\phi_{qs}^{e} = 0 \tag{4.3}$$

And hence from eq. (3.16):

$$i_{qs}^{e} = \frac{-L_m}{L_{ls} + L_m} i_{qr}^{e} \tag{4.4}$$

Substituting for i^{e}_{qs} into eq. (3.27) will result in:

$$T_e = -\frac{3}{2} P \frac{L_m}{L_{ls} + L_m} \phi_{qs}^{e} i_{qr}^{e} \tag{4.5}$$

For 'φ_{ds}' to remain unchanged at zero, '$p\varphi_{ds}$' must be zero. Substituting for '$p\varphi_{ds}$' using

The equation (3.12) and (3.13) will result in $V_{ds}^{e} = r_s i_{ds}^{e}$ Neglecting stator resistance will lead to

V_{ds}^{e}= 0. Substituting for V_{ds}^{e}= 0, eqs. (3.20) and (3.21) will be simplified as follows:

$$P_s^{e} = \frac{3}{2}(\mathrm{V}_{qs}^{e}\, i_{qs}^{e}) \tag{4.6}$$

$$Q_s^e = \frac{3}{2}(\mathrm{V}_{qs}^e\, i_{ds}^e) \tag{4.7}$$

Therefore, the above equati11ons show that active and reactive powers of the stator can be controlled independently.

4.2.2 Decoupling Control scheme

Using stator flux oriented approach with current controlled PWM inverter requires decoupling scheme. In fact, the system is coupled because the inductance matrix is not diagonal. It means that any changes on voltage component in d or q axes results in changes in both current components. In order to combat this problem, equations will be redeveloped in order to compensate for these cross coupling between d and q axes. The leakage factor of the induction machine can be defined as:

Substituting for i_{ds}^e from eq. (3.17) into eq. (3.19) for λ_{ds}^e and from eq. (4.4) into eq. (3.18)

$$\sigma = 1 - \frac{L_m^2}{(L_{ls} + L_m)(L_{lr} + L_m)} \tag{4.8}$$

$$\phi_{dr}^e = \sigma(L_{lr} + L_m) i_{dr}^e + \frac{-L_m}{L_{ls} + L_m} \phi_{ds}^e \tag{4.9}$$

$$\phi_{qr}^e = \sigma(L_{lr} + L_m) i_{qr}^e \tag{4.10}$$

Substituting above equations into eq. (3.14) and (3.15) for V_{dr}^e and V_{dr}^e

$$V_{dr}^e = V_{dr}^{'e} + V_{dr,comp}^e \tag{4.11}$$

$$V_{qr}^e = V_{qr}^{'e} + V_{qr,comp}^e \tag{4.12}$$

Where,

$$V_{dr}^{'e} = r_r i_{dr}^e + \sigma(L_{lr} + L_m)\,\mathrm{p}\, i_{dr}^e \tag{4.13}$$

$$V_{qr}^{'e} = r_r i_{qr}^e + \sigma(L_{lr} + L_m)\,\mathrm{p}\, i_{qr}^e \tag{4.14}$$

$$V^e_{dr,comp} = \frac{-L_m}{L_{ls}+L_m} p i^e_{ds} - (\omega_e - \omega_r)\sigma(L_{lr}+L_m) i^e_{qr} \tag{4.15}$$

$$V^e_{qr,comp} = (\omega_e - \omega_r)\frac{L_m}{L_{ls}+L_m} \phi^e_{ds} - (\omega_e - \omega_r)\sigma(L_{lr}+L_m) i^e_{dr} \tag{4.16}$$

Adding these compensating terms to the corresponding uncompensated voltage terms makes it possible to achieve decoupled performance of the stator flux-oriented control of the rotor-side converter.

4.2.3 Grid side control scheme

The grid-side converter controls the flow of real and reactive power to the grid, through the grid interfacing inductance. The objective of the grid-side converter is to keep the dc-link voltage constant regardless of the magnitude and direction of the rotor power. The vector control method is used as well, with a reference frame oriented along the stator voltage vector position, enabling independent control of the active and reactive power flowing between the grid and the converter. The PWM converter is current regulated, with the *d*-axis current used to regulate the dc-link voltage and the *q*-axis current component to regulate the reactive power. Fig. 4.3 shows the schematic control structure of the grid-side converter.

A similar analysis for the control of the dq currents carried out for the grid-side converter can likewise be done for the control of the converter dq currents.

The d-axis of the reference frame is aligned with the grid voltage angular position θ_e. Since the amplitude of the grid voltage is constant, v_{q_grid} is zero and v_{d_grid} is constant. The active and reactive power will be proportional to i_{q_grid} and i_{d_grid} respectively

So, the real and active powers from the grid-side converter are controlled by i_{d_grid} and i_{q_grid} components of current respectively.

The reference voltage $V^*_{d\_grid}$ and $V^*_{q\_grid}$ are then transformed by inverse-Park transformation to give 3-phase voltage $V^*_{abc\_grid}$ for the final PWM signal generation for the converter IGBT switching.

Based on the grid integration of DFIG, taking in to account the filter connected to the grid, the voltage across the inductor is given by:

$$\begin{bmatrix} V_{as} \\ V_{bs} \\ V_{cs} \end{bmatrix} = R \begin{bmatrix} i_{as} \\ i_{bs} \\ i_{cs} \end{bmatrix} + Lp \begin{bmatrix} i_{as} \\ i_{bs} \\ i_{cs} \end{bmatrix} + \begin{bmatrix} V_{a1} \\ V_{b1} \\ V_{c1} \end{bmatrix} \tag{4.17}$$

Applying phase and rotation transformations to the above equation results in:

$$V_{ds}^{e} = Ri_{ds}^{e} + Lpi_{ds}^{e} - \omega_e Li_{qs}^{e} + V_{dl}^{e} \tag{4.18}$$

$$V_{qs}^{e} = Ri_{qs}^{e} + Lpi_{qs}^{e} - \omega_e Li_{ds}^{e} + V_{ql}^{e} \tag{4.19}$$

Therefore, reference values for front-end converter can be written as:

$$V_{dl}^{ref,e} = -Ri_{ds}^{e} + Lpi_{ds}^{e} + \omega_e Li_{qs}^{e} \tag{4.20}$$

$$V_{ql}^{ref,e} = -Ri_{qs}^{e} + Lpi_{qs}^{e} + (\omega_e Li_{ds}^{e} - V_{qs}^{e}) \tag{4.21}$$

Where, the term in bracket represents the decoupling terms. Neglecting harmonics, the capacitor leakages and losses in the inductor resistance and converter itself.

$$Ei_{os} = \frac{3}{2} V_{qs}^{e} i_{qs}^{e} \tag{4.22}$$

$$V_{qs}^{e} = \frac{M_1 E}{2\sqrt{2}} \tag{4.23}$$

$$i_{os} = \frac{3}{4\sqrt{2}} M_1 i_{qs}^{e} \tag{4.24}$$

$$CPE = i_{os} - i_{or} \tag{4.25}$$

Assuming rotor-side converter DC-link current as disturbance and combining eqs. (4.24) and (4.25)

$$E = \frac{3}{4\sqrt{2}} M_1 i_{os} \tag{4.26}$$

4.3 CONTROLLER DESIGN

The tuning of PI controllers in this control scheme is done by using the Internal Model Control (IMC) technique.

The idea behind IMC is to augment the error between system, G(S), and the model of the system, $G\hat{}\,(s)$, by a transfer function C(S). For a first-order system the controller is an ordinary PI controller which can be represented as follows:

$$F(s) = K_p + \frac{K_i}{s} = \frac{\alpha}{s}\hat{G}(s) \tag{4.27}$$

Where, $G\hat{}\,(s)$ is the transfer function of the system.

4.3.1 Grid side Current control loop

In simplified design the small time constants such as power converter dead time, feedback filter and digital signal processing delay are neglected. Thus, only the dynamics of supply-side filter is taken into account. Fig.4.4 shows the current-control loop of stator-side converter. Based on Eqs.(4.20) and (4.21) and considering compensation terms as disturbance, the plant for the current control loop is given by:

$$\hat{G}(\mathrm{s}) = \frac{i_{ds}^{e}(\mathrm{s})}{(\mathrm{R}+\mathrm{Ls})i_{ds}^{e}(\mathrm{s})} = \frac{1}{(\mathrm{R}+\mathrm{Ls})} \tag{4.28}$$

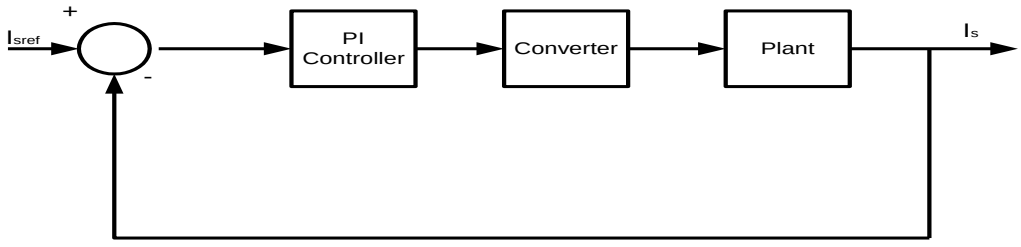

Fig.4.4 Current control loop of stator side converter

Given converter model as:

$$k_{cs} = \frac{M_1 E}{2V_{tri}} \tag{4.29}$$

And substituting for eq. (4.25)

$$k_p = \frac{\alpha_{cs} L}{k_{cs}} \tag{4.30}$$

$$k_i = \frac{\alpha_{cs} R}{k_{cs}} \tag{4.31}$$

4.3.2 DC link voltage control loop

The DC link voltage control loop is shown in Fig. 4.5.

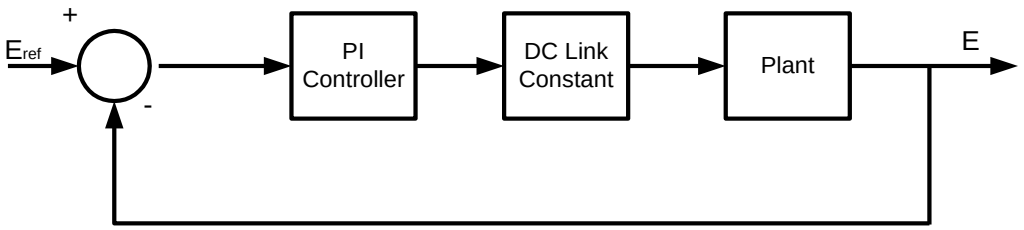

Fig.4.5 DC link voltage control loop

The plant transfer function is expressed as:

$$E = \frac{3}{4\sqrt{2}} M_1 i_{os} \tag{4.32}$$

$$\hat{G}(s) = \frac{1}{Cs} \tag{4.33}$$

And substituting for eq. (4.26) leads to

$$k_p = \frac{4\sqrt{2}\alpha_g C}{3M_1} \tag{4.44}$$

There will be a remaining error when the induction machine is loaded and active power flows between DC-link and the machine. The remaining error can be eliminated by adding an integrator to the DC-link voltage controller. The following is often adopted for the selection of the controller integration time:

4.3.3 Rotor side current control loop

As mentioned previously, in order to keep the switching frequency constant, it is necessary to calculate the required rotor voltages. The i_{qr} and i_{dr} errors are processed by the

PI controller to give V_{qr} and V_{dr}, respectively. Using eq. (4.18) and (4.19), the plant can be represented by transfer functions below:

$$i_{dr}^{e} = \frac{1}{r_r + \sigma(L_{lr} + L_m)} V_{dr}^{'e}(\mathrm{s}) \tag{4.47}$$

$$i_{qr}^{e} = \frac{1}{r_r + \sigma(L_{lr} + L_m)} V_{qr}^{'e}(\mathrm{s}) \tag{4.48}$$

Therefore, the transfer function of the Plant is given by:

$$\hat{G}(\mathrm{s}) = \frac{1}{r_r + \sigma(L_{lr} + L_m)} \tag{4.49}$$

Incorporating dynamics of PWM converter makes the block diagram as shown in Fig.4.6.Where converter can be represented as:

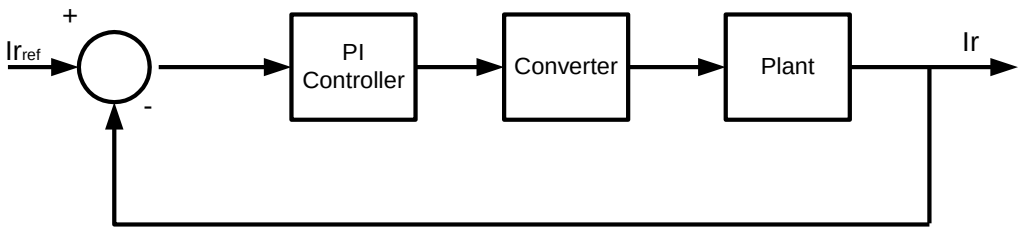

Fig.4.6 Current-control of rotor side current

$$k_{cr} = \frac{M_2 E}{2V_{tri}} \tag{4.50}$$

This will determine control parameters as follows:

$$k_p = \frac{\alpha_{cr}\sigma(L_{lr} + L_m)}{k_{cr}} \tag{4.51}$$

$$k_i = \frac{\alpha_{cr} r_r}{k_{cr}} \tag{4.52}$$

4.3.4 Speed control loop

Assuming single-mass representation of the mechanical drive train and using Fig.4.7, plant transfer function for speed controller is given by:

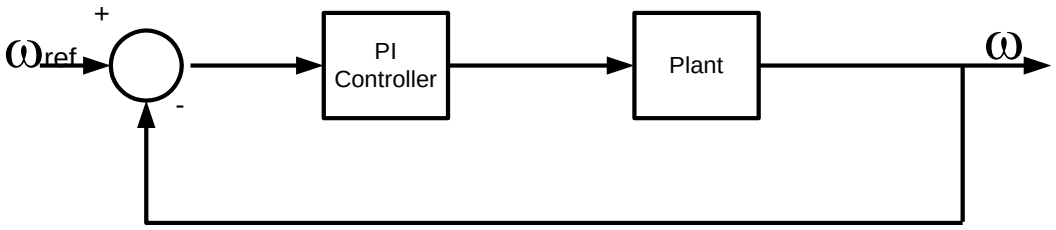

Fig..4.7 Speed control loop of DFIG

$$\hat{G}(s) = \frac{1}{JS + D} \tag{4.53}$$

$$k_{p\omega} = \frac{\alpha_{\omega} JP}{2} \tag{4.54}$$

$$k_{\omega} = \alpha_{\omega} D \tag{4.55}$$

CHAPTER - 5

SIMULATION AND RESULTS

5.1 SYSTEM MODEL

The doubly fed induction generator based wind turbine is directly connected through its stator circuit to the grid and the rotor is connected to the grid via transformer to the converter operating as rectifier. The obtained dc output is connected to converter operating as inverter to yield ac. The controls for both the rectifier and inverter converters is applied. The filters are used to remove the ripples present in the ac voltage. Wind turbines driven doubly-fed induction generator (DFIG) consist of a wound rotor induction generator and an AC/DC/AC IGBT-based PWM converter. The stator winding is connected directly to the 60 Hz grid while the rotor is fed at variable frequency through the AC/DC/AC converter as shown in Fig.5.1. This arrangement of DFIG control allows extracting maximum energy from the wind for low wind speeds by optimizing the turbine speed, while minimizing mechanical stresses on the turbine during gusts of wind.

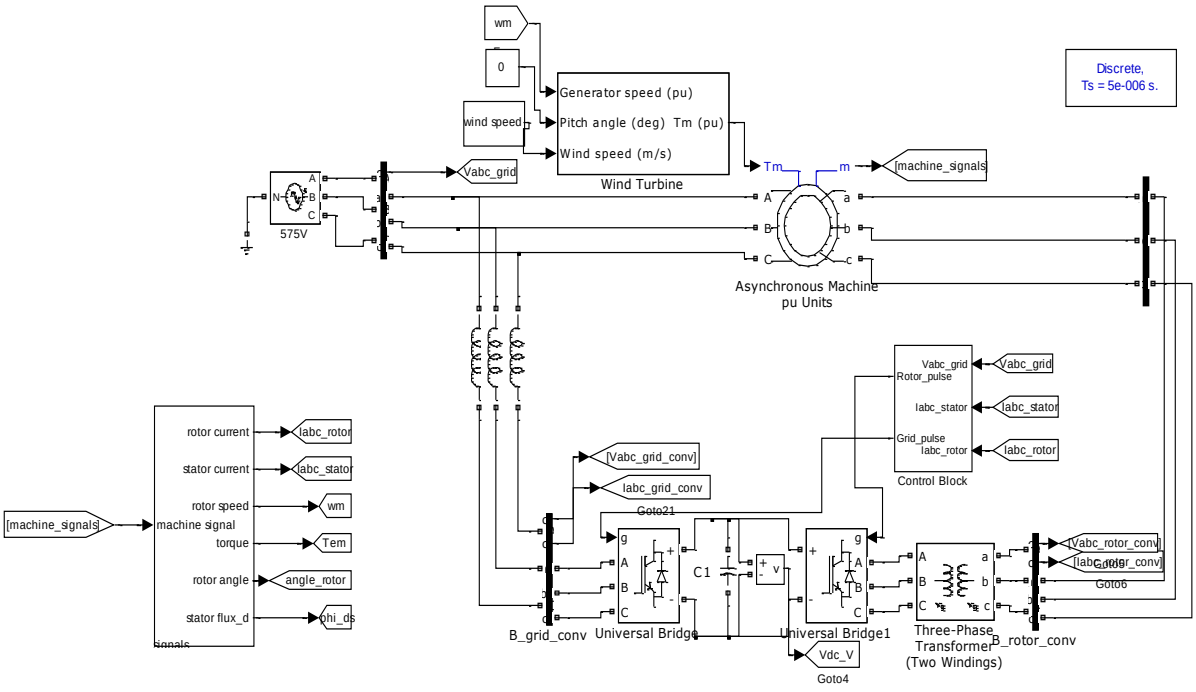

Fig 5.1 System Model of DFIG Grid Integration

The system is modelled in SIMULINK and sub-blocks are discussed. They are-

- **Induction Generator Model**
- **Converter Control Model**
- **Wind turbine Model**

5.1.1 Induction Generator Model

The electrical part of the machine is represented by a fourth-order state-space model and the mechanical part by a second-order system The model of induction generator is shown in Fig. 5.2. The electrical variables and parameters are referred to the stator. All stator and rotor quantities are in the arbitrary d-q axis reference frame (dq frame).

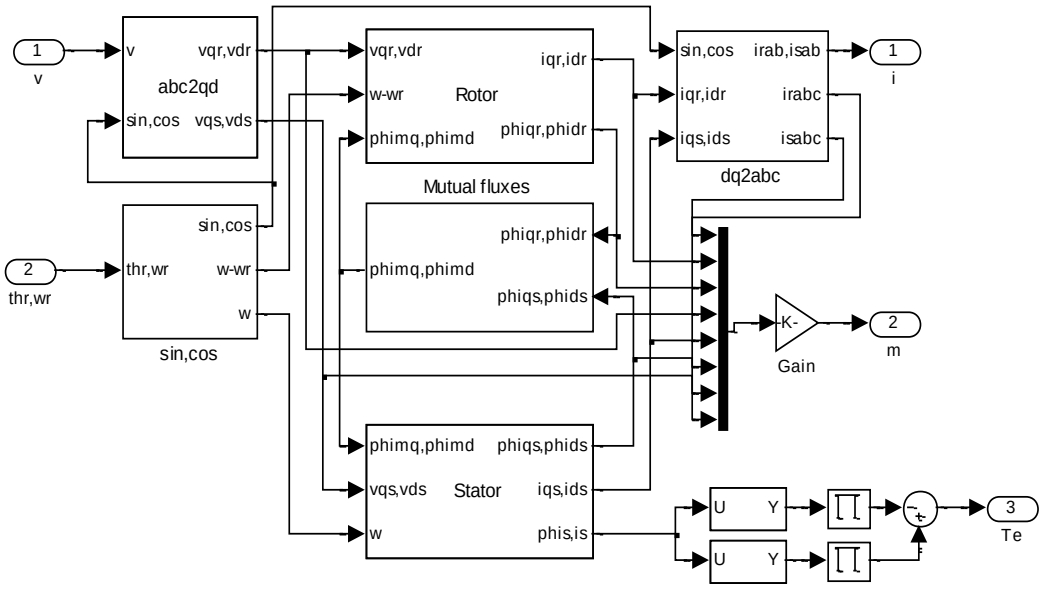

Fig.5.2 Model of Induction Generator

The electrical model suggests that the stator and rotor fluxes are obtained using the numerical integration from eq. (3.16)-(3.19). However, the stator and rotor currents are obtained using the computed fluxes and the inductance parameters. Further, the above model is a d-q variable model and therefore the outcome will be d-q axes fluxes and currents. For the clarity, the dq variables are to be converted back into the phase variables. For computing the fluxes the stator and rotor voltages, which are the input, are to be represented into the d-q variables. Therefore, the implementation is carried out using the following steps:

Step 1. The V_{ds}, V_{qs}, V_{dr}, V_{qr} are obtained from the phase variables V_{sabc} and V_{rabc} through the following sub-steps:

- The sine and cosine values for θ, ω_r and β are calculated where ω_r is the angular speed of rotor θ is angle rotor and $\beta=\theta-\theta_r$
- The stator & rotor voltages (V_{sabc} , V_{rabc}) are transformed into dq axes to form Vdqs and Vdqr using Park transformation to form equation no (3.12) to (3.15)

Step 2 The mutual fluxes for rotor and stator side can be calculated as shown in Fig. A.1 and Fig. A.2.

Step 3: The currents for stator and rotor side I_{dqs} & I_{dqr} are calculated, as shown in Fig. A.3 and Fig. A.4.

Step 4: The rotor and stator side currents are transformed into phase currents.

Step 5: Torque is calculated by using dq axis stator flux and dq axis stator current, as shown in Fig. A.5.

5.1.2 Converter Control Model

The control subsystem model is shown in Fig. 5.3. It is implemented by implementing discrete phase locked loop, rotor side converter and stator side converter.

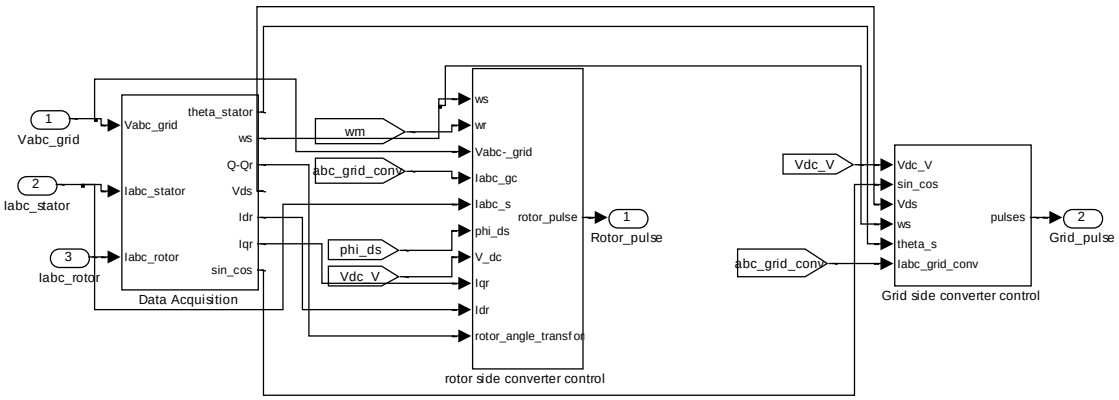

Fig.5.3 representation of control subsystem

5.1.2.1 Discrete phase-locked loop

A discrete phase-locked loop is a control system that tries to generate an output signal whose phase is related to the phase of the input "reference" signal. This circuit

compares the phase of the input signal with the phase of the signal derived from its output oscillator and adjusts the frequency of its oscillator to keep the phases matched. Phase locked loop system is used to synchronize on a set of variable frequency, three phase sinusoidal signals. This 'Discrete 3-phase PLL' has three inputs and two output signals defined as-

Input: Three phase voltage signals [V_a, V_b, V_c]

Output 1: Measured frequency [Hz] = $\frac{\omega}{2\pi}$

Output 2: Phase varying ωt from 0 to 2pi.

5.1.2.2 Grid Side Converter Control Block

The grid side converter control is shown in Fig.5.4. It is used to regulate the voltage of the DC bus capacitor. In addition, this model allows generation or absorption of reactive power. The operation is explained as the following:

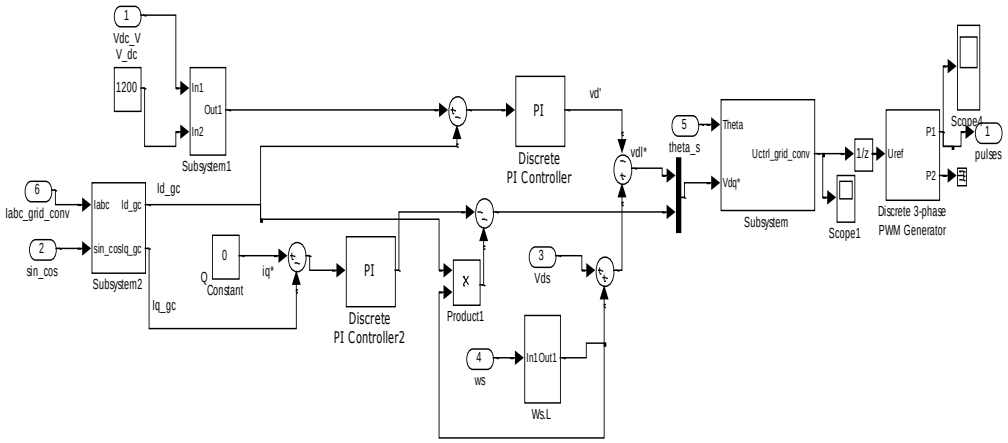

Fig.5.4 Grid side control model

- Transform the voltages and currents 'V_{abcs}' and 'I_{abcs}' into dq reference frame.
- An outer regulation loop consists of a DC voltage regulator. It computes the output reference current 'I_{d_ref} 'between the nominal DC voltage and DC voltage, for the current regulator (I_{d_ref} = current in phase with grid voltage which controls active power flow).
- An inner current regulation loop consisting of a current regulator. The current regulator controls the magnitude and phase of the voltage generated by

converter control grid from the 'I_{d_ref}' produced by the DC voltage regulator and specified '$I_{reference}$'. The current regulator is assisted by feed forward terms which predict the Control grid output voltage. The magnitude of the reference grid converter current is given by:

$$I_{gc\_ref} = \sqrt{(I_{d\_ref}^2 - I_{q\_ref}^2)}$$

The maximum value of this current is limited to a value defined by the converter maximum power at nominal voltage. The stator voltage obtained is delayed by one step and provided to PWM generator. The PWM generated pulses control the stator side converter.

5.1.2.3 Rotor-Side Converter Control Block

The rotor-Side Converter Control System is shown in Fig.5.5. The rotor speed or the reactive power at grid terminals is controlled by the reactive current flowing in the rotor converter.. It's operation is explained as follows-

- Transform the currents of stator, rotor and grid converter into dq reference frame such as 'I_{dq_r}', 'I_{dq_s}' and 'I_{dq_gc}'.
- The actual electrical output power, measured at the grid terminals of the wind turbine, is added to the total power losses (mechanical and electrical) and is compared with the reference power. A Proportional-Integral (PI) regulator is used to reduce the power error to zero. Using the torque regulator the 'I_{dr_ref}' is calculated.
- The output of reactive regulator 'Q Regulator' is the reference rotor current 'I_{qr_ref}' that must be injected in the rotor converter.
- The actual 'I_{qr}' component of positive-sequence current is compared to 'I_{qr_ref}' and the error is reduced to zero by a current regulator (PI). The output of this current controller is the voltage 'V_{qr}' generated by rotor converter. The current regulator is assisted by feed forward terms which predict 'V_{qr}'.
- Voltage at the rotor converter 'V_{dqr}' is transformed into abc reference frame. The rotor voltage obtained is delayed by one step and provided to PWM. The PWM generated pulses controls the rotor side converter.

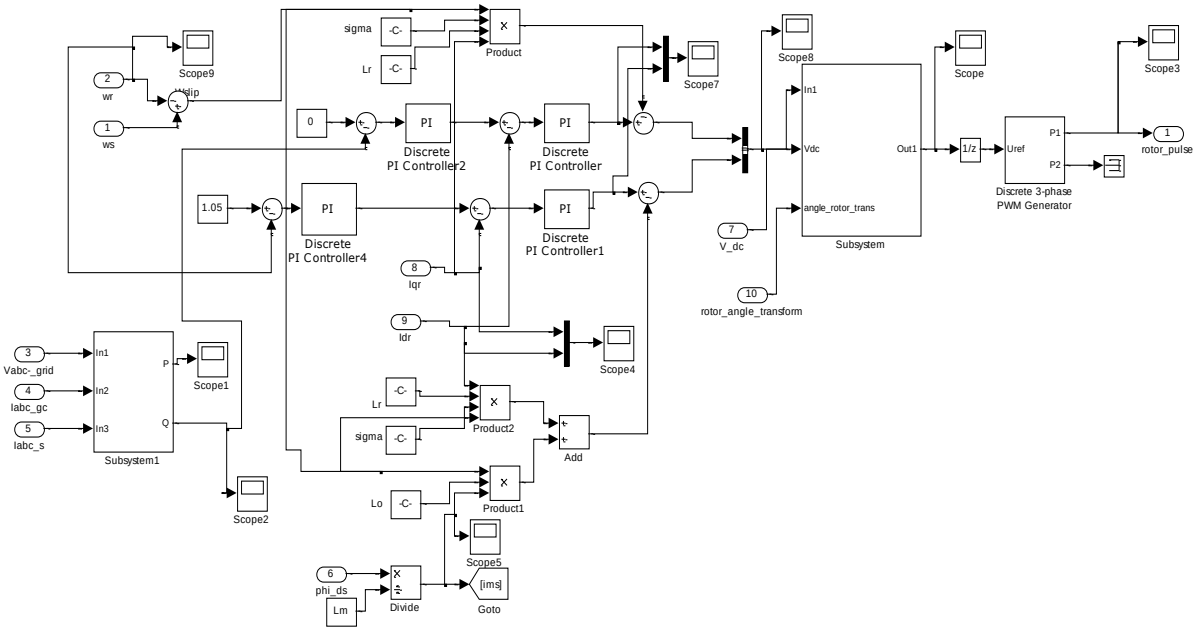

Fig.5.5 Rotor side Control model

The PWM Generator block generates pulses for carrier-based pulse width modulation (PWM) converter using two-level topology. The block can be used to fire the forced-commutated devices IGBTs. The pulses are generated by comparing a triangular carrier waveform to a reference modulating signal. The modulating signals can be generated by the PWM generator itself, or they can be a vector of external signals connected at the input of the block. The amplitude (modulation), phase, and frequency of the reference signals are set to control the output voltage (on the AC terminals) of the bridge connected to the PWM Generator block.

5.1.3 Wind Turbine Model

The wind turbine model is based on the steady-state power characteristics of the turbine as shown in Fig.5.6. The stiffness of the drive train is infinite and the friction actor and the inertia of the turbine must be combined with those of the generator coupled to the turbine. The output power of the turbine is given by the following equation.

$$P_{mech} = 0.5 C_p \rho_{air} \pi R^2 (V_{wind})^3 \quad (5.1)$$

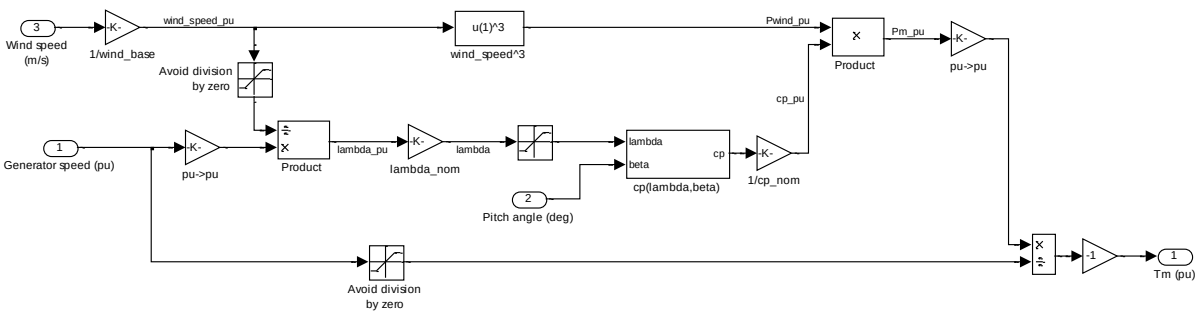

Fig.5.6 Wind turbine model

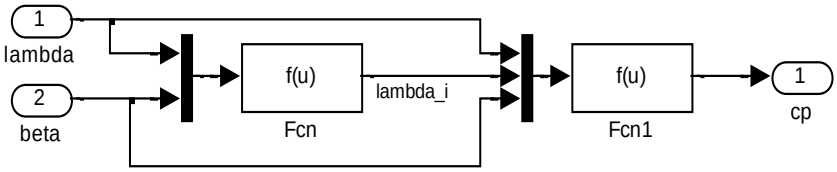

Fig.5.7 Coefficient of performance Cp model

The rotations or speed of wind turbine is controlled by pitch control during the varying wind. The pitch control thus extracts a fraction of the power in the wind. This fraction is expressed as the power efficiency coefficient, Cp, of the wind turbine as shown in Fig. 5.7. The Cp can be expressed as a function of λ and β:

$$C_p = f(\lambda, \beta) \tag{5.2}$$

5.2 RESULTS AND DISCUSSION

The system data is given in Appendix-B. The machine is made to operate in speed control mode. The reference speed of the rotor is specified. The performance is analysed for various wind speed of 9 m/s, 10.5 m/s and 12 m/s at a constant rotor speed of ω_{ref} = 1.05pu. The performance is analysed for the change DC link reference voltage, capacitance and the change in value of inductor connected to the grid. Further the analysis is also made on the rotor reference speed of 1.21 pu and 1.1 pu for simulated wind speed.

5.2.1 Effect of wind speed on DFIG performance

The performance for ω_{ref} = 1.05 pu for different wind speeds as 9 m/s, 10.5 m/s

and12 m/s are shown in Fig.5.8 to 5.18. The effect of wind speed on turbine torque and electromagnetic torque is shown in Fig.5.8 & Fig.5.9 respectively.

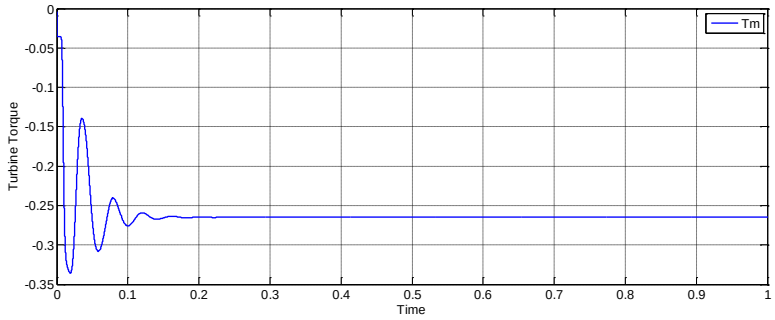

(i) Turbine torque at 9 m/s

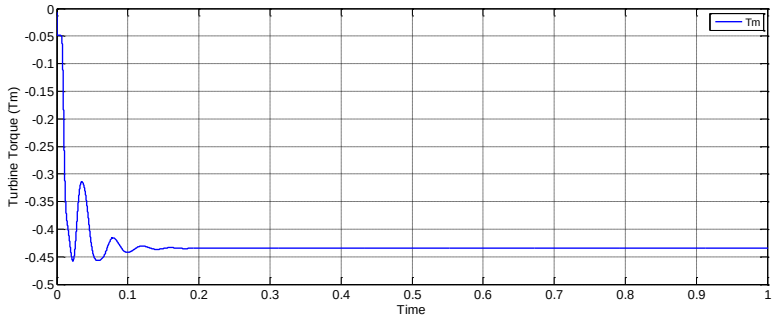

(ii) Turbine torque at 10.5 m/s

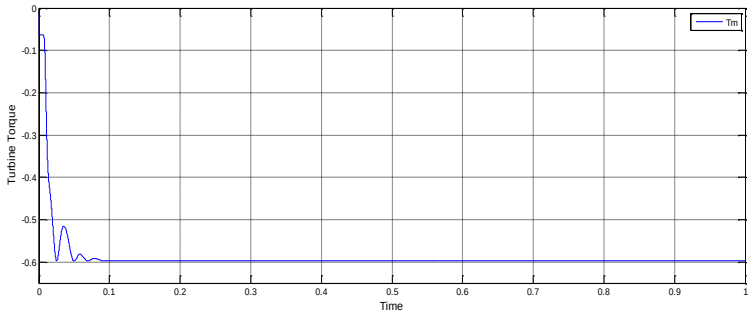

(iii) Turbine torque at 12 m/s

Fig.5.8 Effect of wind speed on turbine torque

As shown in Fig.5.8 with the increase in wind speed the torque generated by the wind turbine increases. The initial transients of about 0.1 sec duration are also resulted.

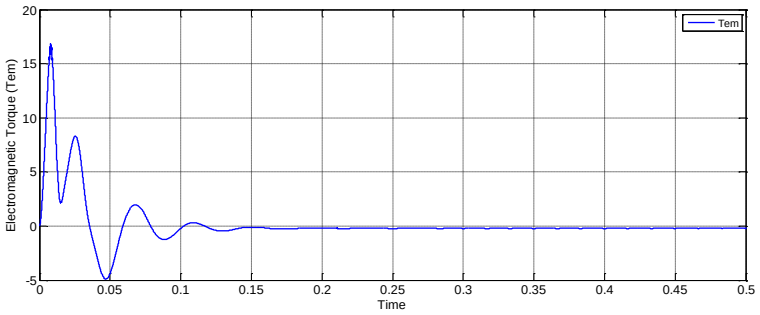

(i) Electromagnetic torque at 9 m/s

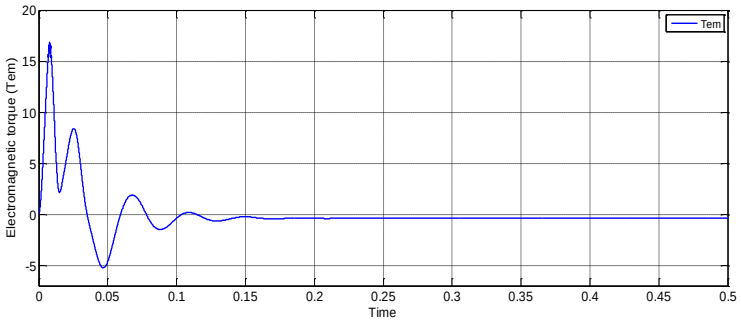

(ii) Electromagnetic torque at 10.5 m/s

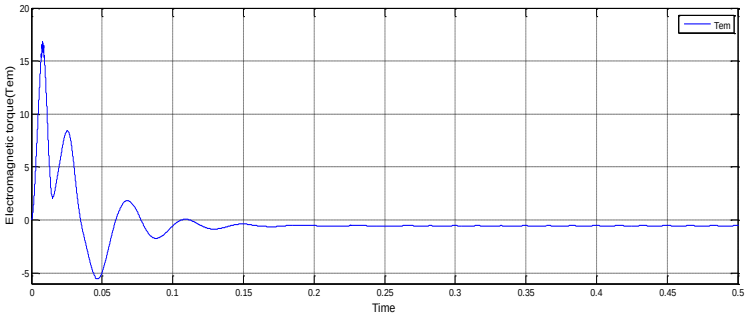

(iii) Electromagnetic torque at 12 m/s

Fig.5.9 Effect of wind speed on electromagnetic torque

As shown in Fig.5.9 after the initial transients of 0.15 sec, the steady state value is violated, electromagnetic torque increases with increase in wind speed as shown in the Fig.5.9. the steady state value of 0.27,0.43 and 0.6 N/m is resulted for wind speed of 9 m/s, 10.5 m/s and 12 m/s respectively as shown in Table.5.1.

Table 5.1- Steady state torque for different wind speeds

Wind speed (m/s)	**Magnitude at steady state (pu)**
9	-0.27
10.5	-0.43
12	-0.60

In Fig.5.9, the initial torque is the indicating of motor mode and thereafter it stabilizes to generating mode yielding negative value.

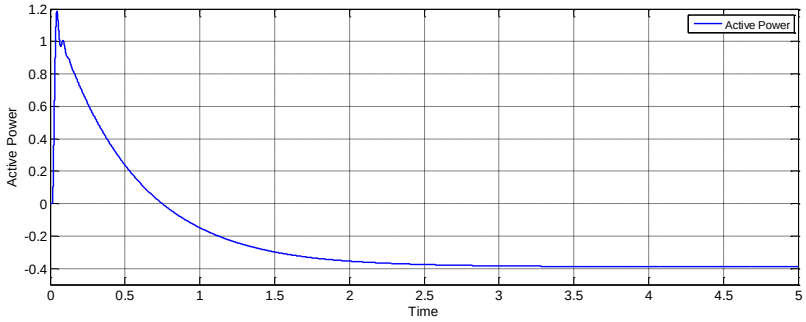

(i) Active power at 9 m/s

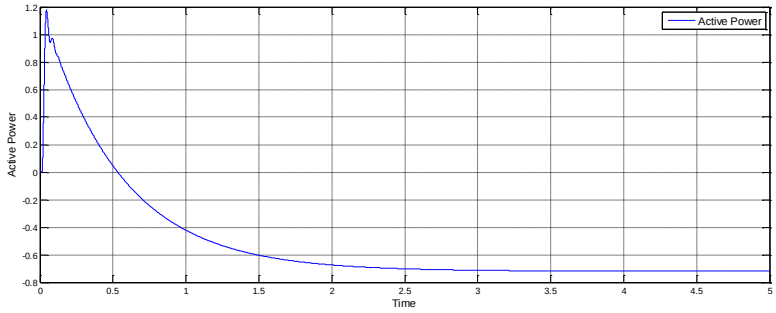

(ii) Active power at 10.5 m/s

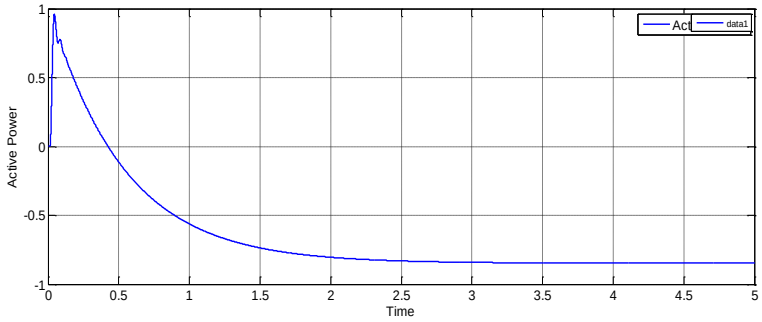

(iii) Active power at 12 m/s

Fig.5.10 Effect of wind speed on the active power generated by DFIG

As shown in Fig.5.10 and summarized in Table 5.2, the active power generated by the DFIG also increases with the increase in wind speed. In line with the observation of Fig.5.9, initially due to operation in the motoring mode and settles to negative value due to operation in generating mode. Increase in active power with increase in speed takes place upto a certain speed of wind, after that the generated power will saturate and will not increase further. In case the wind speed exceeds the safe limit, the turbine will enter into parking mode and no generation of power takes place [5].

Table 5.2- Peak value of Active power for different speeds	
Wind speed (m/s)	**Magnitude at Active power (pu)**
9	-0.38
10.5	-0.71
12	-0.83

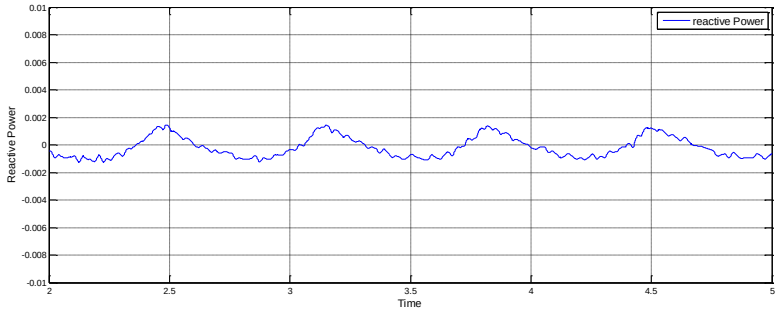

(i) Reactive power steady state at 9 m/s

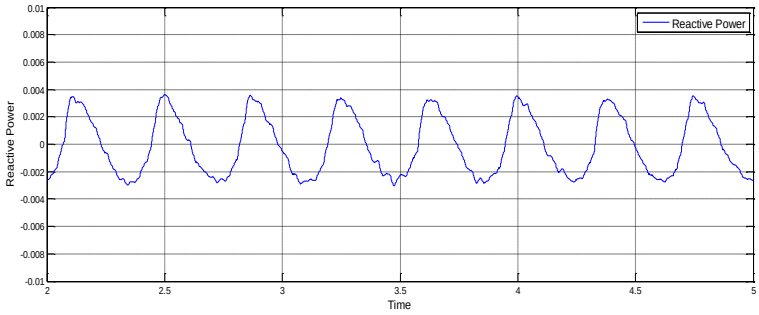

(ii) Reactive Power steady state at 10.5 m/s

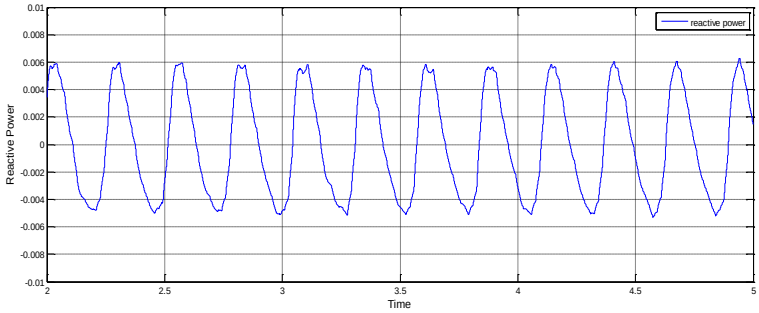

(iii) Reactive Power steady state at 12 m/s

Fig.5.11 Effect of wind speed on the reactive power

The nature of reactive power for different speeds is depicted in Fig.5.11. The reactive power in the system increases in magnitude and frequency as the wind speed increases. As observed from Fig.5.11, although the frequency and magnitude of reactive power is changing, the pattern is symmetric to ‘zero’ value. Thus average will be ‘zero’.

The summary of reactive power magnitude is given in Table 5.3.

Table 5.3- Peak value of reactive power for different speeds	
Wind speed (m/s)	**Peak value of Reactive power (pu)**
9	0.0016
10.5	0.0031
12	0.0060

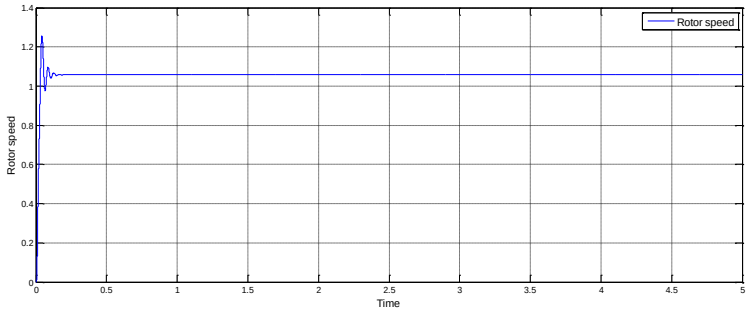

(i) Rotor speed

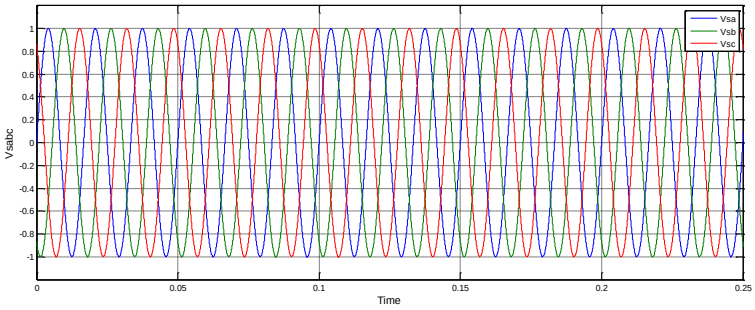

(ii) Stator voltage

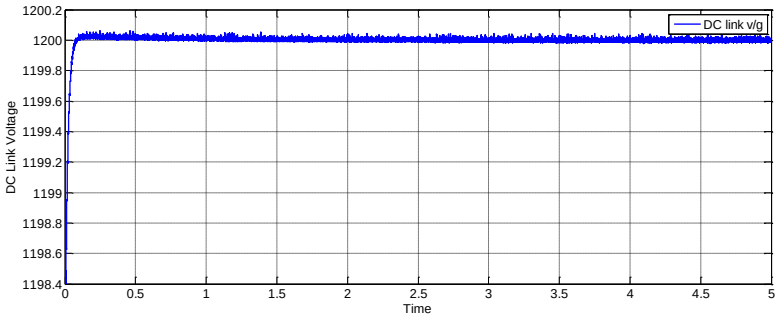

(iii) DC link voltage

Fig.5.12 Illustration of (i) Rotor speed, (ii) Stator voltage and (iii) DC link voltage.

The rotor speed, stator voltage and DC-link voltage is illustrated in Fig.5.12. It is observed that, these parameters remain unchanged due to change in wind speed. This is because the system is used in speed control mode.

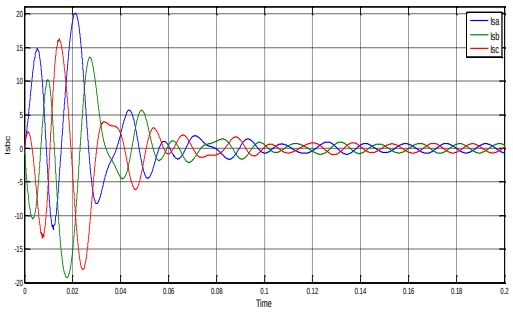

(i) Is_{abc} at 9 m/s

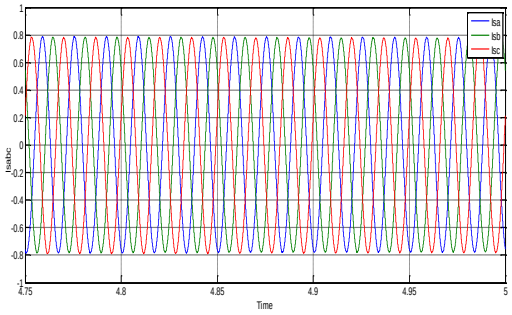

(i) Is_{abc} at 9 m/s

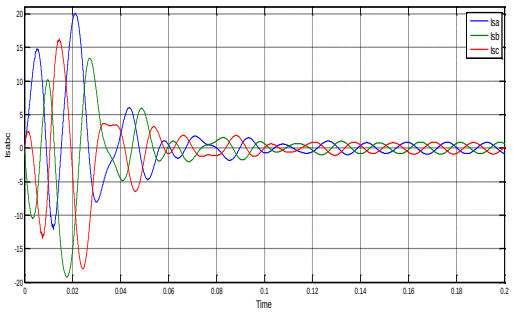

(ii) Is_{abc} at 10.5 m/s

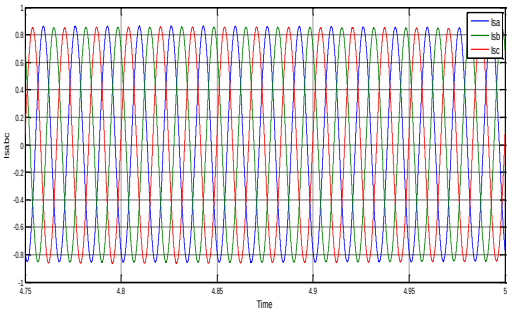

(ii) Is_{abc} at 10.5 m/s

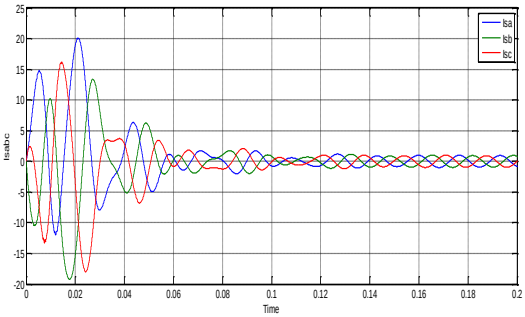

(iii) Is_{abc} at 12m/s

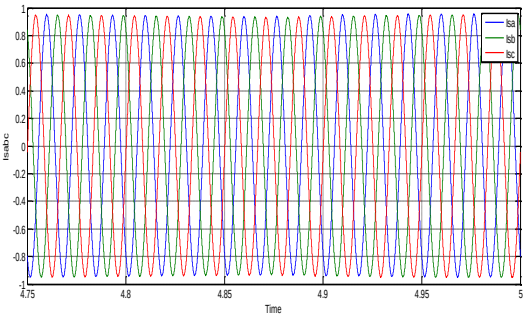

(iii) Is_{abc} at 12m/s

(a) Transient state

(b) Steady state

Fig.5.13 Effect of wind speed on 3- phase stator current

The effect of different speeds on 3-phase stator currents is shown in Fig.5.13 for both initial transient and after attaining steady state. The steady state value of stator current is summarized in Table5.4. It is observed that with the increase in speed the current at the stator terminal increases. On observing the effect of different speeds on stator current it is concluded that with the increase in speed the current at the stator terminal increases. This is in agreement with the increase in electromagnetic torque and active power as observed in Fig.5.9 and Fig.5.10 respectively.

Table 5.4- Summary of stator current for different rotor speeds.	
Wind speed (m/s)	**Magnitude of stator current(pu)**
9	0.79
10.5	0.84
12	0.93

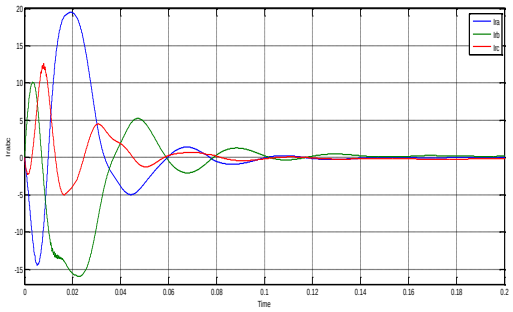

(i) Ir_{abc} at 9 m/s

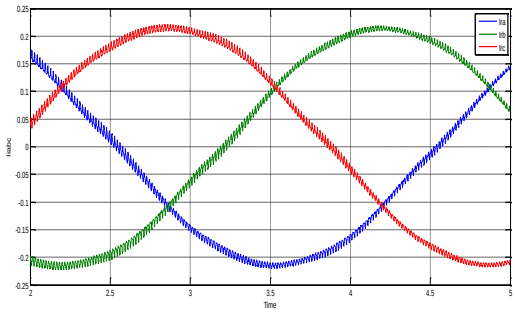

(i) Ir_{abc} at 9 m/s

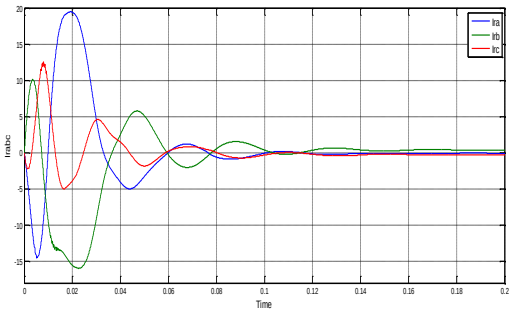

(ii) Ir_{abc} at 10.5 m/s

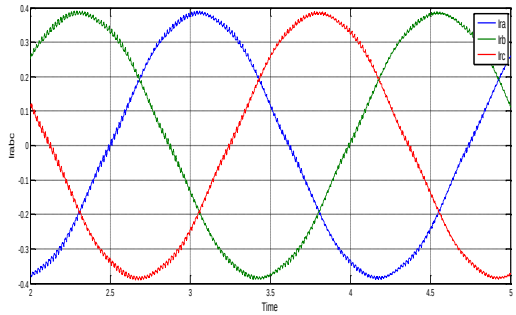

(ii) Ir_{abc} at 10.5 m/s

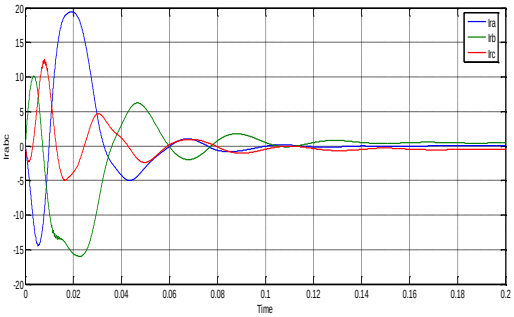

(iii) Ir_{abc} at 12 m/s

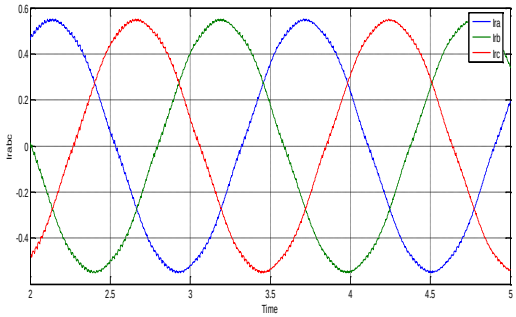

(iii) Ir_{abc} at 12 m/s

(a) Transient state

(b) Steady state

Fig.5.14 Effect of wind speed on 3- phase rotor current

The effect of wind speed on 3-phase rotor currents is shown in Fig.5.14. It is evident that the magnitude and frequency of rotor current increases with increase in wind speed. It is similar to the pattern of reactive power shown in Fig.5.11. the magnitude of rotor current at steady is summarized in Table 5.5.

Table 5.5-Summary of rotor current for different rotor speeds.	
Wind speed (m/s)	**Magnitude of rotor current (pu)**
9	0.22
10.5	0.40
12	0.56

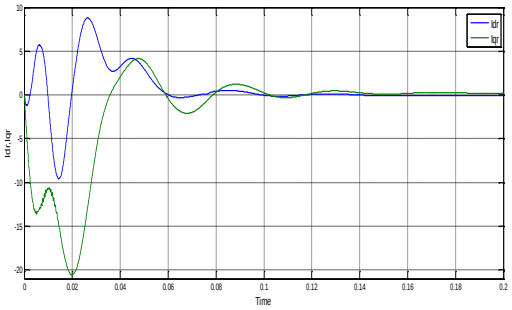

(i) I_{dr}-I_{qr} at 9 m/s

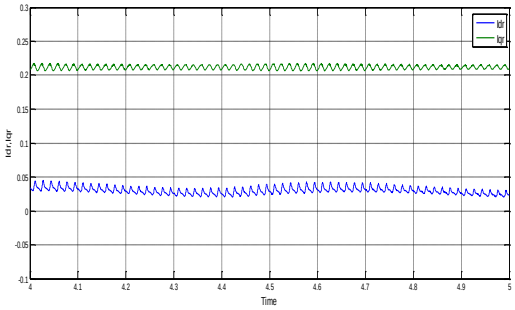

(i) I_{dr}-I_{qr} at 9 m/s

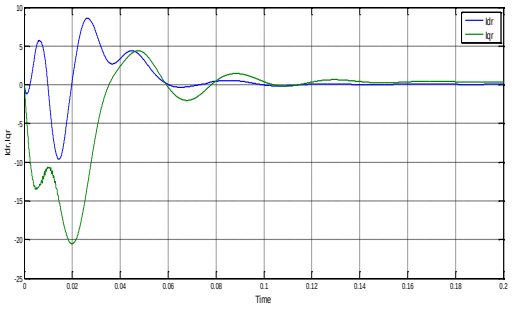

(ii) I_{dr}-I_{qr} at10.5 m/s

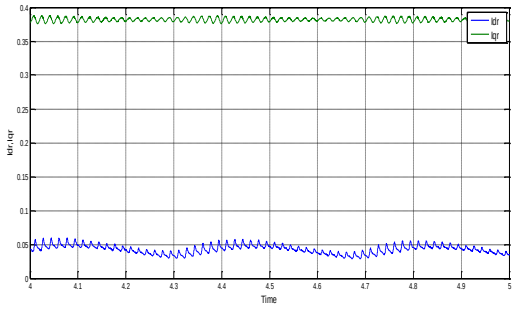

(ii) I_{dr}-I_{qr} at 10.5 m/s

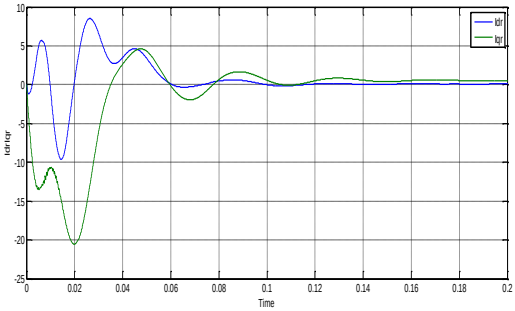

(iii) I_{dr}-I_{qr} at 12 m/s

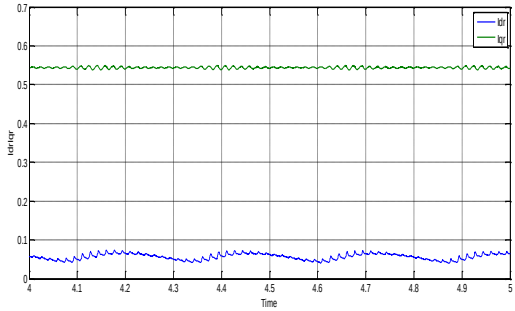

(iii) I_{dr}-I_{qr} at 12 m/s

(a) Transient state | (b) Steady state

Fig. 5.15 Effect of wind speed on rotor current in (d-q) terms

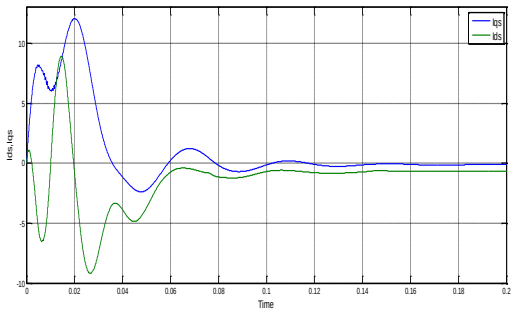

(i) I_{ds}-I_{qs} at 9 m/s

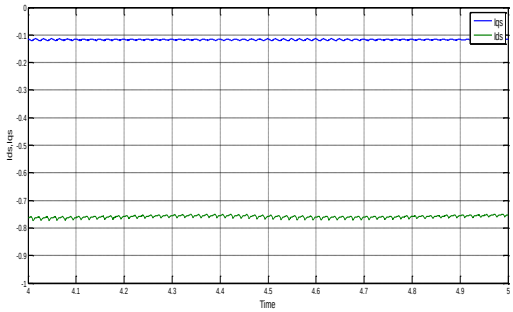

(i) I_{ds}-I_{qs} at 9 m/s

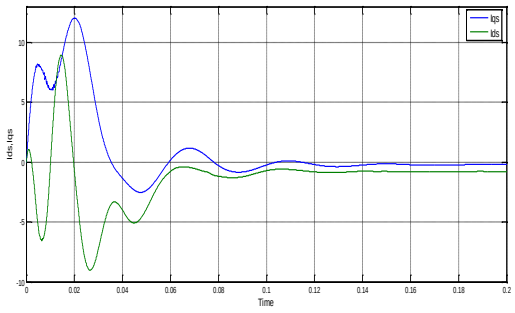

(ii) I_{ds}-I_{qs} at10.5 m/s

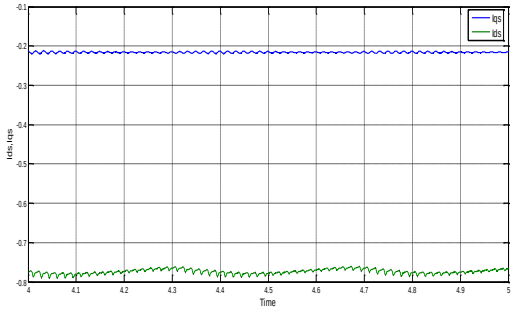

(ii) I_{ds}-I_{qs} at 10.5 m/s

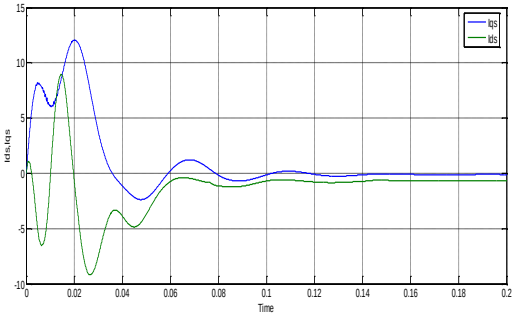

(iii) I_{ds}-I_{qs} at 12 m/s

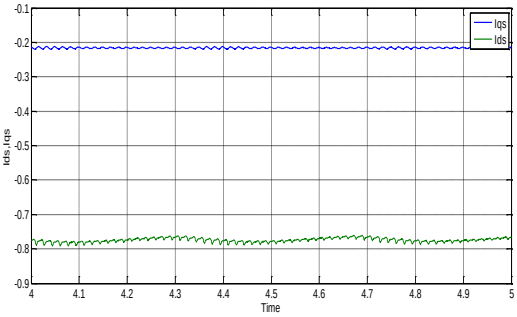

(iii) I_{ds}-I_{qs} at 12 m/s

(a) Transient state

(b) Steady state

Fig.5.16 Effect of wind speed on stator current in (d-q) terms

The influence of wind speed on the d-q components of rotor current and stator current is shown in Fig. 5.15 and 5.16 respectively. The magnitude of rotor current (I_{dr},I_{qr}) and stator currents (I_{ds},I_{qs}) are summarized in Table 5.6 and Table 5.7 respectively. No significant change in transients are observed.

Table 5.6- summary of rotor current in d-q terms

Wind speed (m/s)	**Magnitude of I_{qr} (pu)**	**Magnitude of I_{dr} (pu)**
9	0.21	0.003
10.5	0.38	0.005
12	0.54	0.006

Table 5.7- summary of stator current in d-q terms		
Wind speed (m/s)	**Magnitude of I_{ds} (pu)**	**Magnitude of I_{qs} (pu)**
9	-0.78	-0.11
10.5	-0.78	-0.21
12	-0.78	-0.22

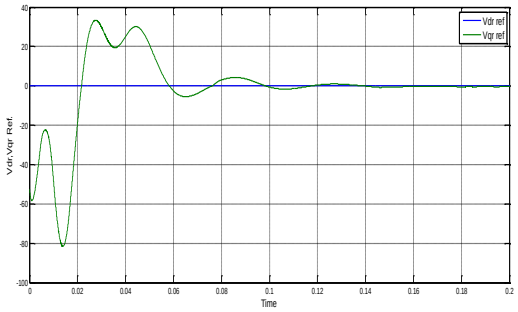

(i) V_{dr}-V_{qr} at 9 m/s

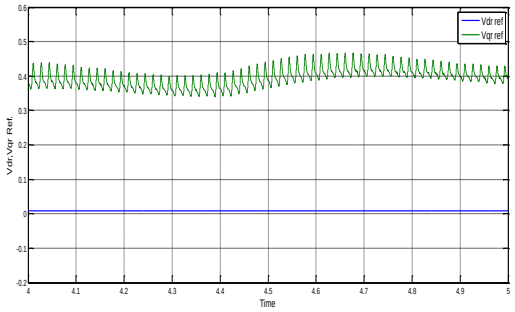

(i) V_{dr}-V_{qr} at 9 m/s

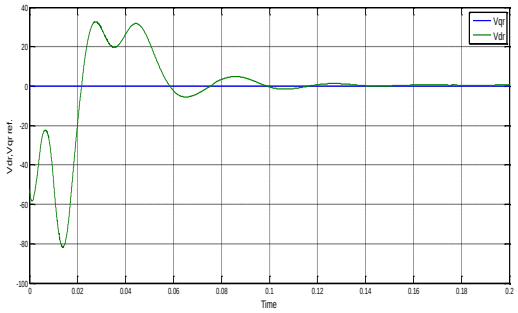

(ii) V_{dr}-V_{qr} at10.5 m/s

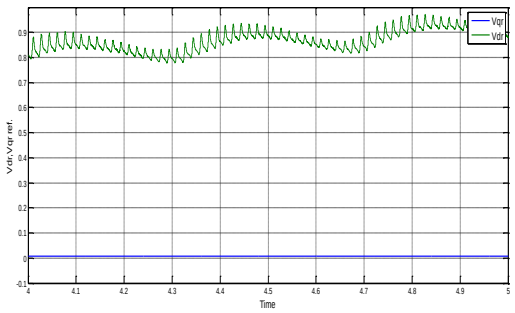

(ii) V_{dr}-V_{qr} at 10.5 m/s

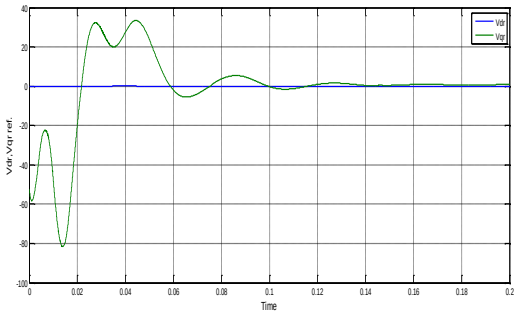

(iii) V_{dr}-V_{qr} at 12 m/s

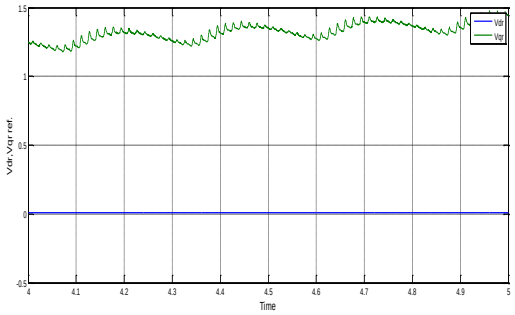

(iii) V_{dr}-V_{qr} at 12 m/s

(a) Transient state

(b) Steady state

Fig.5.17 Effect of wind speed on rotor side reference voltage

It is observed, from Table 5.6, that 'I_{dr}' is around to zero which control the reactive power and maintain it around 'zero' while the 'I_{qr}' control the active power. As shown in Fig.5.16 no significant change in transient pattern is observed for different wind speeds. On steady state, the I_{ds} assumes the same value for all three wind speeds. Since on grid side

'I_{ds}' control the DC link voltage and maintain it so its magnitude remains the same, while 'I_{qs}' control the reactive power of the grid, so its value vary around zero, to maintain the reactive power.

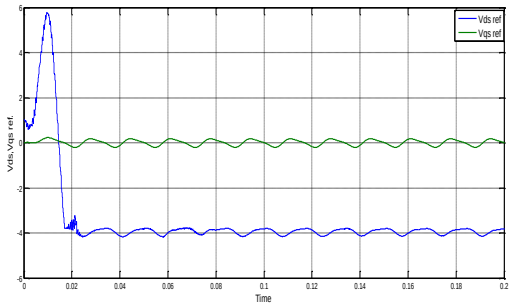

(i) V_{ds}-V_{qs} at 9 m/s

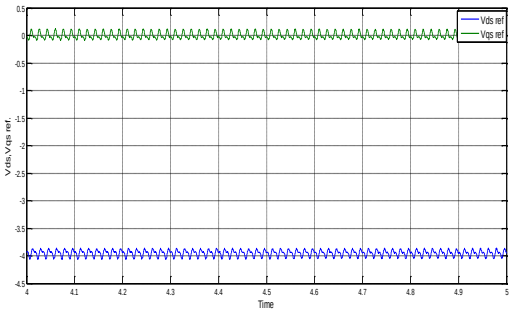

(i) V_{ds}-V_{qs} at 9 m/s

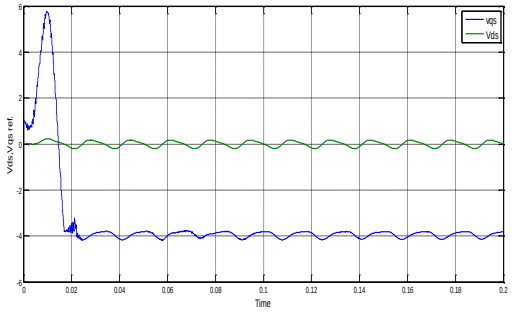

(ii) V_{ds}-V_{qs} at10.5 m/s

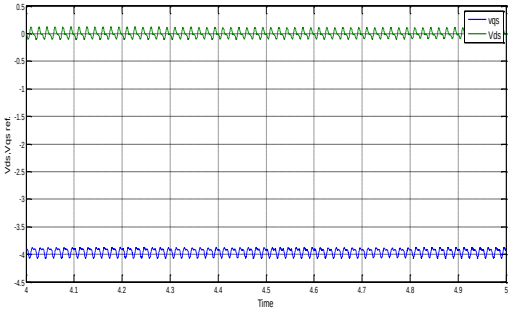

(ii) V_{ds}-V_{qs} at 10.5 m/s

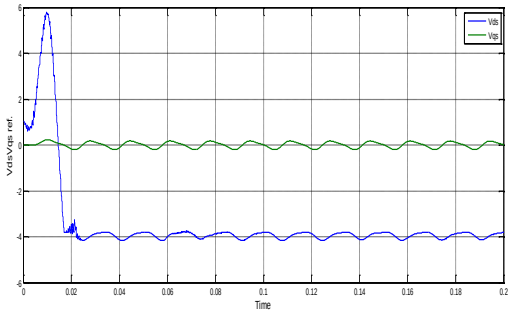

(iii) V_{ds}-V_{qs} at 12 m/s

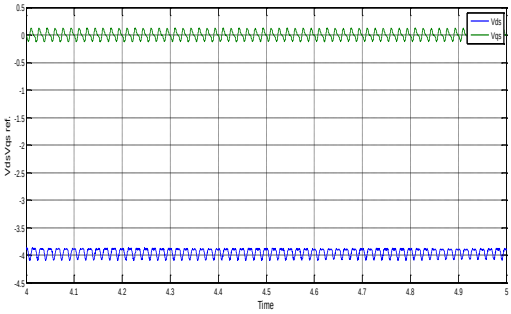

(iii) V_{ds}-V_{qs} at 12 m/s

(a) Transient state

(b) Steady state

Fig. 5.18 Effect of wind speed on stator side reference voltage

The effect of wind speed on rotor side and stator side reference voltages in terms of d-q variables is shown in Fig. 5.17 and Fig. 5.18 respectively. As shown in Fig. 5.17, these are the input signals in d-q terms which are fed to the PWM on rotor side which further produces the control pulses to control the active and reactive power the 'V_{dr}' is nearly 'zero' for all three speeds while the 'V_{qr}' value increases for increase in speed. The pattern is due to the switching devices.

The Fig. 5.18 represents the q-axis and d-axis stator side reference voltage. These are the input signals used to maintain DC link voltage at constant level. These signals are taken from grid side and thus remains unchanged for different wind speeds.

5.2.2 Effect of changing parameters on DFIG performance

The performance of the system is analyzed for change in DC link reference voltage, Dc link capacitor and coupling inductor. For the analysis the DC link reference voltage is reduced by 10% the DC link capacitor is reduced by 20% and coupling inductance is reduced by 20% in one by one manner. The results are presented in comparision with base case, which corresponds to ω_{ref} = 1.05 pu, wind speed of 10.5 m/s, DC link reference voltage as 1000 V, DC link capacitance as 13mF and coupling inductance as 0.04pu. The electromagnetic torque, active power, 3-phase stator current, 3-phase rotor current , d-q rotor current,d-q rotor reference voltage, d-q stator reference voltage are shown in Fig.5.19, 5.20, 5.21, 5.22, 5.23, 5.24 and 5.25 respectively.

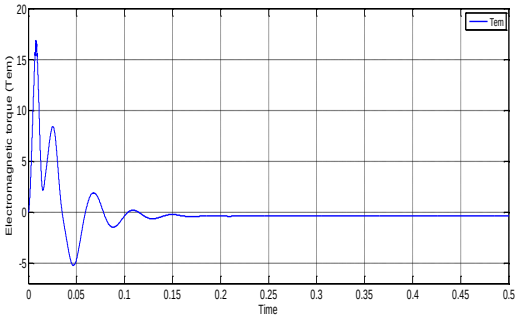

(i) Base case torque

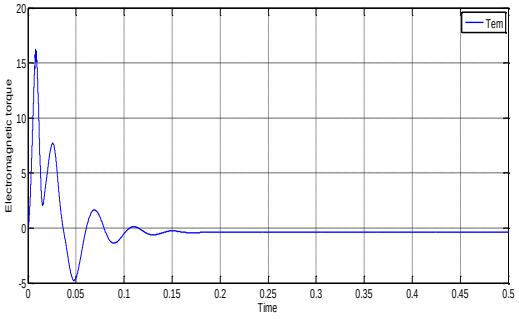

(ii) change in DC link reference voltage

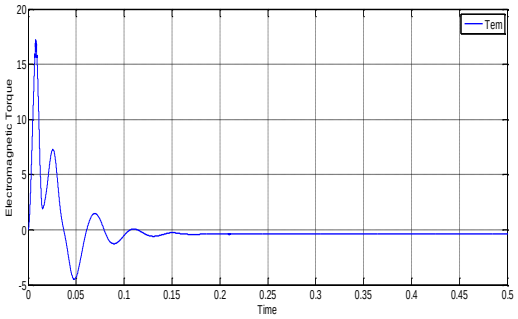

(iii) change in capacitance

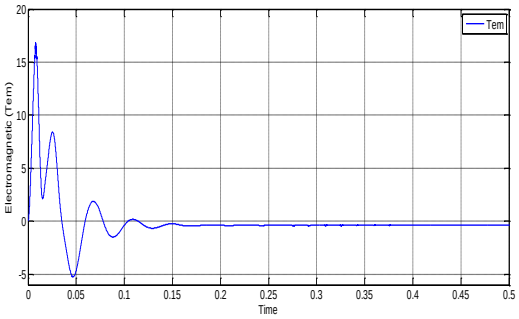

(iv) change in inductance

Fig. 5.19 Effect of changing parameters on Electromagnetic Torque

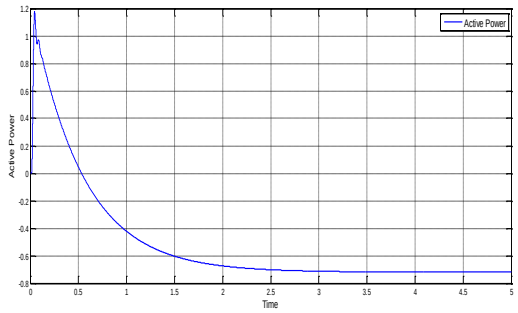

(i) Base Active power

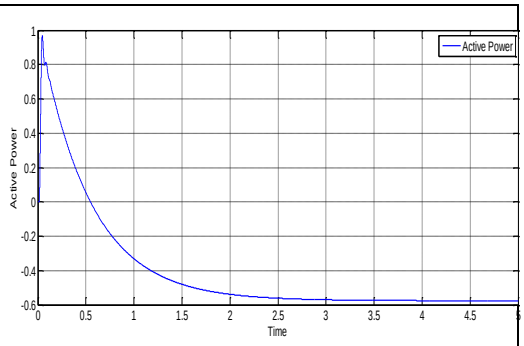

(ii) change in DC link reference voltage

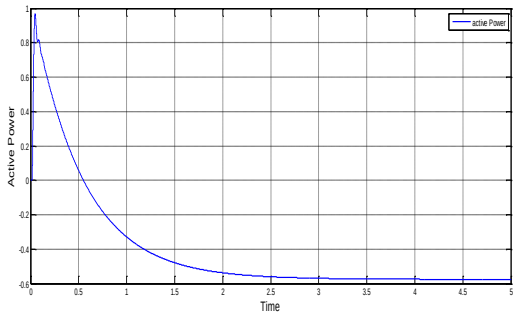

(iii) change in capacitance

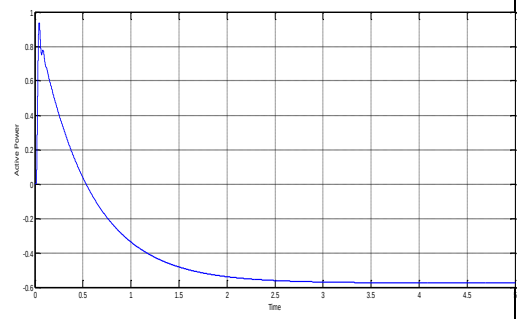

(iv) change in inductor

Fig.5.20 Effect of changing parameters on active power

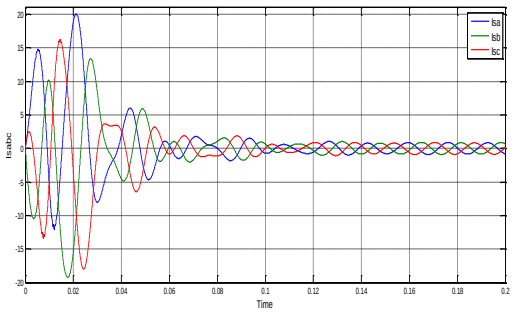

(i) Base stator current (Is_{abc})

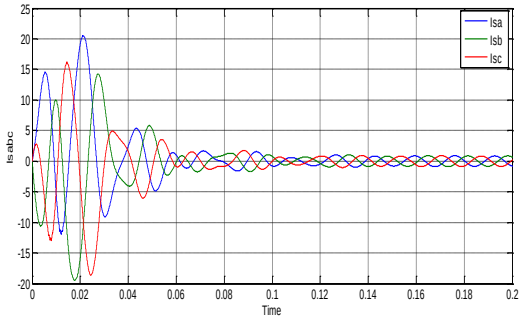

(ii) change in Dc link ref. Voltage

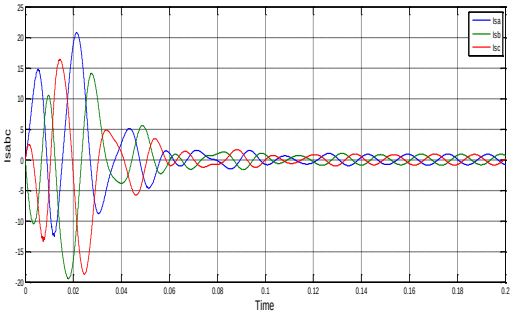

(iii) change in capacitance

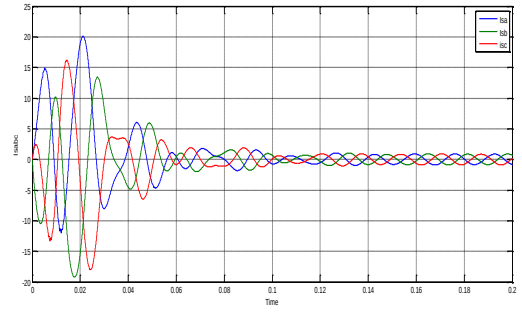

(iv) change in inductance

Fig.5.21 Effect of change in parameters on 3-phase stator current

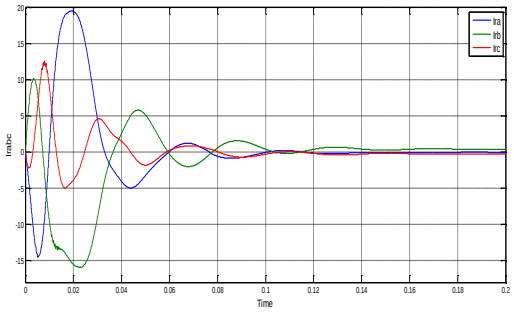

(i) Base rotor current (Ir_{abc}) at 10.5 m/s

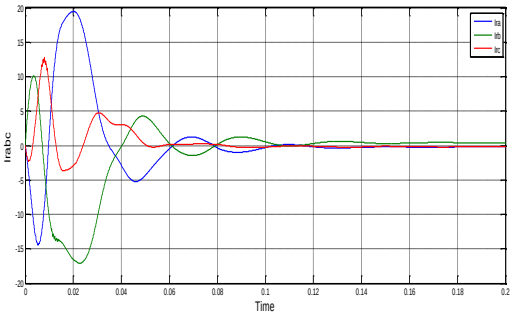

(ii) Rotor current for change in capacitance

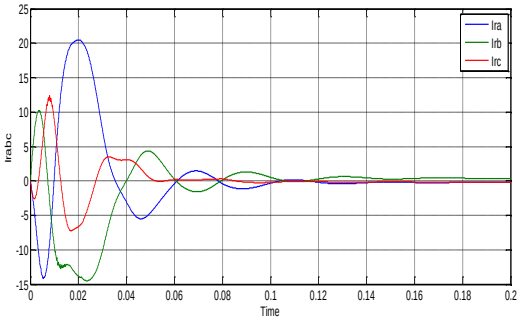

(iii) Rotor current for change in Dc link ref. Voltage

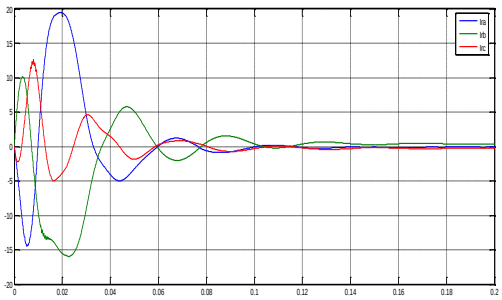

(iv) Rotor current for change in inductance

Fig.5.22 Effect of change in parameters on 3-phase rotor current

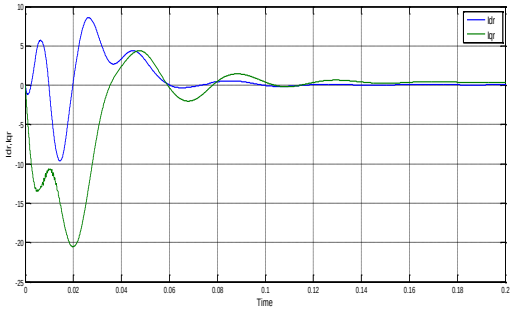

(i) Base case

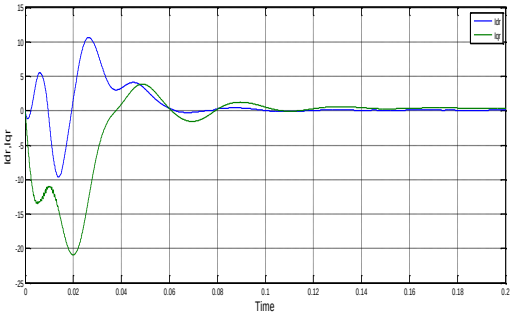

(ii) change in capacitance

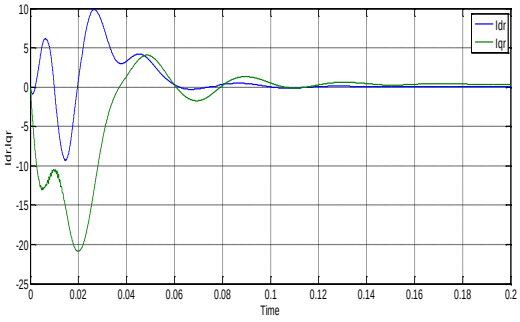

(iii) change in Dc link ref. Voltage

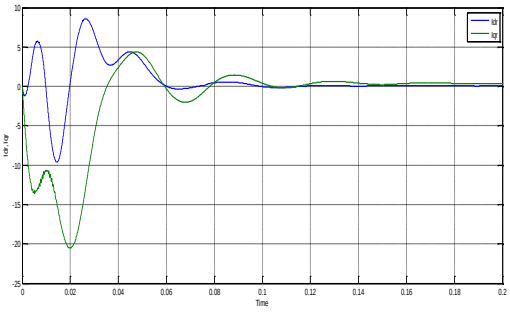

(iv) change in inductance

Fig.5.23 Effect of change in parameters on d-q rotor current

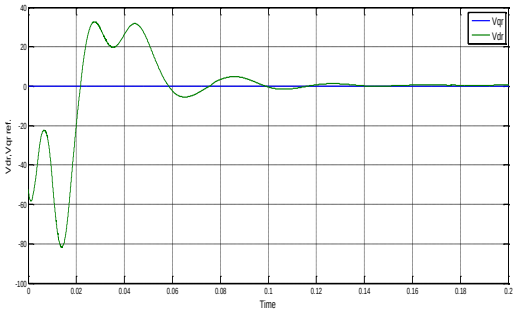

(i) Base V_{dr}-V_{qr} at10.5 m/s

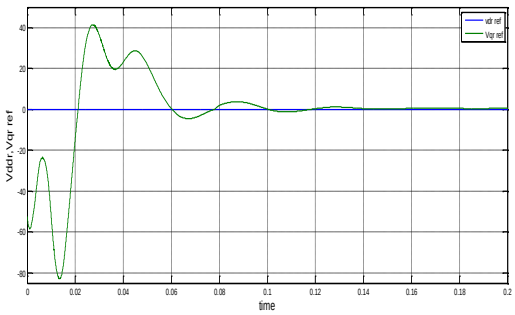

(ii) V_{dr},V_{qr} ref for change in capacitance

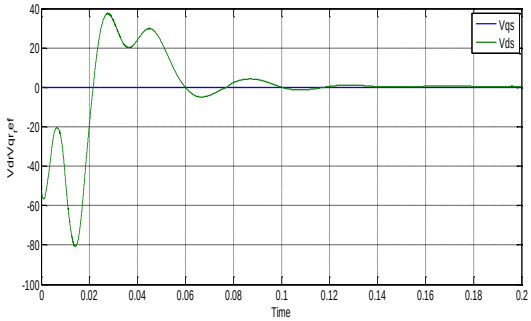

(iii) V_{dr},V_{qr} ref for change in Dc link ref. Voltage

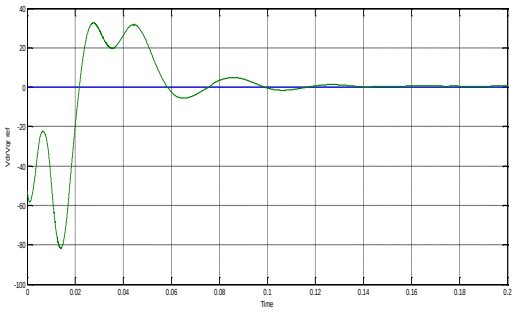

(iv) V_{dr},V_{qr} ref for change in inductance

Fig.5.24 Effect of change in parameters on rotor ref.voltage in (d-q) terms

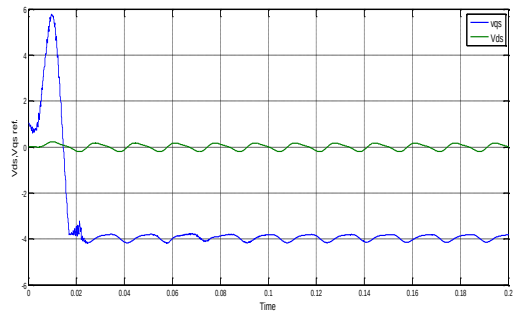

(i) BaseV_{ds}-V_{qs}

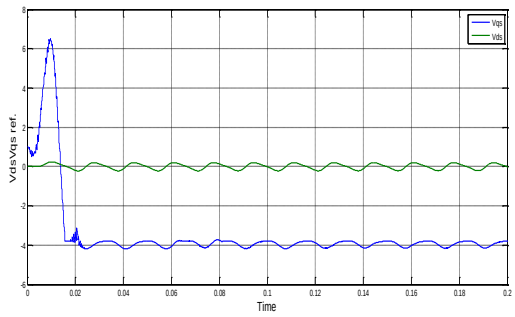

(ii) V_{ds},V_{qs} ref for change in capacitance

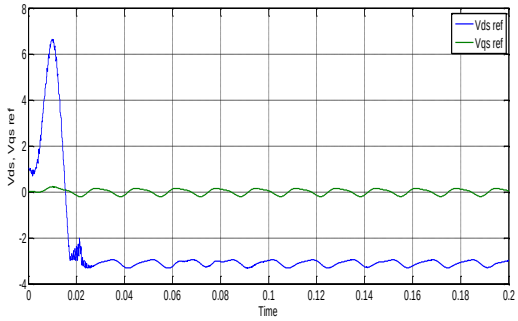

(iii) V_{ds},V_{qs} ref for change in Dc link ref. voltage

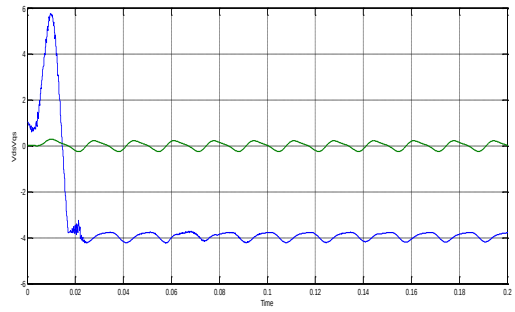

(iv) V_{ds},V_{qs} ref for change in inductance

Fig.5.25 Effect of change in parameters on stator ref.voltage in (d-q) terms

From Fig.5.19 to Fig.5.25 it is observed that the dynamic behaviour and the steady state values does not change significantly due to the change in parameters. This is due to same reference speed and operation in speed control mode. The active power reduces from '0.71' to 0.58 pu due to the selected changes other parameters changes accordingly.

5.2.3 Effect of change in rotor reference speed on the performance of DFIG.

This analysis is carried out at two super- synchronous reference speeds of 1.21 and 1.1 pu. The wind speed is assumed to be varying between 9 m/s and 12 m/s as given in Fig. 5.26(i). The turbine torque, rotor speed, 3- phase stator current, 3- phase rotor current, d-q rotor reference voltages, d-q rotor current, active and reactive powers are shown in Fig. 5.26, Fig. 5.27, Fig. 5.28, Fig. 5.29, Fig. 5.30, Fig. 5.31 and Fig. 5.32 respectively. The DC link reference voltage is taken as 1200 V, DC link capacitor 16 mF and inductor 0.05 pu are taken for simulation study.

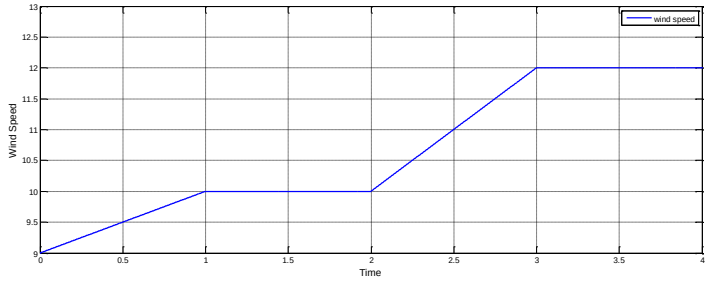

(i) Wind speed

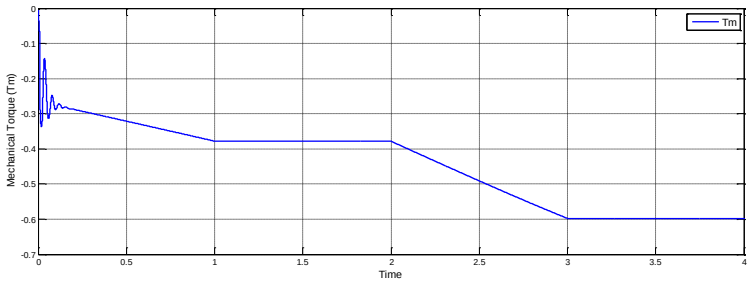

(ii) Torque Generated by Wind Turbine at 1.21pu

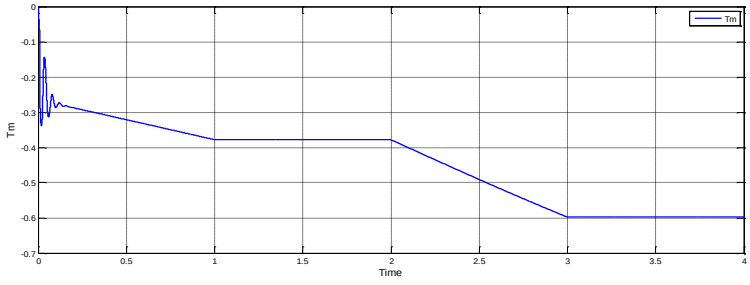

(iii) Torque Generated by Wind Turbine at 1.1pu

Fig.5.26 Turbine Torque for different rotor ref. Speed

As shown in Fig. 5.26, the change in speed results into the change in turbine torque. As the speed increases, the turbine torque also increases (attains higher negative value).

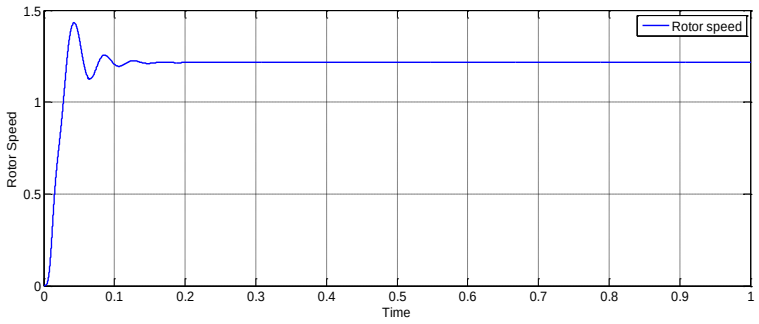

(i) Rotor Speed of the Generator at 1.21pu

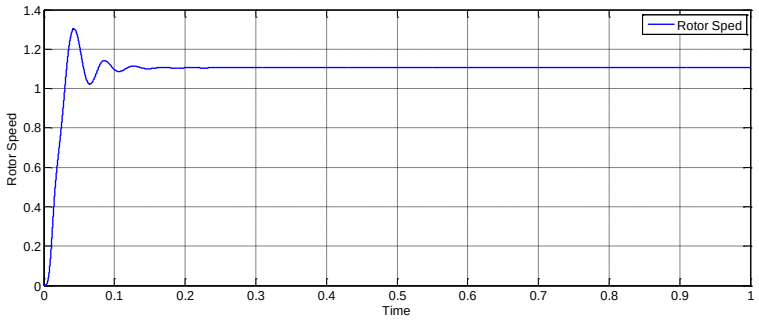

(ii) Rotor Speed of the Generator at 1.1pu

Fig.5.27 Rotor speed for different rotor reference speeds

As shown in Fig. 5.27, as the wind speed in both the cases are same so the rotor assumes the reference speed 1.21 and 1.1 pu after initial transients. No appreciable difference is observed in initial transients. As the input wind speed is same for different references, the electromagnetic torque produced by the wind turbine will be same.

As shown in Fig. 5.28, at the instant of grid connection the three phase grid current oscillates and even attains high magnitude of around 20 p.u. At steady state, it achieve the magnitude of 0.8 pu for both the reference speeds.

As shown in Fig. 5.29, At the instant of grid integration, high magnitude of oscillations can be seen. The magnitude of spikes is very high and it achieves the steady state condition with the magnitude of 0.57 p.u.

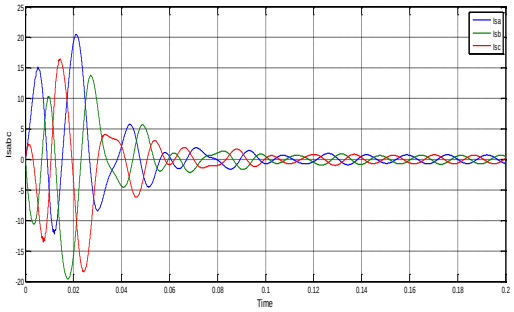	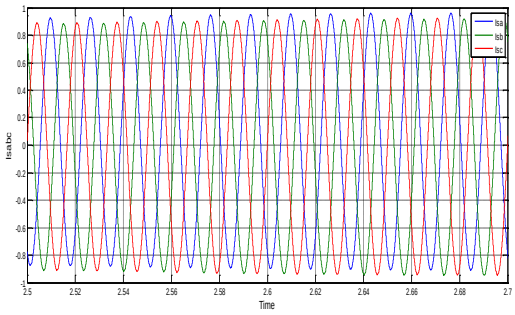
(i) Is_{abc} at 1.21pu	(i) Is_{abc} at 1.21pu
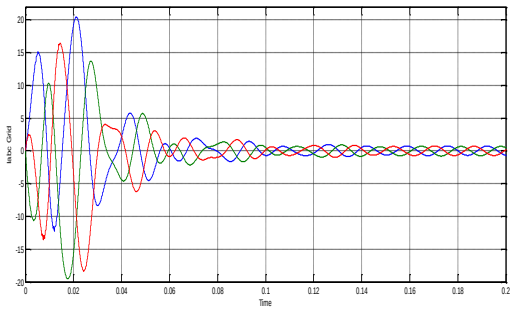	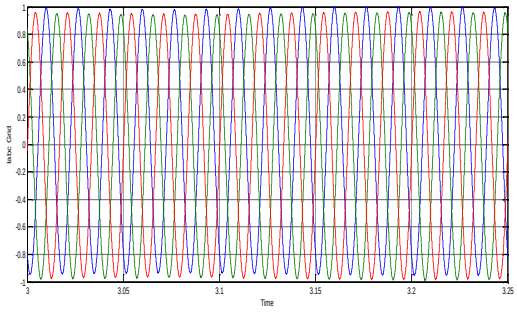
(ii) Is_{abc} at 1.1pu	(ii) Is_{abc} at 1.1pu
Transient state	Steady state

Fig. 5.28 3-phase stator current for different reference speeds

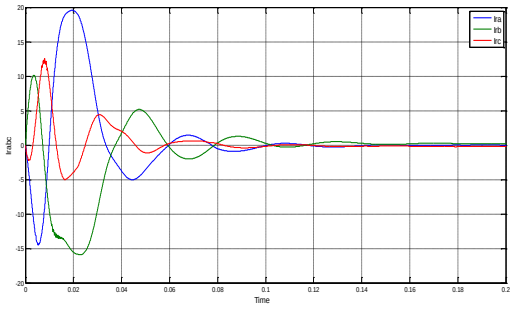	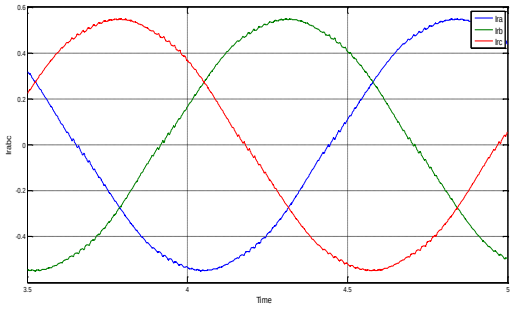
(i) Ir_{abc} at 1.21pu	(i) Ir_{abc} at 1.21pu
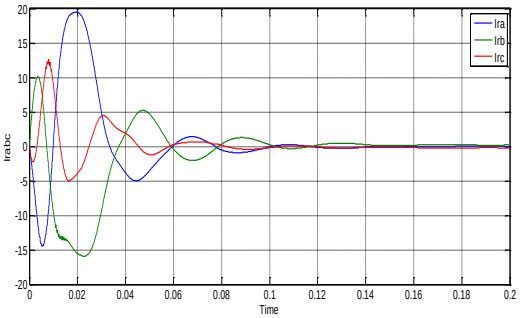	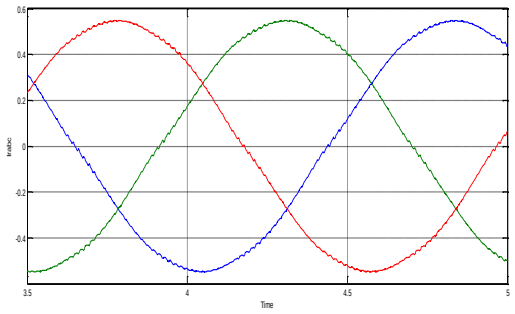
(ii) Ir_{abc} at 1.1pu	(ii) Ir_{abc} at 1.1pu
Transient state	Steady state

Fig.5.29 3-phase rotor current for different reference speeds

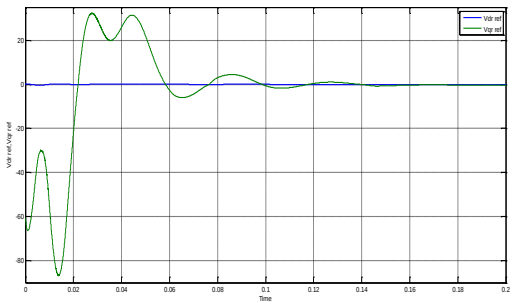

(i) Vr_{dq} ref. At 1.21pu

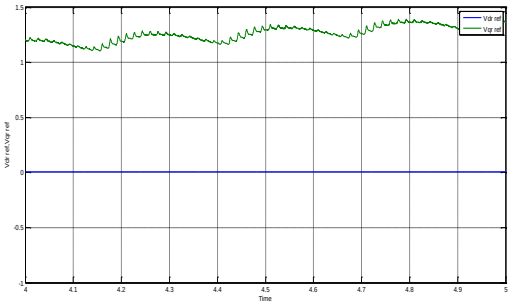

(i) Vr_{dq} ref. at 1.21pu

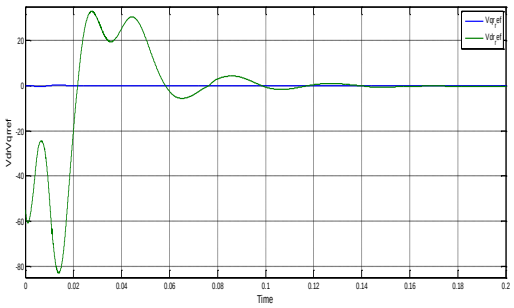

(iii) Vr_{dq} ref. at 1.1pu

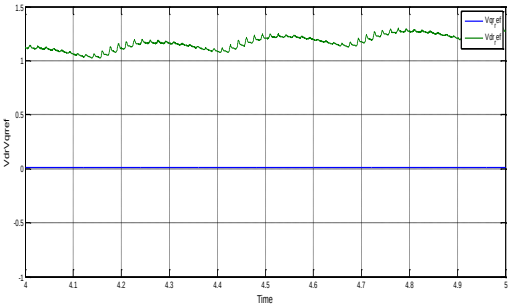

(ii) Vr_{dq} ref. at 1.1pu

Transient state	Steady state

Fig.5.30 d-q rotor reference voltage for different reference speeds

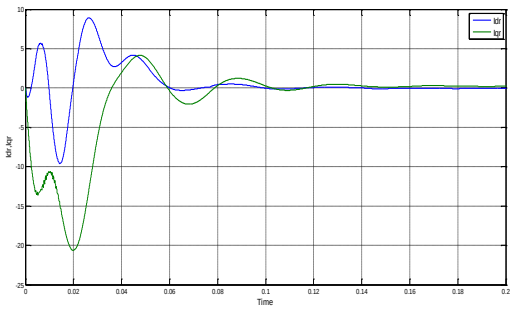

(i) Ir_{dq} at 1.21pu

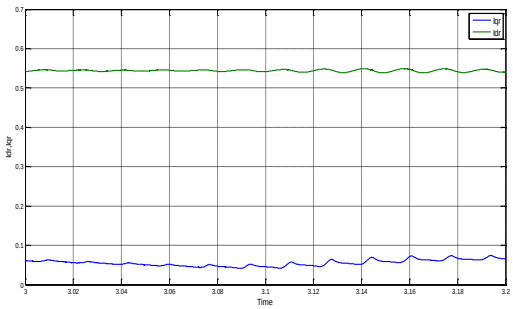

(i) Ir_{dq} at 1.21pu

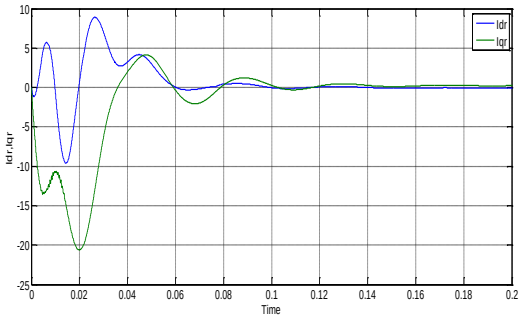

(ii) Ir_{dq} at 1.1pu

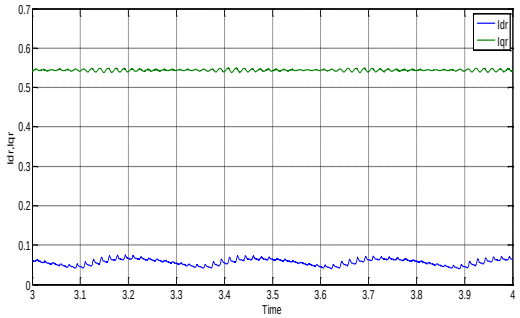

(ii) Ir_{dq} at 1.1pu

Transient state	Steady state

Fig.5.31 d-q rotor current for different reference speeds

As shown in Fig. 5.30, the d-axis rotor voltage control is maintained around zero. This is because, in stator flux orientation method, the d-component controls the reactive power and q-axis control the speed of the machine. The d-axis rotor current oscillates between -10 to 7.5 p.u. and reaches the steady state value with magnitude around zero. The 'iqr' oscillates between 8 to -15 p.u. during the grid integration and attains the steady state with the magnitude of 0.55 p.u. For lower reference speed of 1.1 pu, less transients are observed.

<table>
<tr>
<td> 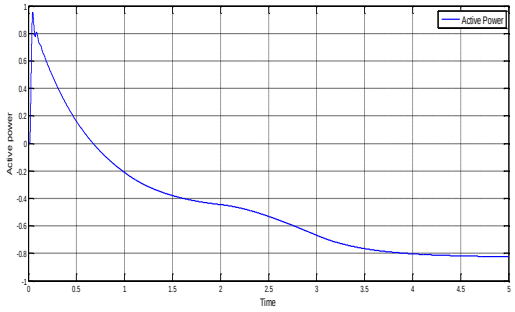

(i) Active power at 1.21pu</td>
<td> 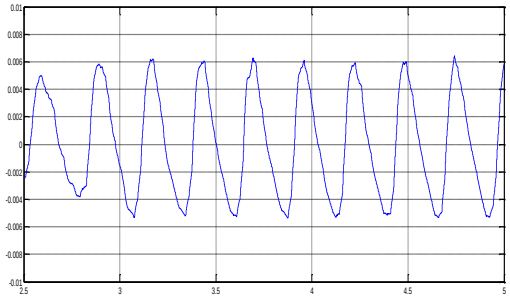
(i) Reactive power at 1.21pu</td>
</tr>
<tr>
<td> 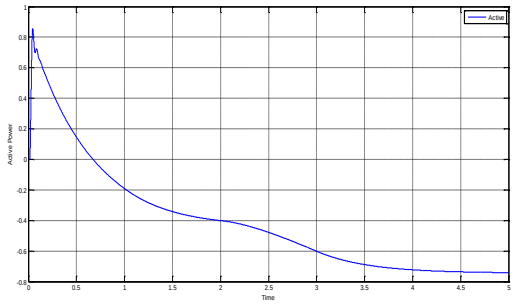

(ii) Reactive power at 1.1pu</td>
<td> 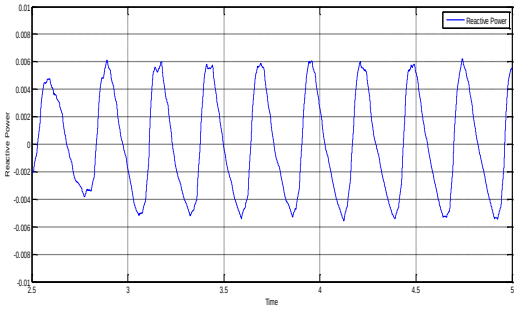

(ii) Reactive power at 1.1pu</td>
</tr>
<tr>
<td>Active power</td>
<td>Reactive power</td>
</tr>
<tr>
<td colspan="2">Fig. 5.32 Active and Reactive Power for different reference speeds</td>
</tr>
</table>

As shown in Fig. 5.32, the active power changes from initial motoring mode to generating mode without oscillating transients. At higher reference speed, slightly higher power is resulted at steady state. The reactive power maintains oscillating nature around zero.

CHAPTER - 6

CONCLUSION AND FUTURE SCOPE OF WORK

6.1 CONCLUSIONS

During this work the operational aspects of grid connected DFIG has been studied and the dynamic performance of grid connected DFIG has been simulated. The dynamic model and control scheme has been realized under simulink environment. The stator flux oriented and stator voltage oriented control schemes are implemented on the rotor and grid side converter respectively while the DFIG is operated in speed control mode. The performance is studied for change in wind speed, reference speed, DC link reference voltage, DC link capacitance and line inductance. The following conclusions are drawn-

- For the given reference speed, the performance characteristics is affected by wind speed. The higher wind speed results in higher amount of torque and power.
- The DFIG is starting in motoring mode and then driven into generating mode. The rotor speed under steady state follows the reference speed irrespective to the varying wind speed.
- In the speed control mode, for given reference and wind speeds, the dynamic and steady state behaviour does not change appreciably for the change (10-20%) in the DC bus reference voltage, DC bus capacitance and inductance.

6.2 SCOPE OF FUTURE WORK

The scope of future work has been identified as-

- The PI controllers have been used. The tuning or design of PI controller parameter is very challenging. There is a scope for formulate an adaptive control scheme to select the control loop parameters.
- The analysis can be done for analyzing power quality and reliability measures when such system is integrated in practical system.
- The model of DFIG wind turbine can be extended to analyze the wind farms.

APPENDIX-A

Subsystem of Induction machine

The subsystems of mutual flux linkages are shown in Fig. A.1 and Fig. A.2.

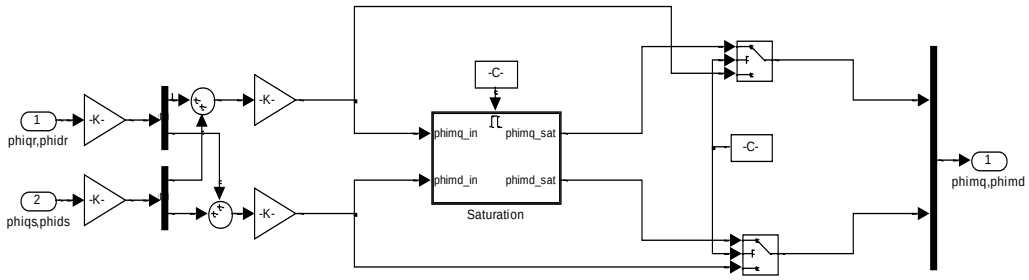

Fig.A.1 Mutual Flux Linkages of Asynchronous Machine

$$\phi_{mq\_in} = \left(\frac{\phi_{qr}}{L_{lr}} + \frac{\phi_{qs}}{L_{ls}} \right) L_{aq} \tag{1}$$

$$\phi_{md\_in} = \left(\frac{\phi_{dr}}{L_{lr}} + \frac{\phi_{ds}}{L_{ls}} \right) L_{ad} \tag{2}$$

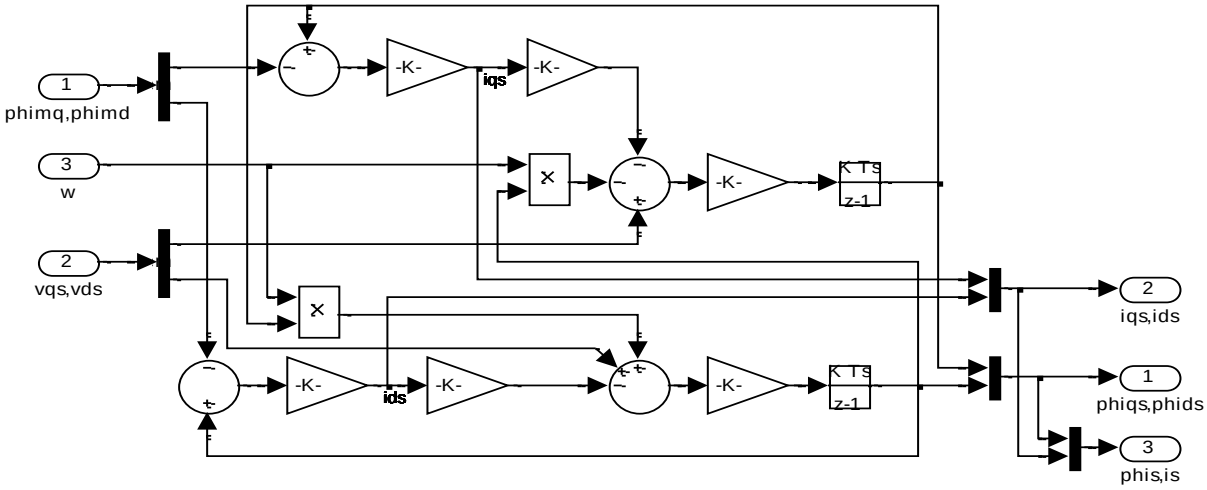

Fig.A.2 Subsystem of mutual flux linkages

$$\phi_{mq\_sat} = \phi_{mq\_in} - \left[(poly\ \ func)\phi_{mq\_in} \right] \frac{L_{aq}}{L_m} \tag{3}$$

$$\phi_{md\_sat} = \phi_{md\_in} - \left[(poly\ \ func)\phi_{md\_in} \right] \frac{L_{ad}}{L_m} \tag{4}$$

Model of rotor side of Induction machine is shown in Fig. A.3.

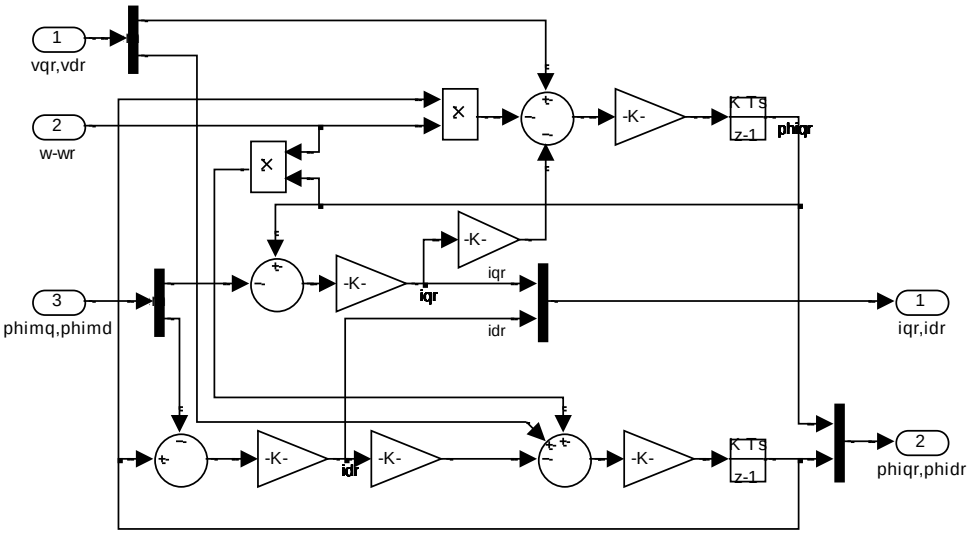

Fig.A.3 Model of rotor side of induction generator

$$i_{qr} = k\phi_{qr} - \phi_{mq} \tag{5}$$

$$i_{dr} = k\phi_{dr} - \phi_{md} \tag{6}$$

$$\phi_{qr} = kV_{qr} - \phi_{dr}\left(\omega - \omega_r\right) i_{qr} \tag{7}$$

$$\phi_{dr} = kV_{dr} - \phi_{qr}\left(\omega - \omega_r\right) i_{dr} \tag{8}$$

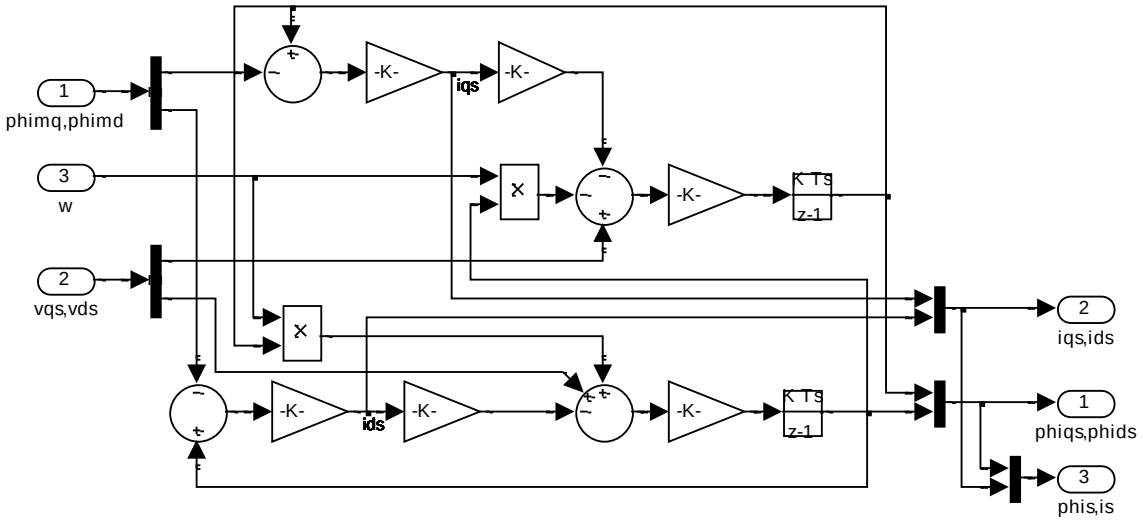

Fig.A.4 Model of stator side of induction generator

Model of stator side of Induction machine is shown in Fig. A.4.

$$i_{qs} = k\phi_{qs} - \phi_{mq} \tag{9}$$

$$i_{ds} = k\phi_{ds} - \phi_{md} \tag{10}$$

$$\phi_{qs} = kV_{qs} - \omega\phi_{ds} - i_{qs} \tag{11}$$

$$\phi_{ds} = kV_{ds} - \omega\phi_{qs} - i_{ds} \tag{12}$$

$$\phi_s = \sqrt{\left(\phi_{qs}^2 + \phi_{ds}^2\right)} \tag{13}$$

$$i_s = \sqrt{\left(i_{qs}^2 + i_{ds}^2\right)} \tag{14}$$

Mechanical model of Induction machine is shown in Fig. A.5.

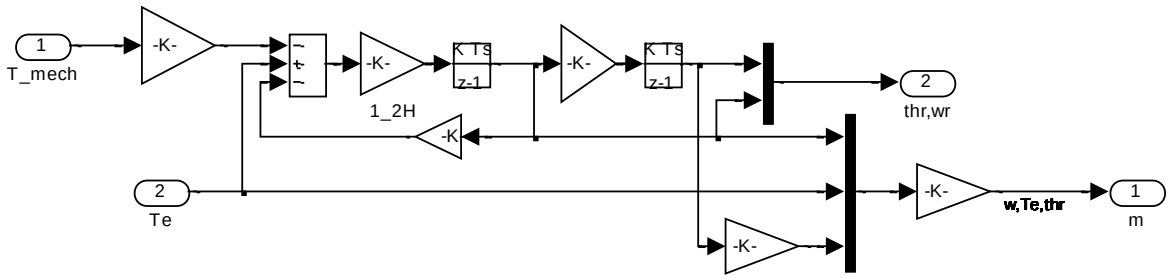

Fig.A.5 Mechanical Model of Induction Generator

Following equations are implemented to simulate the mechanical model as shown in figure A.5..

$$\frac{d\theta_r}{dt} = k\left(\frac{1}{2H}\right)T_e - T_m - \omega_r \tag{15}$$

$$\theta_r = \left(\frac{1}{2H}\right)T_e - T_m - \omega_r \tag{16}$$

APPENDIX-B

Parameters and specifications

Parameters	Values
ASYNCHRONOUS MACHINE DATA	
Nominal power(VA), Pnom	2 MW
Line-Line voltage (Vrms), Vnom	567
Nominal Frequency, Fnom	60
Stator Resistance, Rs (p.u.)	0.01965
Stator Inductance Lls (p.u.)	0.0397
Rotor Resistance, Rr (p.u.)	0.01909
Rotor Inductance, Llr (p.u.)	0.0397
Mutual Inductance, Lm (p.u.)	1.354
Inertia constant, H (p.u.)	0.09526
Friction constant(pu),F (p.u.)	0.05479
Number of Pole pair	2
CONTROL SYSTEM OF BOTH SIDE CONVERTER	
PWM frequency rotor side	1620
PWM frequency grid side	2700
Nominal DC Voltage	1200 Volts
Capacitance of DC link	16mF
Reactive power regulator Kp, Ki	10, 0.1
Dc bus regulator gains Kp, Ki	1, 0.0001
Grid side current regulator gain Kp,Ki	5, 0.001
Rotor side current regulator gain Kp, Ki	5, 0.001
Speed regulator Kp, Ki	10, 3

LIST OF PUBLICATIONS

- Ashwani kumar, Sanjay K. Jain, "A Review on the Operation of Grid Integrated Doubly Fed Induction Generator", *International Journal of Enhanced Research in Science Technology & Engineering (IJERSTE)*, Vol. 2 Issue 6, June – 2013, pp: (25-37)

REFERENCES

[1] Carrasco et al., “Power-Electronic Systems for the Grid Integration of Renewable Energy Sources: A Survey,”, *IEEE Transactions on Industrial Electronics* , vol. 53, pp: 1002-1016, 2006.

[2] WWEA, “World Wind Energy Report 2009,” 2010.

[3] Rechsteiner R. “Wind Power in Context –clean Revolution in the Energy Sector,” 2008.

[4] Ofualagba, G., and. Ubeku E. U. "Wind *Energy Conversion* system-wind turbine modeling", *In Power and Energy Society General Meeting-Conversion and Delivery of Electrical Energy in the 21st Century, 2008 IEEE*, pp. 1-8, IEEE, 2008.

[5] T. Ackermann, Wind Power in Power System, Wiley, Ltd, 2005.

[6] Hau E., Wind Turbines: Fundamental Technologies, Application, Economics, 2nd edition, Springer, 2005.

[7] Blaabjerg F., Chen Z., Power Electronics for Modern Wind Turbines, Morgan & Clay- pool Publishers, 2006.

[8] Slootweg, J. G., De Haan, S. W. H., Polinder, H., & Kling, W. L., "General model for representing variable speed wind turbines in power system dynamics simulations", *IEEE Transactions on Power Systems*, vol. 18, No. 1, pp.144-151, 2003.

[9] L. Holdsworth, X. G. Wu, J. B. Ekanayake, and N. Jenkins,“ Comparison of fixed speed and doubly-fed induction wind turbines during power system disturbances,” *Proc. Inst. Elect. Eng., Commun.*, vol. 150, no. 3, pp. 343– 352, May, 2003.

[10] Wang, R., Lin F., Hao R., You X., and Zheng T. Q., "Vscf doubly-fed induction generator control strategy and simulation research, "*In Industrial Electronics and Applications, ICIEA 2008. 3rd IEEE Conference on Power System*, pp. 2045-2050, IEEE, 2008.

[11] V. Akhmatov, Induction Generators for Wind Power, Multi-Science Publishing Co. Ltd., 2005.

[12] Ekanayake, J. B., Holdsworth L, Wu X.G., and Jenkins N.. "Dynamic modeling of doubly fed induction generator wind turbines," *IEEE Transactions on Power Systems*, 18, no. 2 (2003): 803-809.

[13] Hunt L. J., "A new type of induction motor," Institution of Electrical Engineers, Journal, pp: 648-677, 1907.

[14] Williamson S., Ferreira A. C., and Wallace A. K., "Generalized theory of the brushless doubly-fed machine. Part 1: Analysis," *IEE Proceedings - Electric Power Applications*, vol. 144, No.2, pp: 111-122, 1997.

[15] Broadway A. R. W., Burbridge L., "Self-cascaded machine: a low-speed motor or high frequency brushless alternator," *Proceedings, Institution of Electrical Engineers*, vol. 117, pp: 1277-1290, 1970.

[16] Müller S., Deicke M., and Doncker de R. W., "Doubly Fed Induction Generator Systems for Wind Turbines," *IEEE Industry Applications Magazine*, Vol. 8, No.3, pp: 26-33, 2002.

[17] B. Wu, High-Power Converters and AC Drives, Wiley-IEEE Press, 2006.

[18] Mikhail A., Cousineau K., Howes L., Erdman W., and Holley W., "Variable Speed Distributed Drive Train Wind Turbine System," *United States Patent*, US 7,042,110 B2, 2006.

[19] Babu, B. C., and Mohanty K. B., "Doubly-Fed induction generator for variable speed wind *Energy Conversion* systems-modeling & simulation," *International Journal of Computer and Electrical Engineering 2*, no. 1: 1793-8163, 2010.

[20] Mustafa, Milanovic, Jovica V., "DFIG modling and the relevance of model simplification," 8th International Conference and Eexhibition on Electricity Distribution, CIRED, pp. 1-5, June , 2005.

[21] Battista D., Puleston H., Mantz P.F., Christiansen R.J., "Sliding Mode Control of Wind Energy Systems with DFIG-Power Efficiency and Torsional Dynamics Optimization," *IEEE Trans. On Power Systems*, Vol. 15, No.2, pp: 728-734, May 2000.

[22] Cadirci I., Ermis M., "Double-Output Induction Generator Operating at Sub-synchronous and Super-Synchronous Speeds: Steady-State Optimization and

Wind-Energy Recovery," *IEE Proc. Electric Power Applications*, Vol. 139, No. 5, pp: 429-442, Sept. 1992.

[23] Uctug M.Y., Eskandarzadeh I., Ince H., "Modeling and Output Power Optimization of a Wind Turbine Driven Double Output Induction Generator," *IEE Proc. Electric Power Applications*, Vol. 141, No. 2, pp: 33-38, March 1994.

[24] Pena R., Clare J.C., Asher G.M., "Doubly Fed Induction Generator Using Back-to-Back PWM Converters and its Application to Variable-Speed Wind-Energy Generation," *IEE Proc. Electric Power Applications*, Vol. 143, No. 3, pp: 231-241, May 1996.

[25] Rabelo B., Hofmann W., "Optimal Active and Reactive Power Control with the Doubly-Fed Induction Generator in the MW-Class Wind-Turbines," *4th IEEE International Conference on Power Electronics and Drive Systems*, Vol. 1, pp: 53-58, Oct. 2001.

[26] Abbey C., Joos G., "A Doubly-Fed Induction Machine and Energy Storage System for Wind Power Generation," *Canadian Conference on Electrical and Computer Engineering, Vol. 2*, pp: 1059-1062, May 2004.

[27] Datta R., Ranganathan V.T., "A Method of Tracking the Peak Power Points for a Variable Speed Wind *Energy Conversion* System," *IEEE Transactions on Energy Conversion*, Vol. 18, No. 1, pp: 163-168, March 2003.

[28] Datta R., Ranganathan V.T., "Direct Power Control of Grid-Connected Wound Rotor Induction Machine Without Rotor Position Sensors", *IEEE Trans. on Power Electronics*, Vol. 16, No. 3, pp: 390-399, May 2001.

[29] Bhowmik S., Spee R., "Wind Speed Estimation Based Variable Speed Wind Power Generation," *Proc. of the 24th Annual Conference of the IEEE Industrial Electronics Society*, Vol. 2, pp: 596-601, Sept. 1998.

[30] Qizhong, L, Lan Y., and Guoxiang W.. "comparison of control strategy for double-fed induction generator (DFIG)," *In Measuring Technology and Mechatronics Automation (ICMTMA), 2011 Third International Conference on Power System*, vol. 1, pp. 741-744. IEEE, 2011.

[31] Jia-bing, H., Yi-Kang H., and Guo Z. J., "The internal model current control for wind turbine driven doubly-fed induction generator," *In Industry Applications*

Conference, 2006. 41st IAS Annual Meeting. Conference Record of the 2006 IEEE, vol. 1, pp. 209-215. IEEE, 2006

[32] Pena R., Clare J.C., Asher G.M., "Doubly Fed Induction Generator Using Back-to-Back PWM supplying an isolated load from a variable-speed turbine," *IEE Proc. Electric Power Applications*, Vol. 143, No. 5, pp: 380-387, September 1996.

[33] Li S., Haskew T.A., "Analysis of decoupled d-q vector control in doubley-fed induction generator using back-to-back PWM converter," *IEEE conference on power engineering society*, June, 24-28, pp:1-7,Tampa, FL, 2007.

[34] Yao X., Yi C., Ying D. ,Guo J.,Yang L., "The grid-side PWM converter of the wind power generation system based on fuzzy sliding mode control," *International conference on advanced intelligent mechatronics*, Xian,CHINA, July, 2, 2008.

[35] Sun H., Ren Y., Li H., Liu H., "Doubly-fed induction generator wind power generation based on back-to-back PWM Converter," *IEEE international conference on mechatronics and automation*, Changchun, CHINA, Aug, 9-12, 2009.

[36] Chittibabu B., Mohanty K.B., "Converter performance of grid connected of wind power generating systems," *5th IET conference on power electronics machine and drives*, pp.1-6,Bringhton,U.K., April,19-21, 2010.

[37] Zhan P., Lin W., Wan J., Yao M., Li N., "Design of LCL filters for the back-to-back converter in a doubly-fed induction generator," *IEEE conference on Innovative smart grid technologies in ASIA*, pp:1-6,Tianjin, May, 21-24, 2012.

[38] Salman, S. K., and Badrzadeh B., "New Approach for modelling Doubly-Fed Induction Generator (DFIG) for grid-connection studies," *In European wind energy conference an exhibition, London. 2004*.

[39] S. Li and T. A. Haskew, "Analysis of decoupled d-q vector control in DFIG back-to-back PWM converter," *in Proc. Power Eng. Soc. General Meet., Tampa, FL*, pp. 1–7, Jun. 24–28, 2007.

[40] Zhang L., Watthanasarn C., Shepherd W., "Application of a Matrix Converter for the Power Control of a Variable-Speed Wind- Turbine Driving a Doubly-Fed Induction Generator," *23rd International Conference on Industrial Electronics, Control and Instrumentation*, Vol. 2, pp: 906-911, Nov. 1997.

[41] Keyuan H., Yikang H., "Investigation of a Matrix Converter- Excited Brushless Doubly-Fed Machine Wind-Power Generation System," *The 5th International Conference on Power Electronics and Drive Systems,* Vol. 1, pp: 743-748, Nov. 2003.

[42] Zhang L., Wattahanasaran C., Shepherd W., "Application of a matrix converter for the power control of a variable-speed wind-turbine having a DFIG," *23rd International conference on Industrial electronics, Control and instrumentation,* vol.2, pp:906-911, New Orleans, LA., Nov, 9-14, 1997.

[43] Zhang L., Wattahanasaran C., "A matrix excited doubly fed induction generator machine as a wind power generator," *7th International conference on power electronics and variable speed drives,* pp:532-537, London, Sep, 21-23, 1998.

[44] Cardenas R., Pena R., Tobar G., Clare J., Wheeler P., Asher G., "Stability analysis of a wind *Energy Conversion* system based on a doubly fed induction generator fed by a matrix converter," *IEEE transaction on industrial electronics,* vol.56, no.10, October, 2009.

[45] Jeong J., Ju Y., Hon B., "Wind power system using DFIG and matrix converter with simple modulation scheme," *IEEE conference on power electronics and machines in wind application,* pp:1-6, Lincoln,NE, june, 24-26, 2009.

[46] Yarahmadi A., Khaburi D.A., Behnia H., "Direct virtual torque control of doubly fed induction generator connection using indirect matrix converter," *3rd International conference on power electronics and drives systems technology, ,* pp:115-120, Tehran, Feb,15-16, 2012

[47] Ashfaq H., Tripathi S.K., "Performance improvement of wind *Energy Conversion* system using matrix converter," *IEEE 5th Indian international conference on power electronics,* pp:1-5, Delhi, Dec,6-8, 2012.

[48] Poitiers F., Machmoum M., Doeuff R.l.,Zaim M. E., " Control of Doubly-fed induction generator for wind *Energy Conversion* system" AUPEC01

[49] Arifujjaman, Iqbal, M.T., Quaicoe J.E., "Vector Control of a DFIG based wind turbines," *Journal of Electrical & Electronics Engineering*, Vol. 9, No. 2, 2009.

[50] Almeida R.G. de, and Lopes J.A.P., “Participation of Doubly Fed Induction Wind Generators in System Frequency Regulation,” *Power Systems*, vol. 22, pp: 944-950, 2007.

[51] Dendouga, A., Abdessemed R., Bendaas M. L., and Chaiba A., "Decoupled active and reactive power control of a Doubly-Fed Induction Generator (DFIG),” *In Control & Automation, 2007. MED'07. Mediterranean Conference on*, pp. 1-5. IEEE, 2007

[52] Unchim, T., & Oonsivilai, A.,"A Study of Wind Speed Characteristic in PI Controller based DFIG Wind Turbine,” *World Academy of Science, Engineering and Technology 60* (2011).

[53] Slootweg, J. G., Polinder, H., & Kling, W. L. (2001), “Dynamic modelling of a wind turbine with doubly fed induction generator,” *In Power Engineering Society Summer Meeting*, vol. 1, pp. 644-649, IEEE, 2001.

[54] Kundur P., Paserba J., Ajjarapu V., Andersson G., Bose A., Canizares C., Hatziargyriou N., Hill D., Stankovic A., Taylor C., Cutsem T. V., and Vittal V., “Definition and classification of power system stability,” *IEEE Tran. Power Systems*, vol. 19, pp: 1387-1401, Aug. 2004.

[55] Sorensen P., Hansen A.D., and Lund T., “Reduced models of doubly fed induction generator system for wind turbine simulations,” *Wind Energy*, vol. 9, pp: 299-311, 2006.

[56] Sang K. H., Gab Y. G., and Pyo H. W., “Active Use of DFIG-Based Variable-Speed Wind-Turbine for Voltage Regulation at a Remote Location,” *Power Systems*, vol. 22, pp: 1916-1925, 2007.

[57] Lund T., Serensen P., and Eek J., “Reactive power capability of a wind turbine with doubly fed induction generator,” *Wind Energy*, vol. 10, pp: 379-394, 2007.

[58] Hansen A.D., Michalke G., and Sorensen P., “Co-ordinated voltage control of DFIG wind turbines in uninterrupted operation during grid faults,” *Wind Energy*, vol. 10, pp: 51-68, 2007.

[59] Ausin J.C., Gevers D.N., and Andresen B., “Fault ride-through capability test unit for wind turbines,” *Wind Energy*, vol. 11, pp: 3-12, 2008.

[60] Lopez J., Gubia E., and Sanchis P., “Wind Turbines Based on Doubly Fed Induction Generator Under Asymmetrical Voltage Dips,” *Energy Conversion,* vol. 23, pp: 321-330, 2008.

[61] Lie X., and Yi W., “Dynamic Modeling and Control of DFIG-Based Wind Turbines Under Unbalanced Network Conditions,” *Power Systems,* vol. 22, pp: 314-323, 2007.

[62] Brekken T.K.A., and Mohan N., “Control of a Doubly Fed Induction Wind Generator Under Unbalanced Grid Voltage Conditions,” *Energy Conversion,* vol. 22, pp: 129-135, 2007.

[63] Ullah N.R., Thiringer T., and Karlsson D., “Temporary Primary Frequency Control Support by Variable Speed Wind Turbines; Potential and Applications,” *Power Systems,* vol. 23, pp: 601-612, 2008.

[64] Short J.A., Infield D.G., and Freris L.L., “Stabilization of Grid Frequency Through Dynamic Demand Control,” *Power Systems,* vol. 22, pp: 1284-1293, 2007.

[65] Keung P.K., Li P., Banakar H. and Ooi B.T., "Kinetic Energy of Wind-Turbine Generators for System Frequency Support,” *IEEE Trans. Power Systems*.

[66] Lara O. A., Hughes F.M., and Jenkins N., “Contribution of DFIG-based wind farms to power system short-term frequency regulation,” *Generation, Transsmision & Distribution,* vol. 153, pp: 164-170, 2006.

[67] Yazhou L., Mullane A., Lightbody G., Yacamini R., “Modeling of the wind turbine with a doubly fed induction generator for grid integration studies,” *IEEE Transaction on Energy Conversion,* Vol.21 (1), March, 2006.

[68] F.M.H.N. Lara O. A., “Rotor flux magnitude and angle control strategy for doubly fed induction generators,” *Wind Energy,* vol. 9, pp: 479-495, 2006.

[69] Hughes F.M., Lara O. A., and Jenkins N., “A power system stabilizer for DFIG-based wind generation,” *Power Systems,* vol. 21, pp: 763-772, 2006.

[70] Karki R., Po H., and Billinton R., “A simplified wind power generation model for reliability evaluation,” *Energy Conversion,* vol. 21, pp: 533-540, 2006.

[71] Billinton R., and Yi G., "Multistate Wind *Energy Conversion* System Models for Adequacy Assessment of Generating Systems Incorporating Wind Energy," *Energy Conversion*, vol. 23, pp: 163-170, 2008.

[72] Singh B., Kasal G.K., and Gairola S., "Power Quality Improvement in Conventional Electronic Load Controller for an Isolated Power Generation," *Energy Conversion*, vol. 23, pp: 764-773, 2008.

[73] Moura de A.P., and Moura de A.A.F., "Analysis of injected apparent power and flicker in a distribution network after wind power plant connection," *Renewable Power Generation*, vol. 2, pp: 113-122, 2008.

[74] Tao S., Zhe C., and Blaabjerg F., "Flicker study on variable speed wind turbines with doubly fed induction generators," *Energy Conversion*, vol. 20, pp: 896-905, 2005.

[75] Petersson A., Thiringer T., and Harnefors L., "Modeling and experimental verification of grid interaction of a DFIG wind turbine," *Energy Conversion*, vol. 20, pp: 878-886, 2005.

[76] Changling L., and O. Boon-Teck, "Frequency deviation of thermal power plants due to wind farms," *Energy Conversion*, vol. 21, pp: 708-716, 2006.

[77] Lubosny Z., and Bialek J.W., "Supervisory Control of a Wind Farm," *Power Systems*, vol. 22, pp: 985-994, 2007.

[78] Changling L., Far H.G., and Banakar H., "Estimation of Wind Penetration as Limited by Frequency Deviation," *Energy Conversion*, vol. 22, pp: 783-791, 2007.

[79] Sokratis T.T., and Stavros A.P., "An Investigation of the Harmonic Emissions of Wind Turbines," *Energy Conversion*, vol. 22, pp: 150-158, 2007.

[80] Kanellos F.D., and Hatziargyriou N.D., "The effect of variable-speed wind turbines on the operation of weak distribution networks," *Energy Conversion*, vol. 17, pp: 543-548, 2002.

[81] Chen Z., "Compensation schemes for a SCR converter in variable speed wind *Power Systems*," Power Delivery, vol. 19, pp: 813-821, 2004.

[82] Bozhko S., Asher G., and Risheng L., "Large Offshore DFIG-Based Wind Farm With Line-Commutated HVDC Connection to the Main Grid: Engineering Studies," *Energy Conversion*, vol. 23, pp: 119-127, 2008.

[83] Bozhko S.V., Gimenez R. B. and L. Risheng, "Control of Offshore DFIG-Based Wind Farm Grid With ine-Commutated HVDC Connection," *Energy Conversion*, vol. 22, pp: 71-78, 2007.

[84] Dawei X., Li R., and Bumby J.R., "coordinated control of an HVDC link and doubly fed induction generators in a large offshore wind farm," *Power Delivery*, vol. 21, pp: 463-471, 2006.

[85] Bresesti P., Kling W.L., and Hendriks R.L., "HVDC Connection of Offshore Wind Farms to the Transmission System," *Energy Conversion*, vol. 22, pp: 37-43, 2007.

[86] Lie X., Liangzhong Y., and Sasse C., "Grid Integration of Large DFIG-Based Wind Farms Using VSC Transmission," *Power Systems*, vol. 22, pp: 976-984, 2007.

[87] H. Chong A.Q., Huang and M.E. Baran, "STATCOM Impact Study on the Integration of a Large Wind Farm into a Weak Loop Power System," *Energy Conversion*, vol. 23, pp: 226-233, 2008.

[88] Vrionis T.D., Koutiva X.I., and Vovos N.A., "Control of an HVDC Link Connecting a Wind Farm to the Grid for Fault Ride-Through Enhancement," *Power Systems*, vol. 22, pp: 2039-2047, 2007.

[89] M. Godoy Simöes and F. A. Farret, "Alternative Energy Systems: Design and Analysis with Induction Generators", 2nd Edition, CRC Press, 2007.

[90] Spée R., Wallace A. K., and Lauw H. K., "Performance simulation of brushless doubly-fed adjustable speed drives," *In Conference record of the IEEE Industry Applications Society Annual Meeting, San Diego,* CA, 1989.

[91] B. Wu., "Power Conversion and Control of Wind energy Systems", Wiley-IEEE Press, 2011.

[92] Zhang Y., Lin J., Ll G.J., Ll X., "A review on the integration of wind farms with variable speed wind turbines into *Power Systems*," *International conference on sustainable power generation and supply, SUPERGEN'09*, pp:1-6, Nanjing, April,6-7, 2009.